2008

Electrogenerated Chemiluminescence of New Thiophene-Containing Compounds

Jacquelyn T. Price

Electrogenerated Chemiluminescence of New Thiophene-Containing Compounds

(Spine title: ECL of New Thiophene-Containing Compounds)

(Thesis Format: Monograph)

By
Jacquelyn T. Price
Graduate Program in Chemistry

Submitted in partial fulfillment
Of the requirements for the degree of
Master of Science

SGPS
The University of Western Ontario
London, Ontario
May 2008

ABSTRACT

Electrochemically-induced light emission from conjugated organic molecules has received intense interest due to its possible application in fast response displays, sensors, chemical imaging and laser technology. The development in the field has been fueled by the search for improved light-emitting organic materials. Taking advantage of the Sharpless "click" reaction, a library of thiophene derivatives have been made from azidothiophenes and various aromatic acetylenes (Series A-D, below). These reactions were moderate to high yielding (60 - 98 %) and offered an alternative to carbon-carbon coupling reactions more traditionally used to make derivatives of thiophene and made purification by column chromatography unnecessary. Electron-donating or withdrawing groups could easily be introduced by the appropriate choice of the acetylene.

Series A

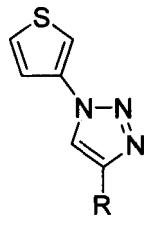

R
1 = C_6H_5
2 = C_6H_5F
3 = $C_6H_4N(CH_3)_2$
4 = SC_4H_3
5 = $C_6H_4OCH_3$

Series B

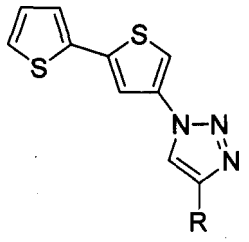

R
8 = C_6H_5
7 = C_6H_4F
8 = $C_6H_4N(CH_3)_2$
9 = SC_4H_3
10 = $C_6H_4OCH_3$

Series C

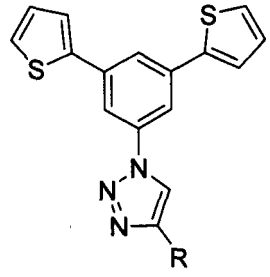

R
11 = C_6H_5
12 = C_6H_4F
13 = $C_6H_4N(CH_3)_2$
14 = SC_4H_3
15 = $C_6H_4OCH_3$

Series D

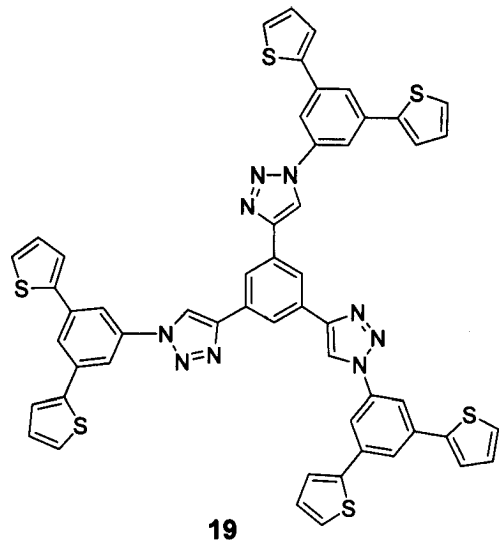

19

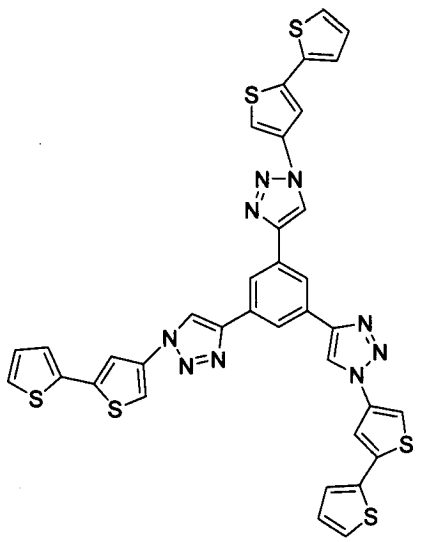

20

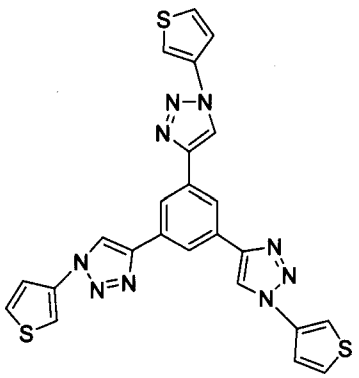

21

The optical and redox properties of compounds in Series A, B and D were investigated in order to determine the relative effects that their electron-donating and –withdrawing substituents had on the thiophene-containing compounds, and to evaluate their potential for electrochemiluminescence (ECL).

The compounds formed unstable radical ions in solution which could be seen from the non-reversible oxidation and reduction potentials in the cyclic voltammograms,

and also from the low efficiencies in the annihilation experiments (0.5 - 1.5 %) relative to 9, 10-diphenylanthracene. However, efficiencies did increase with the use of benzoyl peroxide as coreactant and we were able to achieve efficiencies as high as 17 % for compound **20**. Characteristic low wavelength emissions indicated the presence of excimer (excited dimers) in the ECL spectra. It was also possible to tune the amount of excimer formation by pulsing to different potentials.

Acknowledgements

I would like to thank Dr. Jones my supervisor for giving me the opportunity to work in his lab and for his guidance and support during the course of my project. I would also like to thank Dr. Ding for the use of his electrochemistry instruments and for the many helpful discussions relating to my chemistry. I would also like to express gratitude to Yanhua Chan for her aid in the electrochemiluminescence experiments.

I am also very grateful to the members of the Jones, group, Christine, Angelica, Allison, Kalen, Elizabeth and Steve who have supported and helped me along the way.

I would also like to express thanks to my parents and Craig Stephenson for their support and encouragement during my Master's degree.

I would also like to acknowledge financial assistance from UWO Faculty of Graduate Studies, UWO Chemistry department, the Government of Ontario and the Natural Sciences and Engineering Research Council of Canada (NSERC).

Table of Contents

List of Figures

List of Schemes

List of Tables

List of Appendices

List of Abbreviations

Å	angstroms
bp.	boiling point
BPO	benzoyl peroxide
BPD	dipyromethene
CV	cyclic voltammogram
d	days
δ	chemical shift parts per million
dd	doublet of doublet
DMF	dimethylformamide
DMSO	dimethyl sulfoxide
DPA	9, 10-diphenylantharacene
dppf	1,1'-bis(diphenylphosphino)ferrocene
ECL	electrochemiluminescence
EC	electrochemical
Et_2O	Ether
Fc/Fc^+	ferrocene/ferrocenium
FET	Field effect transistor
HRMS	High Resolution Mass Spectrometry
Hz	Hertz
HH	head-to-head
HOMO	highest unoccupied molecular orbital
HT	head-to-tail
LUMO	lowest unoccupied molecular orbital
λ_{max}	maximum wavelength
m	multiplet
M	molar
n-BuLi	n-butyl lithium
NMR	Nuclear Magnetic Resonance
OLED	Organic light emitting diodes
p-	para
p	pseudo
PT	poly(thiophene)
PHT	poly-3-hexylthiophene
r.t.	room temperature
R_f	distance traveled up a TLC plate relative to the total distance traveled by the solvent
s	singlet
SHE	standard hydrogen electrode
σ_p	sigma para
t	triplet
TBAP	tetra-n-butylammonium perchlorate
THF	tetrahydrofuran
TLC	Thin Layer Chromatography
TPrA	tri-n-propylamine

UV	ultra violet
vis	visible
V	volts
${}^{z}J_{xy}$	coupling constant between x & y over z bonds

1.0 Introduction

1.1 General introduction to conducting polymers

Although known for many years, conjugated polymers containing spatially extended π-bonding systems did not draw significant attention until the mid 1970s. In 1977, Heeger, MacDiarmid and Shirakawa individually showed that poly(acetylene), the simplest polyconjugated system, could be made conductive by reaction with bromine or iodine vapours.[1] Subsequent spectroscopic studies demonstrated that this reaction was in fact redox in nature and converted a neutral polymer chain into polycarbocations. This important discovery initiated extensive and systematic research into the chemistry of conjugated polymers in both their neutral and doped states. Previous to this finding, electrical conductivity had only been observed in metals in their standard states, inorganic polymers and molecular crystals.[1]

In 1979, the first conjugated poly(heterocycle) was reported: highly conductive and homogeneous films of poly(pyrrole) were made *via* the oxidative electropolymerization of pyrrole at a platinum electrode.[2] This quickly led to the development of other conjugated aromatic poly(heterocycles) which included thiophene, furan, indole and carbazole.[3]

1.2 Poly(thiophene) (PT)

Thiophene has become one of the most studied heterocycles because it is easy to make and process, is chemically stable and has many applications. Interest in thiophene has spread from early dye chemistry[4] to block co-polymer self-assembled superstructures,

conductivity-based sensory devices and optoelectronic devices.[5,6] Investigations have focused on thiophene-based conjugated polymers because of their potential use in many applications such as field effect transistors (FET), light emitting diodes (LED) and lasers.[7] The variety of synthetic approaches to PT, both chemical and electrochemical, its capacity to be functionalized with a large number of different substituents, and its unique and tunable electronic properties have resulted in a great interest in this class of polymers as materials for electronic and optoelectronic applications.[7]

Considering the many potential applications of PT, there has been a strong push to develop novel thiophene monomers to vary the electrical and optical properties of the resulting thiophene polymers. Guerrero and co-workers made a series of 3-(*p*-X-phenyl)thiophene monomers to study the role that substitution plays during the n- and p-doping process (Figure 1.1).[8]

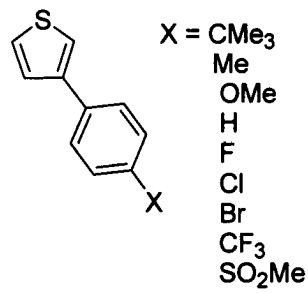

Figure 1.1: Monomers with various electron-donating and -withdrawing substituents.[8]

The trends shown by the monomers were as expected: those containing electron-donating substituents displayed cathodically shifted oxidation potentials, while those containing electron-withdrawing substituents, had potentials that were shifted annodically. The effect of the substituents however was more pronounced in the

monomer than in the polymers.[8] Also, by varying the nature of the substituents in the 3-position of the thiophene monomer, Inganis and coworkers were able to exploit the use of steric hindrance to synthesize PT with emission colours spanning the whole visible spectrum (Figure 1.2).[9]

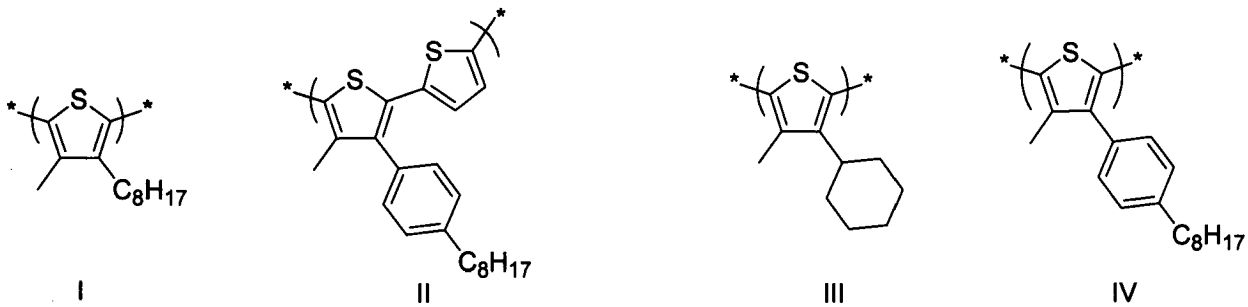

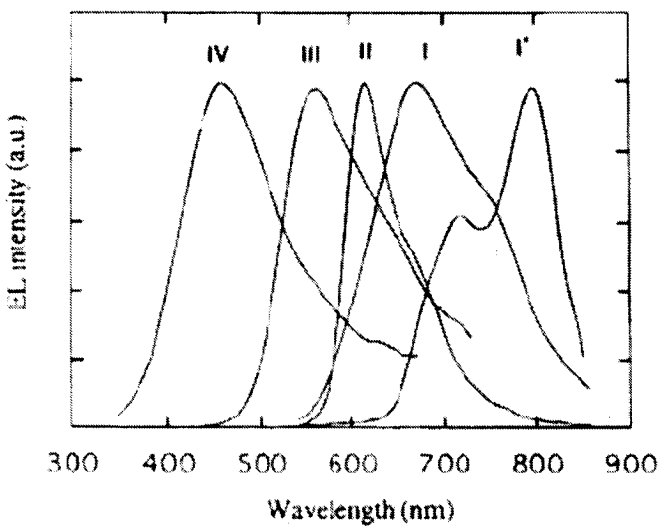

Figure 1.2: The electroluminescence (EL) spectra of the various 3-substituted PT (taken from ref. 9).

The dihedral angle and the π-orbital overlap between adjacent thiophene rings along the polymer backbone determine conjugation along the polymer chain. Short conjugation gives a blue-shifted emission, whereas longer conjugation gives red-shifted emission.

Inganis and coworkers modified the thiophene monomers by adding different numbers and sizes of substituents so that they were able to control the conjugation in the resulting polymer and tune its optical properties. Green, orange, red and NIR electroluminescence (EL) resulted from the polymerization of four different monomers, I-IV (Figure 1.2). The transformation of I to I* occurs upon heating. Polymer I is amorphous, however, upon heating, the crystallinity is increased allowing for greater conjugation causing the emission to be red-shifted.[9]

1.3 Fluorescent dyes

Small conjugated molecules can function as bright fluorescent dyes that can emit light in the red or near infrared (NIR) region of the spectrum. Dyes in the NIR emission have come into high demand for non-invasive and simple diagnostic techniques such as *in vivo* imaging and for biological and analytical applications.[10] Having an optical window of 600 – 900 nm has many advantages. There is significantly less background noise due to low auto absorption and auto fluorescence of biomolecules in the NIR region, low light scattering, deep penetration of light and the possibility of low cost excitation sources.[11] However, many of these fluorescent dyes suffer from low fluorescence quantum yields or lack of photostablity.[12] Squarylium dyes have a zwitterionic structure, which exhibits strong absorption and intense fluorescence. Some of these dyes give enhanced fluorescence and increased quantum yields when bound to proteins. Nakazumi *et al.* prepared new NIR bis-squarylium dyes which are linked by a thiophene spacer that exhibited increased fluorescence in the NIR region in tris buffer containing human serum albumin (HSA) and bovine serum albumin (BSA).[13]

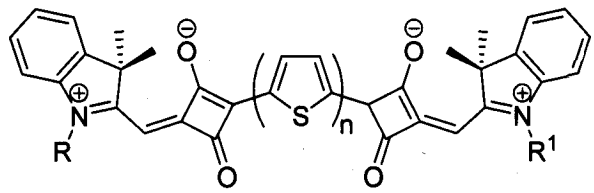

Figure 1.3: Thiophene linked squarylium dyes.[13]

Other small molecules that emit in the NIR region, such as boron-dipyrromethenes (BDP), are currently being explored as alternatives to the standard cyanine-based fluorescent dyes because of their higher fluorescence quantum yields and higher photo- and chemostability.[14] However, these compounds have a relatively short maximum emission wavelength. Umesawa and coworkers were able to develop fluorescent dyes by fusing a furan group into the BDP chromophore. In this way, they made a family of BDP based fluorescent dyes called Keio Fluors (KFL) (Figure 1.4).[15]

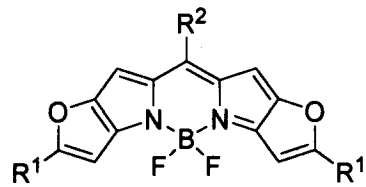

Figure 1.4: Structures of the Keio Fluors (KFL).[15]

By adding π-electron donors and acceptors, these researchers achieved KFLs that had emission in the red and NIR region (500 – 900 nm).[15]

The syntheses of many of these polyaromatic molecules as well as thiophene based monomers for onward polymerization rely on traditional organic reactions such as carbon-carbon couplings which can be used to add functional groups to the parent

molecule. These reactions often require the use of metal catalysts, sometimes at high loadings, and may also need special precautions to avoid oxygen and moisture. They often give low yields and require lengthy purification processes due to various byproducts and intermediates that are formed. As an alternative to the more traditional methods used to functionalize small molecules, we turned to the emerging field of "click" chemistry developed by K.B. Sharpless[16] to tune the optical and electrical properties of thiophene.

1.4 "Click" chemistry

Chemistry research often requires the preparation of structurally complex molecules through rational design, and furthermore, if these molecules are to have any potential application, their syntheses must be as simple as possible and economically viable.[16] This has resulted in a demand for reliable reactions that could potentially provide extensive libraries of chemically diverse compounds.[16] A philosophical approach to this problem has come in the form of "click" chemistry developed by K.B. Sharpless. The term "click" chemistry refers to a collection of reactions that are modular, stereospecific, high yielding and involve simple experimental procedures. These reactions should also make use of readily available starting materials, environmentally friendly conditions and should not require chromatographic isolations. The most widely used "click" reaction is the 1,3-dipolar cycloaddition of azides and alkynes to form 1,2,3-triazoles, known as the Huisgen cyclization (Figure 1.5).[16]

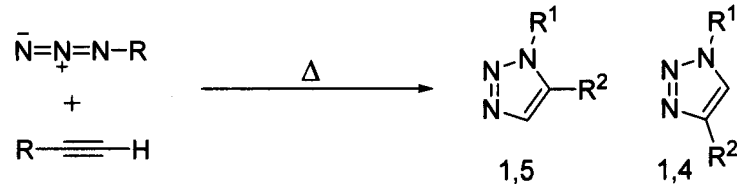

Figure 1.5: 1,4- and 1,5-disubstituted 1,2,3-triazoles by Huisgen cyclization.[17]

The discovery that Cu(I) salts greatly increased the rate of the reaction (up to 10^7 fold) and produced exclusively the 4-substituted regioisomer allowed this reaction to be used more readily.[18] This Cu-catalyzed cycloaddition can be carried out at room temperature in aqueous or biphasic media, and is compatible with most functional groups.

The Cu(I) source is usually generated *in situ* from Cu(II)SO_4 through reduction by sodium ascorbate,[18] but other Cu(I) sources have also been reported in the literature, *e.g.*, simple Cu(I) salts[19] (CuCl, CuI, *etc.*) and Cu(I) complexes.[20] The proposed mechanism for the Cu(I) catalyzed cycloaddition reaction is shown in Scheme 1.1.[17]

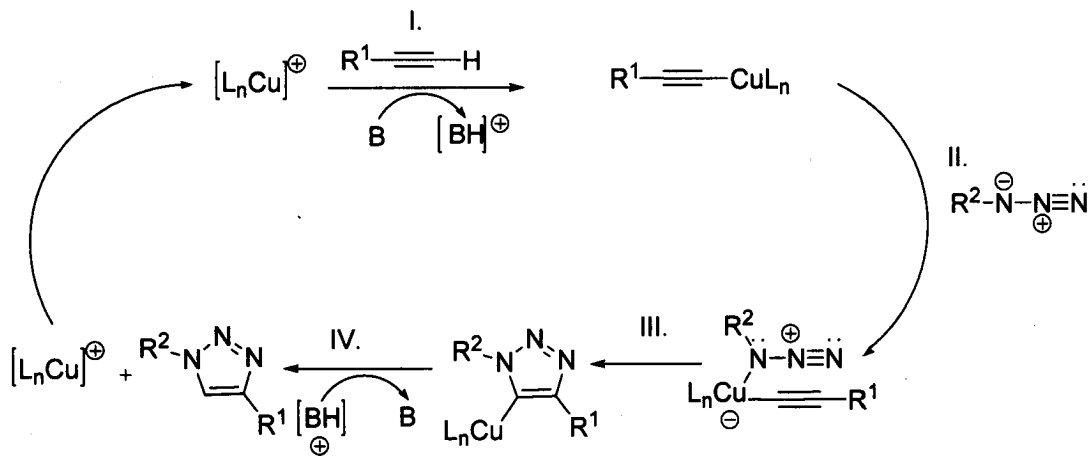

Scheme 1.1: Cu(I) catalyzed synthesis of 1,4-disubstituted 1,2,3-triazoles from azides and alkynes. Ln: an indeterminate number of ancillary ligands.[17]

The reactions steps are the following: I) Cu(I) is able to form a π-complex with the alkyne, lowering the pK_a value of the terminal alkyne proton. Under these conditions, the acetylene group is acidic enough to be deprotonated in an aqueous media; II) the resulting Cu(I) acetylide is attacked by the azide to form a zwitterionic Cu(I) adduct; III) which then undergoes an intramolecular cyclization to yield a copper-containing 1,2,3-triazole; IV) the final protonation of the triazole regenerates the Cu(I) catalyst and the 4-substituted 1,2,3-triazole. During the catalytic cycle, copper occupies the 5-position of the triazole ring, and therefore only the 1,4-regioisomer of the product 1,2,3-triazole is formed.[17]

The triazole ring is compatible with many functional groups and is stable under a variety of reaction conditions. Because of this, much effort has gone into synthesizing triazole-containing peptides, oligosaccharides and natural product analogues. Also, the synthesis of dendrimers and polymeric material has greatly been simplified by using the 1,3-dipolar addition.[17]

An important factor to consider in the production of functionalized polymers is the synthetic availability of the monomer itself. Thibault and coworkers used the Cu(I) catalyzed "click" reaction to synthesize 4-vinyl-1,2,3-triazole monomers possessing many of the same features of traditional monomers (*e.g.*, styrene, acrylate and vinyl pyridine). These monomers possess many of the same features of vinyl systems, such as aromaticity, stability to acid and base, a large dipole moment, and access to structural diversity through N1 on the triazole ring (Figure 1.6).[21]

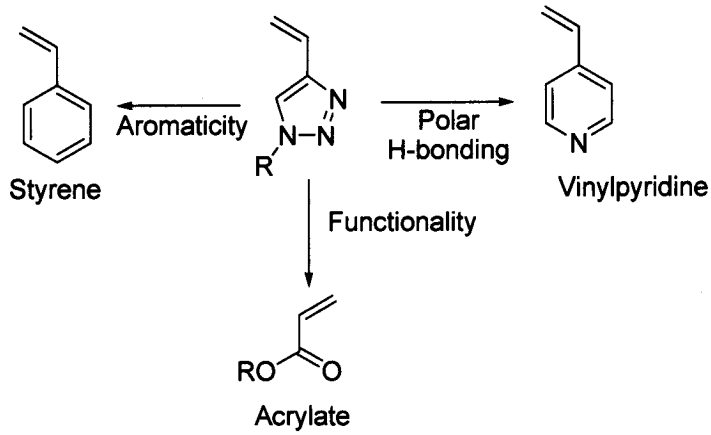

Figure 1.6: Similarities between the 4-vinyl-1,2,3-triazole monomer and traditional vinyl systems. [21]

By using the click reaction, the researchers were able to expand the monomer library easily (Figure 1.8), and found that the homopolymerization and copolymerization of the monomers using reversible addition-fragmentation chain transfer (RAFT) conditions proceeded with a high degree of control to give materials with a wide range of physical properties.[21]

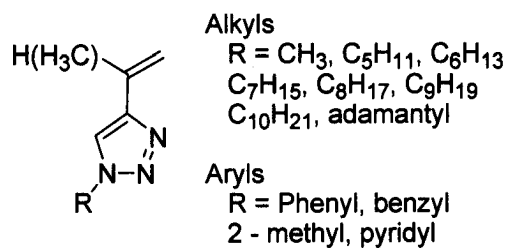

Figure 1.7: Structure and functional variety in the 4-vinyl-1,2,3-triazole monomer.[21]

Click chemistry has also been applied to the synthesis of new conjugated polymers based on poly(fluorenes). Starting from 4,4'-azido fluorene and 4,4'-

diethynyl fluorene building blocks, a polyaddition click reaction was carried out (Scheme 1.2).[22]

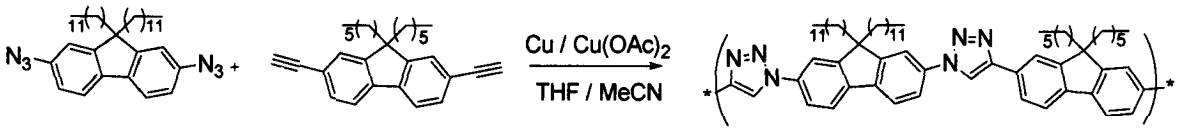

Scheme 1.2: Polymerizatio of fluorene using Cu(I) catalyzed "click" chemistry.[22]

Using this method, van Steenis and co-workers are able to introduce multiple triazole repeating units which could potentially have interesting properties. However, for this class of polymers, they found that there was little electronic communication between the fluorene units from the UV-vis and fluorescence spectra.[22] This could be due to twisting in the polymer chain.

1.4.1 Dendrimers

Dendrimers have received much attention due to their unique properties and applications in medicinal and materials chemistry. However, after 25 years, the syntheses of dendrimers are still plagued by the same problems such as purification and lengthy chromatographic separations of impure or intermediate products. However, these problems can be addressed partially with the use of Cu(I) catalyzed "click" chemistry.[23] The Huisgen 1,3-dipolar addition is a simple and reliable method for the efficient synthesis of chemically differentiated dendrimers. There are three strategies to make the triazole-based dendrimers: I) coupling between a dendron azide and a dendron alkyne, II) between a dendron azide and a polyalkyne or III) between a dendron alkyne and a polyazide (Figure 1.8).[17]

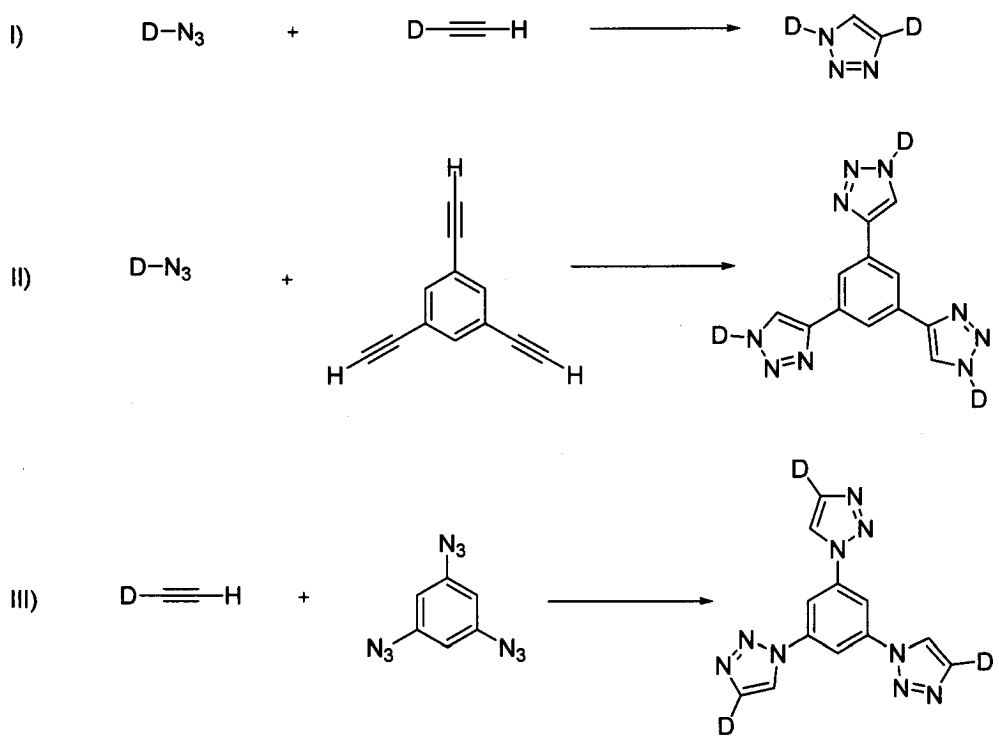

Figure 1.8: Three different strategies using "click" chemistry to 1,2,3-triazole containing dendrimers.

Lee and co-workers were successful in linking dendrons up to the 4th generation using "click" chemistry. Frechet-type dendrons (**A**) could be linked to a bivalent core (**B**) or another azido-substituted dendron (**C**) in yields ranging from 84 to 95 % using 5 mol % of $CuSO_4$/sodium ascorbate in DMF/water mixture. This provides an easy approach to link complex and large structures (Figure 1.9).[24]

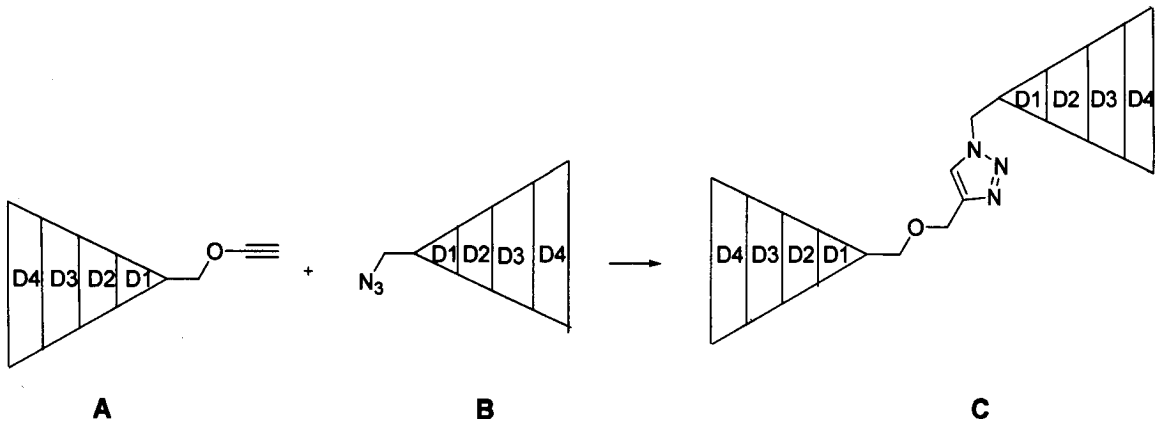

Figure 1.9: Use of "click" chemistry to link two dendrimers.[24]

We have been able to take advantage of the Cu(I) catalyzed 1,3-dipolar addition to make a variety of elaborated thiophene compounds including dendrimers whose electrical and optical properties we studied.

1.5 Electrochemiluminescence (ECL)

Electrochemiluminescence (also called electrogenerated chemiluminescence, or ECL) involves the production of light near an electrode surface by the generation of species that can undergo highly energetic electron transfer reactions to give excited states that emit light. For example, when a potential is applied to an electrode in the presence of $Ru(bpy)_3^{2+}$ (bpy = 2, 2'-bipyridyl), emission of light allows detection of the emitter at very low concentrations ($\leq 10^{-11}$ M).[25] ECL has found application in immunoassays, DNA analyses and display devices.[26] Commercial systems have been developed which use ECL to detect many clinically important analytes (*e.g.*, digoxin, thyrotropin, proteins and steroidal hormones and various antibodies) with high sensitivity and specificity.[26] ECL should not be confused with chemiluminescence, which is initiated and controlled

by the mixing of reagents and careful treatment of fluid flow; ECL, is instead initiated and controlled by switching the electrode voltage.[27]

1.5.1 General reaction mechanisms

The first studies on ECL involved electron transfer reactions between an oxidized and a reduced species, both of which were generated at the same electrode, by scanning the electrode potential between negative and positive values. This type of experiment is called "annihilation". The proposed mechanism is shown in Scheme 1.3.[27]

(1) $A - e^- \rightarrow A^{\bullet+}$ (oxidation at the electrode in the positive potential region)

(2) $A + e^- \rightarrow A^{\bullet-}$ (reduction at the electrode in the negative potential region)

(3) $A^{\bullet+} + A^{\bullet-} \rightarrow A^* + A$ (excited state formation)

(4) $A^* \rightarrow A + h\nu$ (light formation)

Scheme 1.3: Annihilation mechanism for ECL; A = analyte.[27]

Cyclic voltammetry (CV) is commonly used together with ECL to determine the potentials at which the desired reactants are generated. CV is also an excellent probe to determine the stabilities of the oxidized and reduced forms of the analyte and its ability to undergo electron transfer reactions. The presence of stable "reversible" redox waves in the CV and highly efficient, bright photoluminescence are taken in combination as signs that a compound is a good candidate as an ECL luminophore (Figure 1.10).[27]

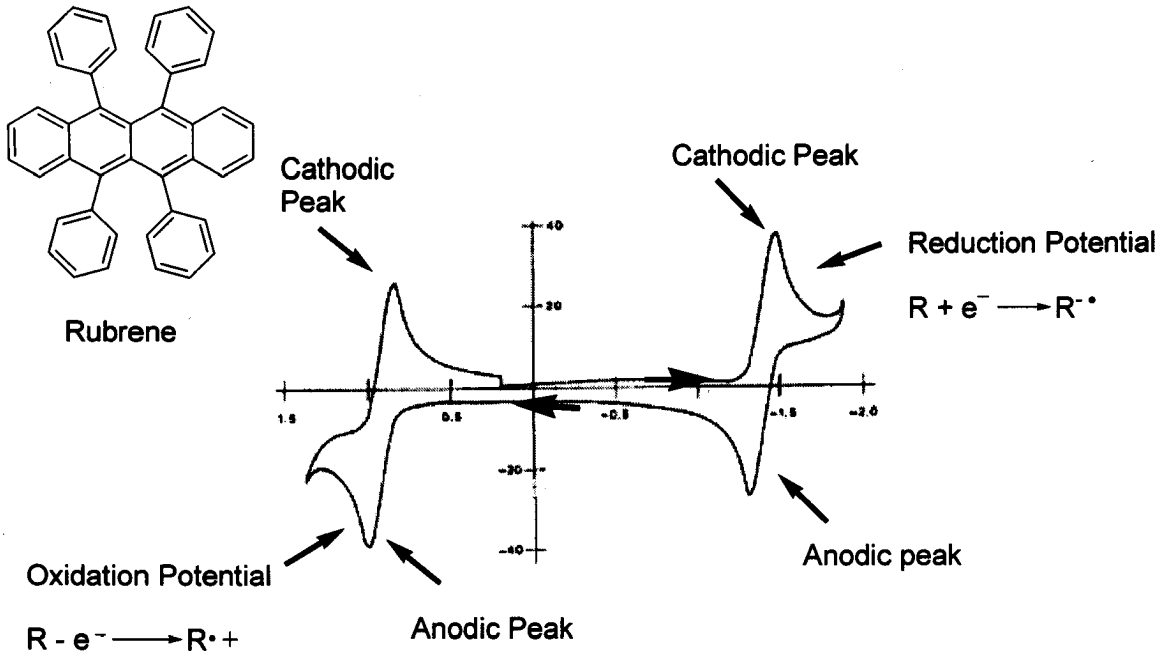

Figure 1.10: Cyclic voltammogram curve of rubrene in benzonitrile solution containing 0.1 M TBAP where the x-axis is the potential (V) and the y axis is current (A) (taken from ref 27).[27]

In a typical annihilation experiment, a platinum electrode is immersed in a solution containing an electrolyte and the compound under study. The electrode is initially held at a potential where no electrochemical activity occurs (0.0 V). The potential is then stepped anodically to a value where an oxidation reaction occurs, and the first reagent is produced ($A^{\bullet+}$), which is accompanied by an obvious peak. In the example shown in Figure 1.10, only one oxidation peak can be seen. This is called an anodic peak because it involves the loss of an electron. Once the potential sweeps past the oxidation potential and reaches the scan limit set by the user, it proceeds in the reverse direction. If the oxidation reaction is reversible (as in Figure 1.10), cathodic peaks are produced in the back scan. The potential is then stepped cathodically until a new cathodic peak is formed (representing gain of an electron) which generates a radical anion ($A^{\bullet-}$). After reaching the end of the cathodic scan, the potential is swept back in

the reverse direction and returned to the initial value. If the reduction is reversible (as in Figure 1.10), an anodic peak is seen for the oxidation of $A^{\bullet-}$. After a complete cycle, both the radical anion and cation exist in the diffusion layer near the electrode. These react, to give an excited molecule (A*), which subsequently gives light by relaxing to its ground electronic state.[27]

1.5.2 Coreactant ECL experiments

ECL can also be generated using a single direction potential sweep if an appropriate coreactant is added to the system. The coreactant is a species that upon oxidation or reduction produces an intermediate that can react with the ECL luminophore to produce excited states. This usually occurs because bond cleavage of the coreactant forms a strong oxidant or reductant. Typical coreactants for oxidations include tri-n-propylamine (TPrA), which produces a strong reducing agent (TPrA radical, $TPrA^{\bullet}$) and a strong oxidizing agent (TPrA radical cation, $TPrA^{\bullet+}$) oxalate ion ($C_2O_4^{2-}$), which produces a strong reducing agent ($CO_2^{\bullet-}$), and benzoyl peroxide (BPO) which produces a strong oxidizing agent ($C_6H_5CO_2^{\bullet}$). The general mechanism for the coreactant system is shown in Scheme 1.4 where R is the emitter, CR is a coreactant, X is the reactive oxidizing agent produced from the CR radical anion and X′ is a reaction product of X.[26]

$$R + e^- \rightarrow R^{\bullet-}$$

$$CR + e^- \rightarrow CR^{\bullet-}$$

$$CR^{\bullet-} \rightarrow X$$

$$R^{\bullet-} + X \rightarrow R^* + X'$$

Scheme 1.4: General reaction mechanism for a coreactant system.

1.5.3 Thiophene ECL

The photo and electroluminescence of thiophene monomers and polymers have been studied extensively. However, very few studies have investigated the ECL properties of thiophene. Yang and co-workers made fluorescent donor-acceptor π-conjugated systems containing thiophene chromophores (Figure 1.11).[28]

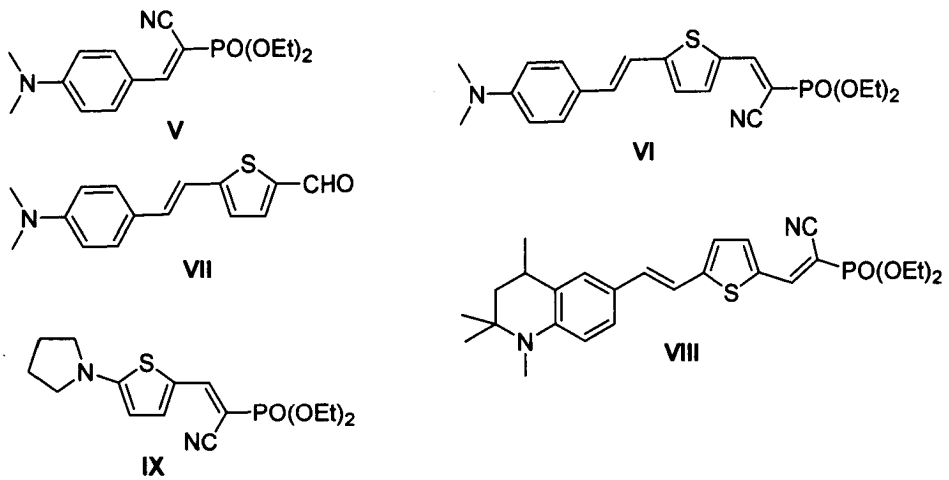

Figure 1.11: The structures of A-π-D compounds made by Yang and coworkers.

In these systems, the *para*-N,N-dimethylaniline group is the donor (D), while the diethyl cyanomethylphosphonate as the acceptor (A) and the thienylvinyl unit acts as the bridge. The first oxidation and reduction waves in these molecules were reversible, and therefore the electrogenerated radical ions were stable. Compounds **VI-IX** all exhibited ECL whereas **V** did not. This is believed to be due to the increased delocalization of the π-electrons in compounds containing thiophene.

ECL studies have also been done on poly(3-hexylthiophene) (PHT). From the CV (Figure 1.12), there is good reversibility for the p-type doping. During the cathodic

scan, there was an obvious threshold potential for the reduction of PHT (n-type doping) (-1.2), but significant current flow was not seen until -1.8 V.

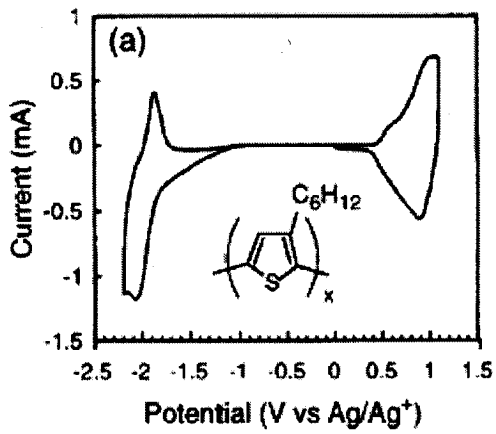

Figure 1.12: Cyclic voltammograms of PAT6 (taken from ref 23).

A cathodic peak current appeared around -2.1 V and a clear undoping current appeared at -1.9 V. This suggested that some nonelectrochemical undoping reactions took place during the cathodic scan. The ECL intensity for a double potential-step electrolysis of PHT film with a thickness of 0.24 μm is shown in Figure 1.13. The electrode was pulsed between 1.1 and -2.2 V, and the durations were 0.6 and 0.9 s for the anodic and cathodic scans, respectively.[23]

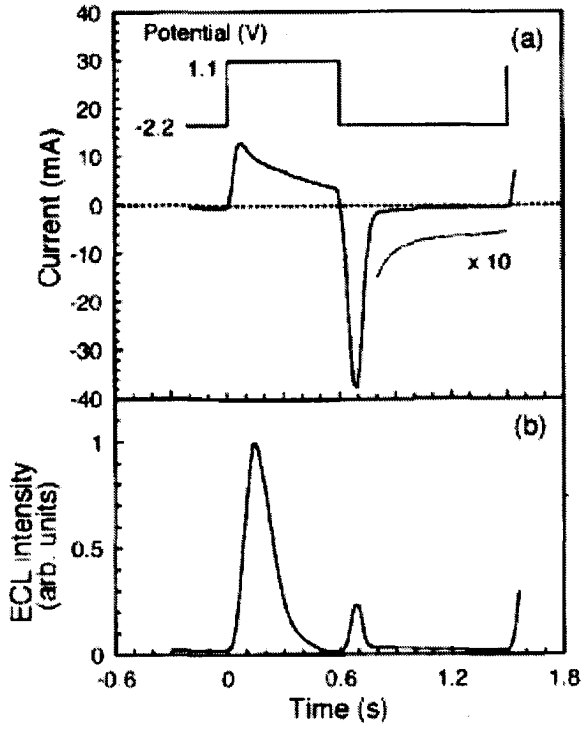

Figure 1.13: (a) Current and (b) ECL for double potential step electrolysis of PHT (taken from ref 23).

In the PHT polymer, ECL was much more intense and long-lived at positive potentials than at negative potentials.[23] ECL studies on thiophene compounds, whether they be small molecules or π-conjugated polymers are quite rare and there is much room in this field for exploration into the potentially tunable ECL.

1.6 Goals and scope of this thesis

The goal of this project was to develop a simplified method to modify thiophene so as to create poly(aromatic) thiophene-containing compounds and dendrimers that do not rely on C-C coupling reactions. We then set out to study the electrochemical and optical properties of these elaborated thiophene compounds. The motivation stemmed

from the growing interest in thiophene-containing materials for optoelectronic devices which derives from the tunability of their properties by minor structural modification. This has allowed the realization of a great diversity of chemical structures with varying optical properties.

In this work, we were able to take advantage of the Sharpless "click" reaction between thienylazides and arylacetylenes to synthesize several series of elaborated thiophene compounds containing both electron-withdrawing and -donating substituents in high yielding reactions requiring very little purification (Figure 1.14)

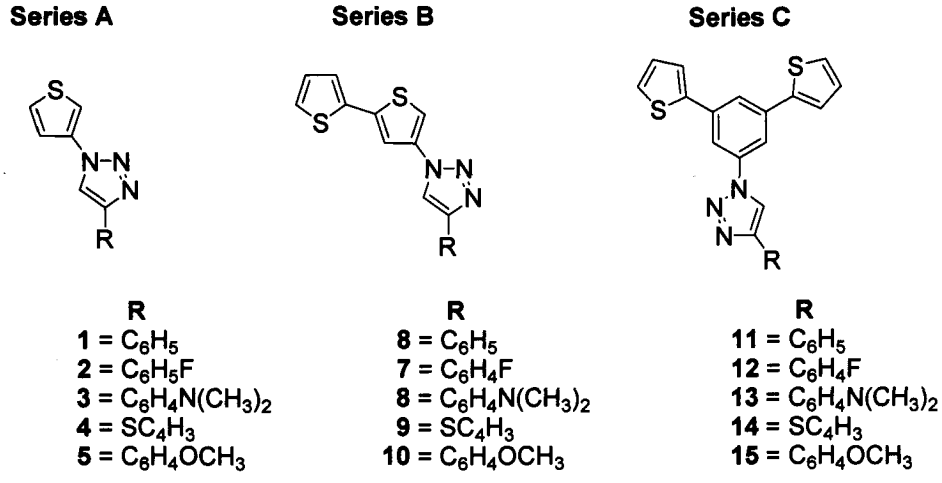

Figure 1.14: 1,4-disubstituted triazoles made in this work.

Furthermore, a series of C_3-symmetric thiophene-containing dendrimers was also synthesized using similar protocols (Figure 1.15).

Series D

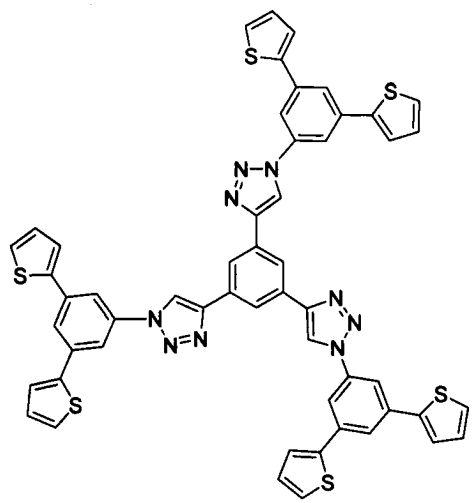

19

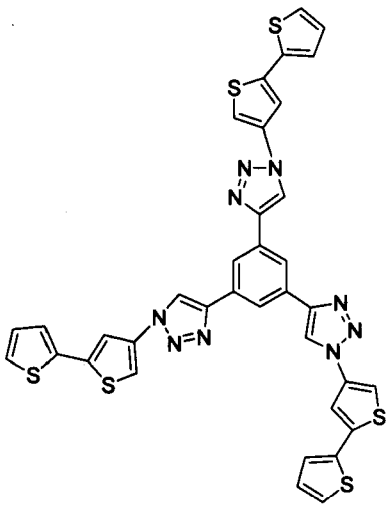

20

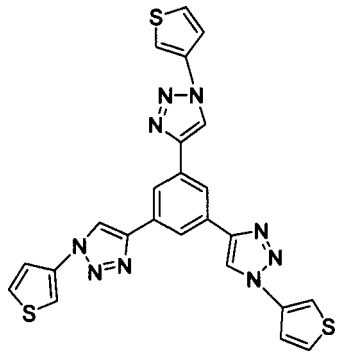

21

Figure 1.15: C_3-Symmetric dendrimers made by Cu(I) catalyzed "click" reaction

We were then able to characterize these compounds by ^{1}H NMR and ^{13}C spectroscopic, mass spectrometry and crystallographic methods. We also studied the physical and optical properties through cyclic voltammetry, ECL, photoluminescence and UV-vis

spectroscopy and compared the effects the various functional groups had on the properties of the series of compounds studies.

1.7 References

(1) Pron, A.; Rannou, P. *Prog. Polym. Sci* **2002**, *27*, 135.
(2) Diaz, A. F.; Danazawa, K. K. *Chem. Soc., Chem Commun.* **1979**, 635.
(3) Roncali, J. *Chem. Rev* **1992**, *17*, 711.
(4) King, W. J.; Nord, F. F. *J. Org. Chem.* **1949**, *14*, 638.
(5) Verizema, D. M.; Hoogboom, J.; Velonia, K.; Takazawa, K.; Christianen, P. C. M.; Maan, J. C.; Rowan, A. E.; Nolte, R. J. M. *Angew. Chem. Int. Ed.* **2003**, *42*, 772.
(6) Yu, H.; Pullen, A. E.; Bushel, M. G.; Swager, T. M. *Angew. Chem. Int. Ed.* **2004**, *43*, 3700.
(7) Barbarella, G.; Melucci, M.; Sotgiu, G. *Adv. Mater.* **2005**, *17*, 1581.
(8) Guerrero, D. J.; Ren, X.; Ferraris, J. P. *Chem. Mater.* **1994**, *6*, 1437.
(9) Andersson, M. R.; Berggren, M.; Inganas, O.; Gustafsson, G.; Gustafsson-Carlberg, J. C.; Selse, D.; Hjerthberg, T.; Wennerstrom, O. *Macromolecules* **1995**, *28*, 7525.
(10) Weissleder, R.; Tung, C. H.; Mahmood, U.; Bogdanov, A. *Nat. Biotechnol* **1999**, *17*, 375.
(11) Weissleder, R. *Nat. Biotechnol.* **2001**, *19*, 316.
(12) Ballou, B.; Ernst, L. A.; Waggoner, A. S. *Curr. Med. Chem* **2005**, *12*, 795.
(13) Nakazumi, H.; Ohta, T.; Etoh, H.; Uno, T.; Colyer, C.; Hyodo, Y.; Yagi, S. *Synth. Met.* **2005**, *153*, 33.
(14) Loudet, A.; Burgess, K. *Chem. Rev.* **2007**, *107*, 4891.
(15) Umezawa, K.; Nakamura, Y.; Makino, H.; Citterio, D.; Suzuki, K. *J. Am. Chem. Soc.* **2008**, *130*, 1550.
(16) Kolb, H. C.; Finn, M. G.; Sharpless, K. B. *Angew. Chem. Int. Ed.* **2001**, *40*, 2004.
(17) Gil, M. V.; Arevallo, M. J.; Lopez. O. *Synthesis* **2007**, *11*, 1589.
(18) Rostovtsev, V. V.; Green, L. G.; Fokin, V. V.; Sharpless, K. B. *Angew. Chem. Int. Ed.* **2002**, *41*, 2596
(19) Tornoe, C. W.; Christiensen, C.; Meldal, M. *J. Org. Chem.* **2002**, *67*, 3057.
(20) Perez-Balderas, F.; Ortega-Munoz, M.; Morales-Sanfrutos, J.; Jerandez-Mateo, F.; Calvo-Flores, F. G. *Org. Lett.* **2003**, *5*, 1951.
(21) Thibault, R. J.; Takizawa, K.; Lowenheilm, P.; Helms, B.; Mynar, J.; Frechet, J. M. J.; Hawker, C. J. *J. Am. Chem. Soc.* **2006**, *128*, 12084.
(22) van Steenis, D. J. C.; David, O. R. P.; van Strijdonck, G. P. F.; van Maarseveen, J. H.; Reek, J. N. H. *Chem. Commun.* **2005**, 4333.
(23) Moses, J. E.; Moorehouse, A. D. *Chem. Soc. Rev.* **2007**, *36*, 1249.
(24) Binder, W.; Sachsenhofer, R. *Macromol. Rapid. Commun.* **2007**, *28*, 15.
(25) Leland, J. K.; Powell, M. J. *J. Electroanal. Chem.* **1991**, *318*, 91.

(26) Bard, A.; Debad, J. D.; Leland, J. K.; Sigal, G. B.; Wilbur, J. L.; Wohlstadter, J. N. *Encyclopedia of Analytical Chemistry* **2000**, 9842.
(27) Richter, M. M. *Chem. Rev.* **2004**, *104*, 3003.
(28) Yang, X.; Jiang, X.; Zhao, C.; Chen, R.; Qin, P.; Sun, L. *Tetrahedron Lett.* **2006**, *47*, 4961.

2.0 Experimental Details

2.1 General Considerations

Dry DMF (99.8%) in a Sure Seal bottle was purchased from Aldrich and stored in an N_2-filled glove box. Other reagents, 9, 10-diphenylanthracene (DPA), benzoyl peroxide (BPO) and sulfuric acid were purchased from Aldrich and used without purification. The supporting electrolyte, tetra-*n*-butylammonium perchlorate (TBAP) was purchased from Alfa Aesar (Electrochemical grade) and used without purification. A suspension of 500Å alumina in water was used along with a polishing pad microcloth purchased from Buehler Ltd.

UV-vis absorbance spectra were recorded on a Varian Cary 50 spectrophotometer over a range of 230 – 800 nm. The photoluminescence experiments were performed on a Fluorolog (QM-7/2005) instrument with a slit width of 0.5 nm. All solutions were diluted to a concentration of 1 μM using CH_2Cl_2 or DMF and analyzed in a quartz cuvette. High-resolution mass spectrometry data were collected by Mr. Doug Harisine using a Finnigan MAT 8400 instrument. Melting points were obtained using a Fisher-John melting point apparatus.

NMR spectra were recorded using a Varian Mercury 400 spectrometer (400.089 MHz for ^1H and 100.613 for ^{13}C) or a Varian Inova spectrometer (399.762 MHz for ^1H and 100.520 MHz for ^{13}C) at 293 K in DMSO-d_6 unless other wise indicated using residual solvent proton (relative to external $SiMe_4$ = δ 0.00) or solvent carbon (relative external $SiMe_4$ = δ 77.0) as internal reference. Downfield shifts were taken as positive. All coupling constants are given in Hz; s = singlet, d = doublet, t = triplet, m = multiplet, p = psudo. ^1H NMR data are correlated with the structure shown in each section.

2.2 ECL(electrochemiluminescence)/Pulsing:

Electrochemical experiments were carried out in a photochemical cell with a flat Pyrex window at the bottom for detection of light generated from the working electrode and was fitted with a Teflon cap. These experiments were conducted using 2 mm platinum disc inlaid in a glass tube as the working electrode, a coiled Pt wire as the counter electrode and a Ag wire as the quasi reference electrode. After each experiment, the working electrode was polished using a 0.5 μM solution of alumina on a felt pad and then electrochemically polished using a 0.1 M aqueous solution of H_2SO_4 by scanning many times between 1.3 and -0.5 V. The electrodes and cell were then dried at 85°C for 30 min and left to cool to r.t. over 3h.

2.2.2 General Experimental details for ECL/pulsing:

All solutions for ECL and pulsing experiments were prepared in a drybox using anhydrous solvent in an airtight vessel equipped with a Teflon cap through which the electrodes were inserted. Solutions were made from 2 mg of compound and 3 mL of DMF; the supporting electrolyte was 0.1 M TBAP. For systems containing coreactant, 3.6 mg of BPO was also added. After each experiment, the potentials obtained were calibrated using ferrocene as an internal standard. ECL-voltage curves were obtained using the Electrochemical Analyzer (CHI610a, CH instruments) coupled with a photomultiplier tube (PMT, R928, Hamamatsu, Japan) held at 750 V with a high voltage power supply. The ECL generated at the working electrode was collected by the PMT under the flat Pyrex window at the bottom of the cell. The photocurrent from the PMT

was transformed into a voltage signal by an electrometer (Model 6517, Keithley, Cleveland, OH). This signal, the potential and current signals from the electrochemical work station was sent through a DAQ board (DAQ 6052E, National Instruments, Austin TX) to the computer where the entire data acquisition system was controlled by a homemade lab VIEW (National Instruments) program. Also, ECL was generated with a potentiostat (Model AFCBPI, Pine Instrument Co) connected to an EG&G PAR 175 Universal Programmer. These instruments were used to pulse the potential through the system. The potential, current and ECL signals were recorded at the same time with the above computer acquisition system. The electrochemical potential was calibrated at the end of each ECL experiment by the addition of ferrocene as an internal standard (Fc^+/Fc = 0.400 V vs SHE).[1] ECL quantum yields are calculated relative to DPA (Φ_{ECL} = 10 %).[2]

The ECL spectra was collected using a spectrometer with a CCD (charge coupled device) camera (Andor Technology, Model DV420-BV). The camera was cooled to -55 °C and the accumulation times were varied accordingly. The intensity was recorded by Andor Technology program.

2.2.3 Cyclic Voltammetry

These experiments were conducted using 2 mm platinum disc inlaid in a glass tube as the working electrode, a coiled Pt wire as the counter electrode and Ag wire as the reference. The cyclic voltammograms were recorded on a CH instrument (Austin Texas) model 610A Electrochemical Work station. Solutions for the voltammograms were made up of 3 mL of DMF, 2 mg of compound and 0.1M of TBAP electrolyte. These

experiments were carried out by scanning to the positive and then negative potentials at a scan rate of 0.1 Vs^{-1}. Ferrocene was used as an internal standard and added by hand after the ECL, pulsing and the ECL spectra had been collected, however it is not shown on the cyclic voltammograms. All potentials are reported vs. Ag/Ag^{+} and the y axes of the cyclic voltammograms are uncorrected for the internal standard used.

2.3 Calculations of Quantum Yields of PL and ECL

Calculation of quantum yields for thiophene photoluminescence (PL): The quantum yield (Φ) of the thiophene PL was found by comparing the integrated photoluminescence intensities and the absorbance values of the thiophene sample with the reference diphenylanthracene (DPA). The quantum yield was calculated using Equation 2.1.

$$\phi = 100 \times \left(\frac{\int_{a}^{b} PL d\lambda}{\int_{c}^{d} Ab d\lambda} \right)_{x} \Big/ \left(\frac{\int_{a}^{b} PL d\lambda}{\int_{c}^{d} Ab d\lambda} \right)_{st}$$

Equation 2.1: Equation used to calculate the photoluminescence quantum efficiency.

Where Φ is the quantum efficiency (%) relative to the reference, PL is the photoluminescence intensity, Ab is the absorbance value, St is the standard and X is the sample

Calculations of quantum yields of thiophene ECL: The quantum yield of the thiophene ECL was found by comparing the integrated ECL intensities and the current values (charge) of the thiophene sample with the reference DPA. The quantum yield was calculated using Equation 2.2:

$$\phi = 100 \times \left(\frac{\int_a^b ECLdt}{\int_a^b Currentdt} \right)_x \Big/ \left(\frac{\int_a^b ECLdt}{\int_a^b Currentdt} \right)_{st}$$

Equation 2.2: Equation used to calculate the ECL quantum efficiency

Where Φ is the quantum efficiency (%) relative to the reference DPA, ECL is the ECL intensity, Current the electrochemical current value, st is the standard t is time and x is the sample.

2.4 Synthesis of precursors to click reactions

The following compounds were made according to published procedures: tosylazide,[3] 3-azidothiophene,[4] 2-ethynylthiophene,[5] 5,5'dibromo-2,2'bithiophene,[6] 4,4',5,5'-tetrabromo-2,2'bithiophene,[6] 2,3-dibromothiophene,[7] 2,3,5-tribromothiophene,[8] 2,4-dibromothiophene,[9] 2-thienylmagnesium bromide,[10] 4-bromo-2,2'bithiophene,[10] 4-azido-2,2'bithiophene,[4] 1,3,5-triethynylbenzene,[11] 1-bromo-3,5-bis(2'-thienyl)benzene,[12] $PdCl_2(dppf)$,[12] $Pd(PPh_3)_4$,[12] 1,3,5-tri(2'-thienyl)benzene.[12]

2.5 Click reactions

2.5.1 1,4-disubstituted 1,2,3-triazoles (Series A and B)

The title compounds were made according to Scheme 2.1.

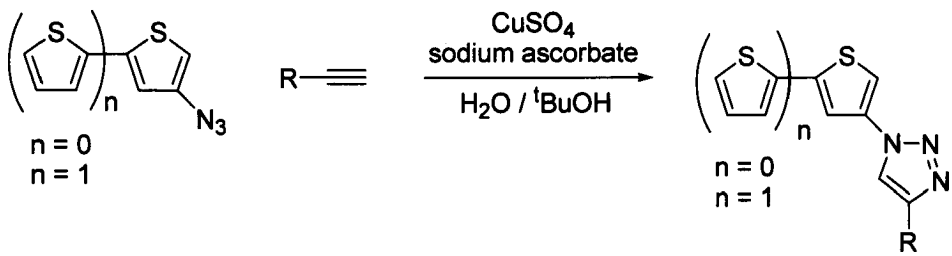

Scheme 2.1: General reaction scheme for the synthesis of 1,4 disubstituted triazoles.

3-azidothiophene or 4-azido-2,2'-bithiophene (0.50 mmol) and arylacetylene (0.50 mmol) were suspended in a 1:1 mixture of H_2O and t-BuOH (3.0 mL total) in a 30 mL thick walled glass tube sealed with a Teflon screw top. To this, sodium ascorbate (0.08 mmol) and $CuSO_4$ (0.25 mmol) were added. The mixture was heated on an oil bath to 80 °C for 90 min, and then allowed to cool to r.t. The product precipitated from solution as a brown solid. The mixture was diluted with H_2O (10 mL) and filtered. The solid residue was washed several times with H_2O (10 mL) and 5 % by vol. HCl (5 mL) and finally with Et_2O (10 mL).

2.5.2 4-Phenyl-1-thiophen-3-yl-1*H*-[1,2,3]triazole, 1

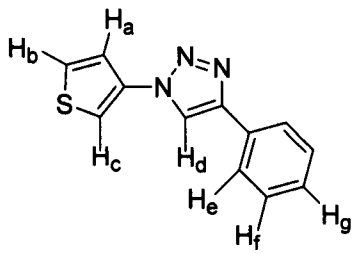

^{1}H NMR ($CDCl_3$): δ 9.97 (t, 1H, H_g, $^3J_{HH}$ = 7.6), 10.05 (pt, 2H, H_f), 10.08 (m, 2H, H_a/H_b,), 10.37 (dd, 2H, H_c, $^4J_{HH}$ = 3.2, $^4J_{HH}$ = 1.6), 10.47 (d, 1H, H_e,$^3J_{HH}$ = 8.4), 11.69 (s, 1H, H_d). $^{13}C\{^1H\}$ NMR δ: 113.86, 117.43, 120.66, 125.83, 126.01, 127.32, 128.98, 129.24, 129.72, 130.79, 136.04, 138.80, 147.55. HRMS calcd. for $C_{12}H_9N_3S$: 227.0517; found: 227.0509. m.p. 169 – 170 °C. Yield: 0.045 g (60 %).

2.5.3 4-(4-Fluoro-phenyl)-1-thiphen-3-yl-1*H*-[1,2,3]triazole, 2

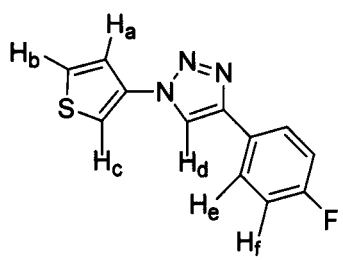

^{1}H NMR ($CDCl_3$): δ 7.15 (d, 2H, H_e, $^3J_{HH}$ = 9.2), 7.50 (m, 2H, H_a and H_b,), 7.61, (dd, 2H, H_c, $^3J_{HH}$ = 2.8, $^4J_{HH}$ = 1.6), 7.87 (dd, 2H, H_f, $^3J_{HH}$ = 8.4, $^3J_{HF}$ = 4.8), 8.1 (s, 1H, H_d). $^{13}C\{^1H\}$ NMR δ: 115.43, 116.55, 116.76, 120.36, 121.34, 127.45, 128.01, 128.09,

129.21, 136.07, 146.64. HRMS calcd. for $C_{12}H_8FN_3S$: 245.0423; found: 245.0413. m.p. 194 – 196 °C. Yield: 0.108 g (88 %).

2.5.4 Dimethyl-[4-(1-thiophen-3-yl-1*H*-[1,2,3]triazole-4-yl)-phenyl]-amine, 3

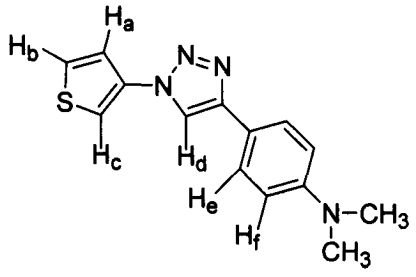

^{1}H NMR: δ 3.05 (s, 6H, *CH*$_3$), 7.52 (br, s, 2H), 7.61 (dd, 1H, H_c, $^4J_{HH}$ = 1.2, $^3J_{HH}$ = 5.2), 7.77 (dd, 1H, H_a, $^4J_{HH}$ = 3.2, ^3J = 5.2), 7.91 (d, 2H, H_e/H_f, $^3J_{HH}$ = 8.4), 8.0 (dd, 1H, H_b, $^4J_{HH}$ = 1.2, $^3J_{HH}$= 2.8), 9.06 (s, 1H, H_d). $^{13}C\{^1H\}$ NMR δ: 113.03, 114.81, 118.57, 118.65, 121.30, 126.94, 129.03, 136.36, 148.18, 150.94. HRMS calcd. for $C_{14}H_{14}N_4S$: 270.0939; found: 270.0933. m.p. 180 – 183 °C. Yield: 0.096 g (71 %).

2.5.5 4-Thiophen-2-yl-1-thiophen-3-yl-1H-[1,2,3]triazole, 4

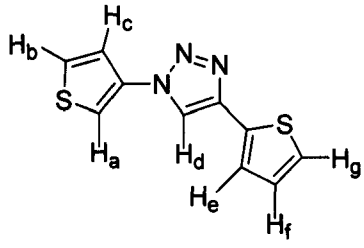

^{1}H NMR: δ 7.16 (t, 1H, H_f, , $^3J_{HH}$ = 4.4), 7.47 (d, 1H, H_b, $^3J_{HH}$ = 2.8), 7.58 (d, 1H, H_e/H_g, CH, $^3J_{HH}$ = 5.2), 7.65 (d, 1H, H_e/H_g, $^3J_{HH}$ = 5.6), 7.81 (dd, 1H, H_c, $^3J_{HH}$ = 4.0, $^4J_{HH}$ = 3.2),

8.04 (d, 1H, H_a, $^3J_{HH}$ = 1.6), 9.10 (s, 1H, H_d). $^{13}C\{^1H\}$ NMR δ: 115.58, 119.89, 121.26, 125.60, 128,70, 129.21, 132.94, 135.90, 142.90. HRMS calcd. for $C_{10}H_7N_3S_2$: 233.0081; found: 233.0079. m.p. 151 – 152 °C. Yield: 0.084 g (72 %).

2.5.6 4-(4-Methoxy-phenyl)-1-thiophen-3-yl-1*H*-[1,2,3]triazole, 5

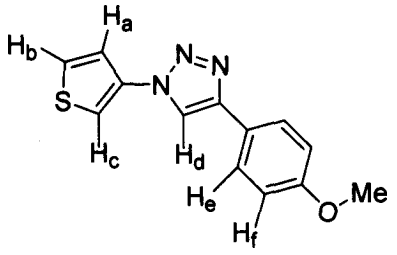

^1H NMR: δ 3.78 (s, 3H, *CH*$_3$), 7.04 (d, 2H, H_f, $^3J_{HH}$ = 8.8), 7.64 (dd, 1H, H_c, $^3J_{HH}$ = 5.2, $^4J_{HH}$ = 1.6), 7.81 (m, 3H, H_e and H_a), 8.00 (dd, 1H, H_b, $^3J_{HH}$ = 3.2, $^4J_{HH}$ = 1.2), 9.08 (s, 1H). $^{13}C\{^1H\}$ NMR δ: 55.87, 115.11, 119.70, 121.33, 123.40, 127.39, 129.13, 136.22, 147.45, 159.97. HRMS calcd. For $C_{13}H_{11}N_3OS$: 257.0623; found: 257.0613. m.p. 152 – 153 °C. Yield: 0.107 g (83 %).

2.6.1 1-[2,2']Bithiophenyl-4-yl-4-phenyl-1H-[1,2,3]triazole, 6

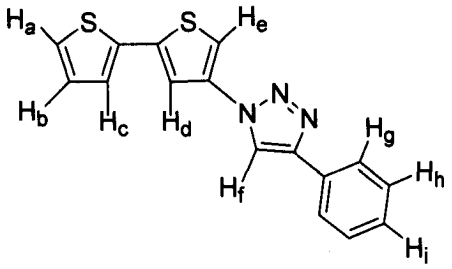

^1H NMR δ: 6.31 (dd, 1H, H_c, $^3J_{HH}$ = 3.6, $^4J_{HH}$ = 0.8), 6.54 (pt, 1H, H_h), 6.62 (d, 1H, H_a/H_b, $^3J_{HH}$ = 3.6), 6.65 (t, 2H, H_i, $^3J_{HH}$ = 7.6), 6.77 (d, 1H, H_a/H_b, $^3J_{HH}$ = 4.8), 7.03 (d,

1H, H_d/H_e, $^4J_{HH}$ = 1.2), 7.07 (d, 2H, H_g, $^3J_{HH}$ = 7.6), 7.14 (d, 1H, H_d/H_e, $^4J_{HH}$ = 1.2), 8.21 (s, 1H, H_f). $^{13}C\{^1H\}$ NMR (DMSO-d_6) δ: 113.58, 117.41, 120.64, 125.81, 125.98, 127.31, 128.96, 129.21, 129.69, 130.77, 136.01, 138.78, 147.52. HRMS calcd. for $C_{16}H_{11}N_3S_2$: 309.0394; found: 309.0385. m.p. 158 – 161°C . Yield: 0.113 g (73%).

2.6.2 1-[2,2']Bithiophenyl-4-yl-4-(4-fluoro-phenyl)-1*H*-[1,2,3]triazole, 7

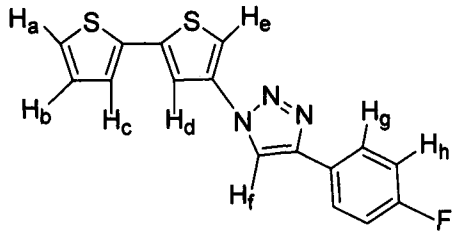

^1H NMR: δ 7.11 (dd, 1H, H_b, $^3J_{HH}$ = 4.8, $^3J_{HH}$ = 3.6), 7.31 (t, 2H, H_g, C*H*, $^3J_{HH}$ = 9.2), 7.42 (dd, 1H, H_a/H_c $^4J_{HH}$ = 0.8, $^3J_{HH}$ = 5.2), 7.57 (dd, 1H, H_a/H_c, $^4J_{HH}$ = 0.8, $^3J_{HH}$ = 5.2), 7.81 (d, 1H, H_d/H_e, $^4J_{HH}$ = 1.2), 7.91 (m, 3H, H_d/H_e, H_h), 9.19 (s, 1H, H_f). $^{13}C\{^1H\}$ NMR δ: 113.92, 116.57, 116.79, 117.39, 120.59, 125.82, 127.32, 128.00, 129.22, 135.96, 138.81, 146.65, 161.46, 163.90. HRMS calcd. for $C_{16}H_{10}FN_3S_2$: 327.0300; found: 327.0297. m.p. 182 – 184 °C. Yield: 0.138 g (84 %).

2.6.3 [4-(1-[2,2']Bithiopheny-4-yl-1*H*-[1,2,3]triazole-4-yl)-phenyl]-dimethyl-amine, 8

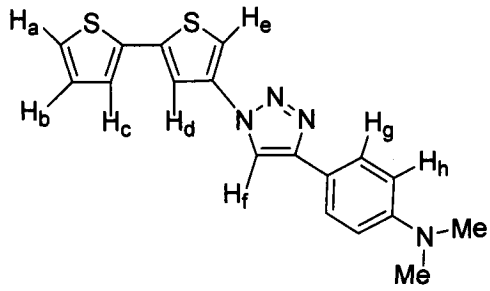

^{1}H NMR: δ 2.97 (s, 6H, CH_3), 6.88 (br s, 2H, H_h), 7.15 (dd, 1H, H_c, $^3J_{HH}$ = 3.2, $^4J_{HH}$ = 2.4), 7.47 (dd, 1H, H_a/H_b, $^3J_{HH}$ = 2.4, $^4J_{HH}$ = 0.8), 7.62 (dd, 1H, H_a/H_b, $^3J_{HH}$ = 3.6, $^4J_{HH}$ = 0.8), 7.75 (d, 2H, H_g, $^3J_{HH}$ = 6.0), 7.86 (d, 1H, H_d/H_e , $^4J_{HH}$ = 0.8), 7.94 (d, 1H, H_d/H_e, $^4J_{HH}$ = 0.8), 9.05 (s, 1H, H_f). ^{13}C{^{1}H} NMR (DMSO-d_6): δ 113.03, 113.32, 117.39, 118.46, 118.60, 125.78, 126.94, 127.26, 129.22, 136.11, 136.27, 138.67, 150.98. HRMS calcd. for $C_{18}H_{16}N_4S_2$: 352.0816; found: 352.0828. m.p. 198 – 200 °C. Yield: 0.125 g (71 %).

2.6.4 1-[2,2']Bithiophenyl-4-yl-4-thiophen-2-yl-1*H*-[1,2,3]triazole, 9

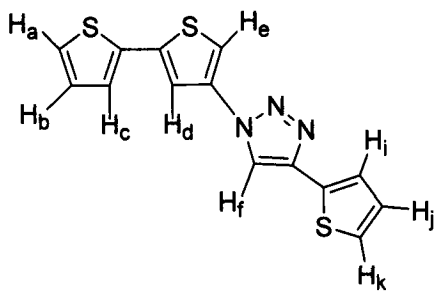

^{1}H NMR: δ 7.11 (dd, 1H, H_j/H_b, $^3J_{HH}$ = 4.0, $^3J_{HH}$ = 5.2), 7.14 (dd, 1H, H_j/H_b, $^3J_{HH}$ = 3.6, $^3J_{HH}$ = 4.8), 7.42 (dd, 1H, H_i/H_k, $^4J_{HH}$ ≒ 0.8, $^3J_{HH}$ = 3.6), 7.46 (dd, 1H, H_i/H_k, $^4J_{HH}$ = 1.2, $^3J_{HH}$ = 3.6), 7.56 (dd, 2H, H_a and H_c, $^4J_{HH}$ = 1.2, $^3J_{HH}$ = 6.0), 7.82 (d, 1H, H_d/H_e, $^4J_{HH}$ =

1.6), 7.94 (d, 1H, H_d/H_e, $^4J_{HH}$ = 1.6), 9.11 (s, 1H, H_f). $^{13}C\{^1H\}$ NMR: δ 114.05, 117.42, 119.83, 125.28, 125.85, 126.66, 127.33, 128.73, 129.22, 132.85, 135.80, 135.99, 138.80, 142.92. HRMS calcd. for $C_{14}H_9N_3S_3$: 314.9959; found: 314.9953. m.p. 160 – 162 °C. Yield: 0.113 g (72 %).

2.6.5 1-[2,2']Bithiophenyl-4-yl-4-(4-methoxy-phenyl)-1H-[1,2,3]triazole, 10

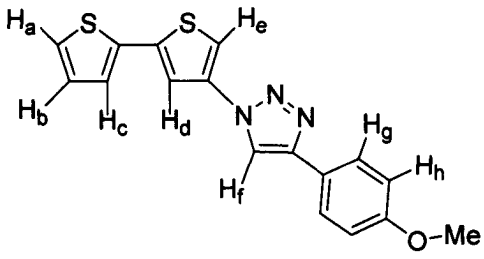

^1H NMR: δ 3.78 (s, 3H, CH_3), 7.04 (d, 2*H*, H_g, ^3J = 9.2), 7.13 (dd, 1*H*, H_b, $^3J_{HH}$ = 5.2, $^3J_{HH}$ = 3.6), 7.44 (dd, 1*H*, H_a/H_c, $^3J_{HH}$ = 3.6, $^4J_{HH}$ = 1.2), 7.60 (dd, 1*H*, H_a/H_c, $^3J_{HH}$ = 5.2, $^4J_{HH}$ = 1.2), 7.82 (d, 2*H*, H_h, $^3J_{HH}$ = 8.8), 7.84 (d, 1*H*, H_e/H_d, $^4J_{HH}$ = 1.6), 7.95 (d, 1*H*, H_e/H_d, $^4J_{HH}$ = 1.6), 9.13 (s, 1H, H_f). $^{13}C\{^1H\}$ NMR: δ 55.88, 113.64, 115.14, 117.41, 119.65, 123.32, 125.81, 127.39, 129.23, 136.13, 138.75, 147.49, 160.01. HRMS calcd. for $C_{17}H_{13}N_3OS_2$: 339.4346; found: 339.05135. m.p. 202 – 204 °C. Yield: 0.169 g (98 %).

2.7 Synthesis of 1-azido-3,5-di(2'-thienyl)benzene

This compound was made in manner similar to 3-azidothiophene and 4-azido-2,2'-bithiophene[2] (Scheme 2.2).

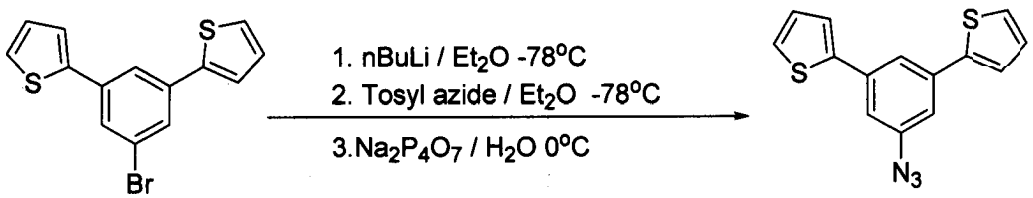

Scheme 2.2: Reaction scheme for the synthesis of 1-azido-3,5-Di(2'-thienyl)benzene.

Under an Ar atmosphere, a solution of 1-bromo-3,5-di(2'-thienyl)benzene (2.7g, 8.4mmol) in dry Et_2O (100 mL) was cooled to -78 °C in a acetone/dry ice bath and a 1.6 M solution of n-BuLi in hexanes (5.2 mL, 8.4 mmol) was added dropwise. After stirring for 1 h at this temperature, a solution of tosyl azide (1.65 g, 8.4mmol) in dry Et_2O (20 mL) was added dropwise to yield a yellow precipitate. The reaction mixture was stirred at -78 °C for 5 h. The mixture was then poured directly into a solution of $Na_2P_4O_7$ (3.74 g, 8.4 mmol) in water (100 mL) and stirred for 12 h at r.t. The aqueous layer was discarded and the organic layer was washed with brine, dried over $MgSO_4$ and reduced to a dark red liquid by rotary evaporation. The desired product, a yellow liquid, was obtained by flash column chromatography using hexanes as eluent ($R_f = 0.33$).

1-azido-3,5-Di(2'-thienyl)benzene

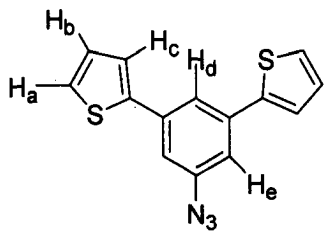

^{1}H NMR ($CDCl_3$): δ 7.11 (dd, 1H, H_b, $^3J_{HH}$ = 3.6, $^3J_{HH}$ = 4.8), 7.15 (d, 2H, H_e, $^4J_{HH}$ = 1.6), 7.34 (dd, 1H, H_a/H_c, $^3J_{HH}$ = 5.2, $^4J_{HH}$ = 1.6), 7.37 (dd, 1H, H_a/H_c, $^3J_{HH}$ = 3.6, $^4J_{HH}$ = 1.2), 7.59 (t, 1H, H_d, $^4J_{HH}$ = 1.6). HRMS calcd for $C_{14}H_9N_3S_2$: 283.02379; found 283.02381. m.p. 55 – 57 °C. Yield: 0.80 g (30 %)

2.7.1 Synthesis of 1-(3,5-di-thiophen-2-yl-phenyl) substituted triazoles (Series C)

These compounds were made according to Scheme 2.3

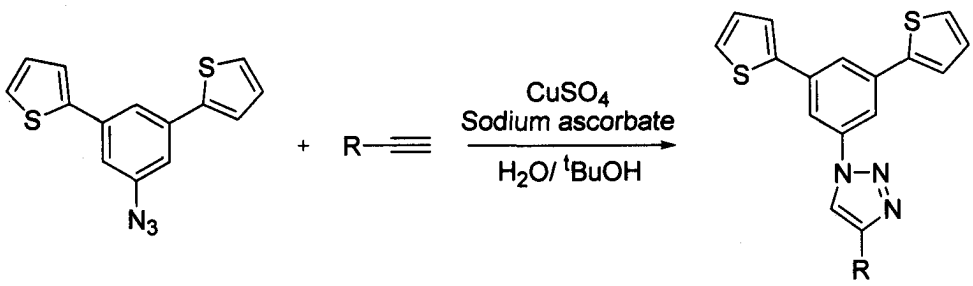

Scheme 2.3: General reaction scheme for the synthesis of the 1-(3,5-Di-thiophen-2-yl-phenyl) substituted triazoles.

1-azido-3,5-di(2'-thienyl)benzene (0.50 mmol) and the appropriate arylacetylene (0.50 mmol) were suspended in a 1:1 mixture of H_2O and t-BuOH (3.0 mL total) in a 30 mL thick-walled glass tube sealed with a Teflon screw top. To this, sodium ascorbate (0.08 mmol) and $CuSO_4$ (0.25 mmol) were added. The mixture was heated on an oil bath to 80 °C for 90 min, then allowed to cool to r.t. The product precipitated from solution as

an orange solid. The mixture was diluted with H_2O (10 mL) and filtered. The solid residue was washed several times with H_2O (10 mL) and 5% vol. HCl (5 mL) and finally with Et_2O (10 mL).

2.7.2 1-(3,5-Di-thiophen-2-yl-phenyl)-4-phenyl-1H-[1,2,3]triazole, 11

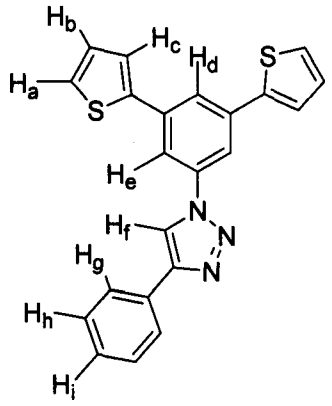

^{1}H NMR: δ 7.23 (dd, 2H, H_b, $^3J_{HH}$ = 3.6), 7.39 (t, 1H, H_i, $^3J_{HH}$ = 7.6), 7.51 (t, 2H, H_h, $^3J_{HH}$ = 7.6), 7.69 (dd, 2H, H_a/H_c, $^3J_{HH}$ = 5.2, $^4J_{HH}$ = 0.8), 7.81 (dd, 2H, H_a/H_c, $^3J_{HH}$ = 3.2, $^4J_{HH}$ = 0.4), 7.95 (s, 1H, H_d), 7.97 (d, 2H, H_e, $^4J_{HH}$ = 1.2), 8.13 (d, 2H, H_g, $^3J_{HH}$ = 1.2), 9.50 (s, 1H, H_f). $^{13}C\{^1H\}$ NMR: δ 116.04, 120.66, 122.52, 126.06, 126.38, 127.85, 129.02, 129.41, 129.71, 130.87, 136.97, 138.62, 142.07, 148.09. HRMS calcd. for $C_{22}H_{15}N_3S_2$: 385.0707; found: 387.0708. m.p. 200 – 202 °C. Yield: 0.095 g (70 %).

2.7.3 1-(3,5-di-thiophen-2-yl-phenyl)-4-(4-fluoro-phenyl)-1H-[1,2,3]triazole, 12

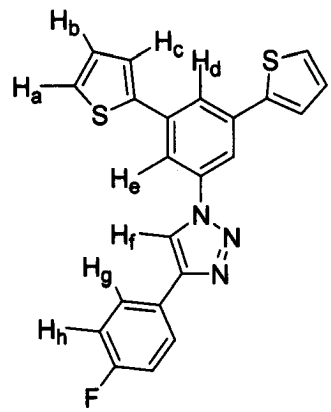

^{1}H NMR : δ 7.21 (dd, 2H, H_b, $^3J_{HH}$ = 3.6, $^3J_{HH}$ = 4.8), 7.35 (t, 2H, H_h, $^3J_{HH}$ = 8.8), 7.68 (d, 2H, H_g, $^3J_{HH}$ = 4.8), 7.79 (d, 2H, H_a/H_c, $^3J_{HH}$ = 3.2), 7.98 (m, 3H, H_a/H_c and H_d), 8.09 (d, 2H, H_e, $^3J_{HH}$ = 1.6), 9.47 (s, 1H, H_f). $^{13}C\{^1H\}$ NMR : δ 116.04, 116.58, 116.80, 120.59, 122.55, 126.39, 127.87, 128.05, 128.12, 129.41, 136.97, 138.57, 142.04, 147.21. HRMS calcd for $C_{22}H_{14}FN_3S_2$ 403.0613; found 403.0613. m.p. 178 – 181 °C. Yield: 0.136 g (70 %)

2.7.4 {4-[1-(3,5-di-thiophen-2-yl-phenyl)-1H[1,2,3]triazole-4-yl]-phenyl}-dimethylamine, 13

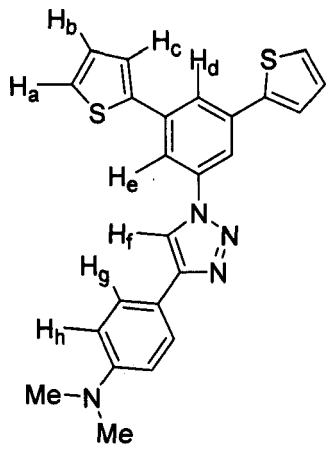

^{1}H NMR: δ 2.64 (s, 6H, CH_3), 6.84 (d, 2H, H_b, $^3J_{HH}$ = 8.8), 7.24 (dd, 2H, H_a, $^3J_{HH}$ = 5.2, $^4J_{HH}$ = 4.0), 7.70 (d, 2H, H_e, $^4J_{HH}$ = 4.4), 7.78 (m, 4H, H_g/H_h), 7.96 (s, 1H, H_d), 8.12 (d, 2H, H_c, $^3J_{HH}$ = 1.6), 9.28 (s, 1H, H_f). ^{13}C{^{1}H} NMR: δ 31.97, 113.01, 115.85, 118.50, 122.29, 126.33, 126.99, 127.79, 129.40, 136.91, 138.75, 142.14, 148.80, 150.99. HRMS calcd. for $C_{24}H_{20}N_4S_2$: 428.1129; found: 428.1123. m.p. 159 – 165 °C. Yield: 0.155 g (95 %)

2.7.5 1-(3,5-Di-thiophen-2-yl-phenyl)-4-thiophen-2-yl-1H-[1,2,3]triazole, 14

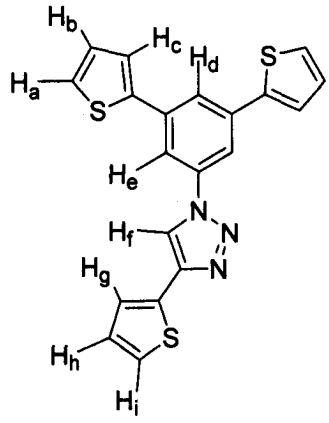

^{1}H NMR : δ 7.18 (m, 3H, H_h/H_b), 7.50 (dd, 1H, H_i/H_j, $^3J_{HH}$ = 3.6, $^4J_{HH}$ = 1.2), 7.57 (dd, 1H, H_i/H_j, $^3J_{HH}$ = 5.2, $^4J_{HH}$ =1.2), 7.65 (dd, 2H, H_a/H_c, $^3J_{HH}$ = 4.8, $^4J_{HH}$ = 0.8), 7.77 (dd, 2H, H_a/H_c, $^3J_{HH}$ = 3.2, $^4J_{HH}$ = 0.8), 7.39 (t, 1H, H_d, $^4J_{HH}$ = 1.6), 8.07 (d, 2H, H_e, $^4J_{HH}$ = 1.6), 9.36 (s, 1H, H_e). $^{13}C\{^1H\}$ NMR: δ 116.11, 119.90, 122.62, 125.36, 126.41, 126.71, 127.85, 128.73, 129.40, 132.95, 136.96, 138.46, 142.02, 143.48. HRMS calcd for $C_{20}H_{13}N_3S_3$: 391.0272; found: 391.0281. m.p. 148 – 150 °C. Yield: 0.13 g (94 %).

2.7.6 Synthesis of 1-(3,5-Di-thiophen-2-yl-phenyl)-4-(4-methoxy-phenyl)-1H-[1,2,3]triazole, 15

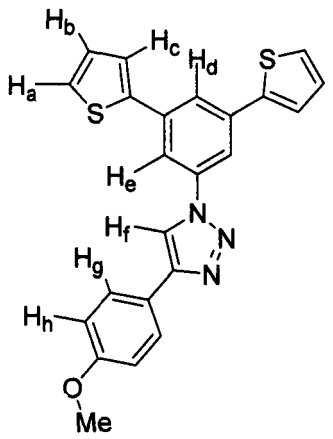

^{1}H NMR : δ 3.79 (s, 3H, CH_3), 7.06 (d, 2H, H_h, $^3J_{HH}$ = 8.8), 7.22 (t, 1H, H_b, $^3J_{HH}$ = 4.0), 7.68 (d, 2H, H_a/H_c, $^3J_{HH}$ = 4.8), 7.79 (d, 2H, H_a/H_c, $^3J_{HH}$ = 3.2), 7.88 (d, 2H, H_g, $^3J_{HH}$ = 8.4), 7.95 (s, 1H, H_d), 8.10 (s, 2H, H_e), 9.37 (s, 1H, H_f). ^{13}C{^{1}H} NMR: δ 55.89, 115.13, 115.94, 119.61, 122.44, 126.36, 127.43, 127.83, 129.41, 136.94, 138.67, 142.10, 148.06, 160.05. HRMS calcd for: $C_{23}H_{17}N_3OS_2$ 415.08130; found: 415.08129. m.p. 165 – 170 °C. Yield 0.107 g (83 %)

2.8 Synthesis of 1,3,5-tri substituted triazole benzenes (Series D)

The title compounds were made according to Scheme 2.4

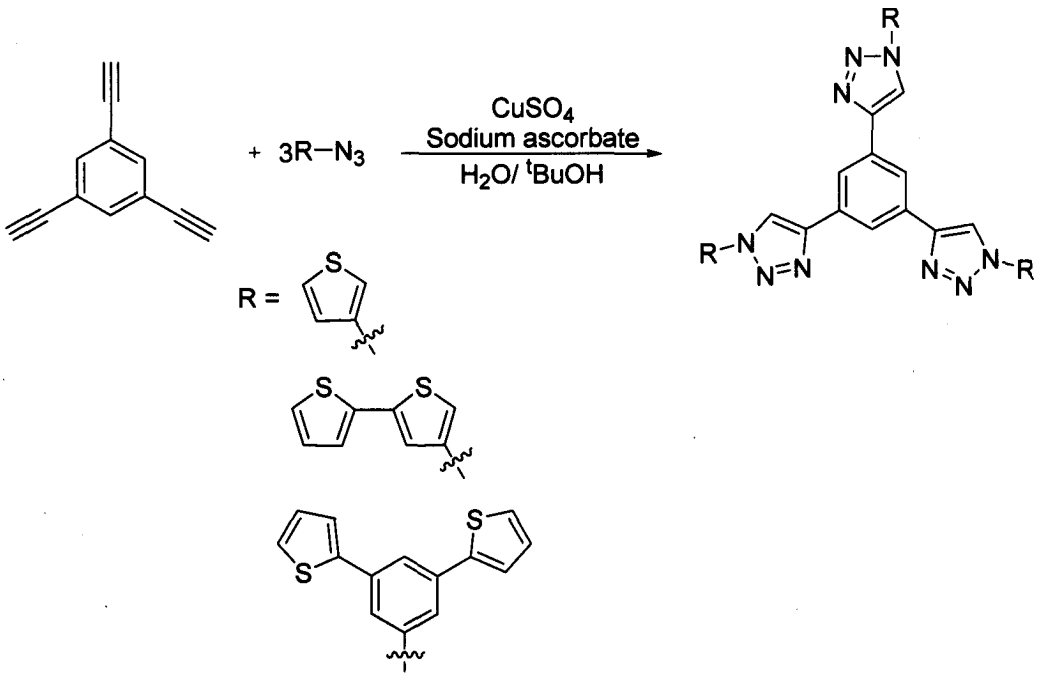

Scheme 2.4: General reaction scheme for the synthesis of 1,3,5-tri substituted triazole benzene.

The appropriate aryl azide (1.50 mmol) and 1,3,5-triethynylbenzene (0.50 mmol) were suspended in a 1:1 mixture of H_2O and t-BuOH (3.0 mL total) in a 30 mL thick walled glass tube sealed with a Teflon screw top. To this, sodium ascorbate (0.08 mmol) and $CuSO_4$ (0.25 mmol) were added. The mixture was heated on an oil bath to 80 °C for 90 min, and then allowed to cool to r.t. The product precipitated from solution. The mixture was diluted with H_2O (10 mL) and filtered. The solid residue was washed several times with H_2O (10 mL) and 5 % vol. HCl (5 mL) and finally with Et_2O (10 mL).

2.8.1 1,3,5-tris(1,- (3,5-di(thiophen-2-yl)phenyl)-1-*H*-1,2,3-triazol-4-yl)benzene, 19

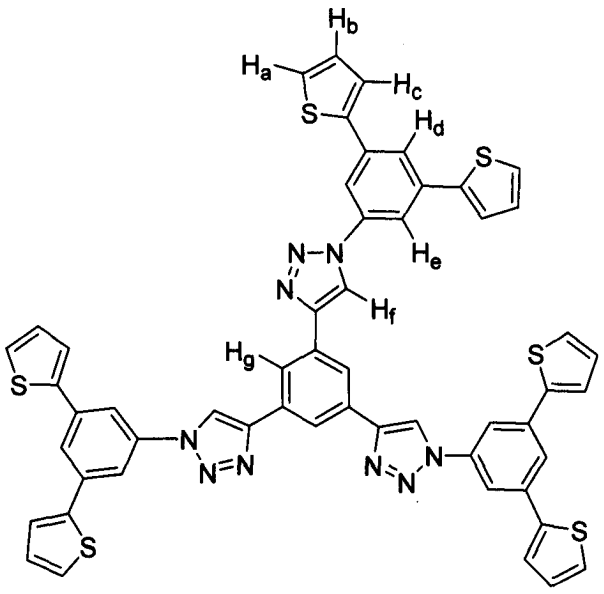

Physical description *e.g.*, yellow solid. ^{1}H NMR: δ 7.23 (dd, 6H, H_b, $^3J_{HH}$ = 4.8, $^3J_{HH}$ = 4.0), 7.70 (d, 6H, H_a/H_c, $^3J_{HH}$ = 5.2), 7.80 (d, 6H, H_a/H_c, $^3J_{HH}$ = 4), 7.93 (s, 3H, H_d/H_g), 8.17 (d, 6H, H_e, $^4J_{HH}$ = 1.2), 8.57 (s, 3H, H_d/H_g), 9.65 (s, 3H, H_f). HRMS calcd. for $C_{54}H_{33}N_9S_6$: 1000.2901; found 1000.1261. m.p. > 300 °C. Yield: 0.24 g (96 %).

2.8.2 1,3,5-tris(1-(2,2'bithiophene-3-yl)-1-*H*-1,2,3-triazol-4-yl)benzene, 20

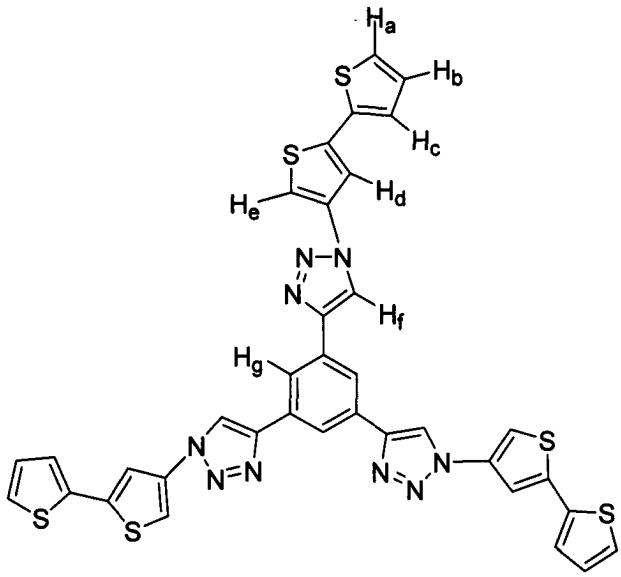

Physical description *e.g.*, brown solid. ^{1}H NMR: δ 7.17 (dd, 3H, H_b, $^{3}J_{HH}$ = 2.0, $^{3}J_{HH}$ = 5.2), 7.49 (d, 3H, H_a/H_c, $^{3}J_{HH}$ = 3.2), 7.63 (d, 3H, H_a/H_c, $^{3}J_{HH}$ = 4.8), 7.95 (s, 3H, H_d/H_e), 8.06 (s, 3H, H_d/H_e), 8.53 (s, 3H, H_g), 9.49 (s, 3H, H_f). ^{13}C{^{1}H} NMR: δ 31.97, 67.61, 109.99, 113.75, 117.31, 121.11, 122.49, 125.76, 127.29, 129.21, 136.09, 138.83. HRMS calcd. for $C_{36}H_{21}N_9S_6$: 772.0022; found 772.0322. m.p. 284 – 286 °C. Yield 0.18 g (46 %).

2.8.3 1,3,5-tris(1-(thiophene-3-yl)-1-*H*-1,2,3-triazol-4-yl)benzene, 21

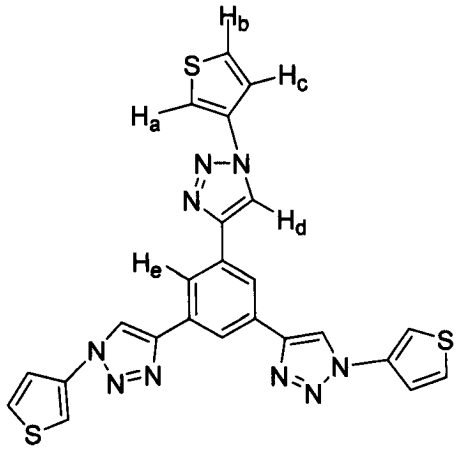

Physical description *e.g.*, brown solid. ^{1}H NMR : δ 7.75 (dd, 3H, H_a, $^{3}J_{HH}$ = 5.2, $^{4}J_{HH}$ = 1.2), 7.86 (dd, 3H, H_c, $^{3}J_{HH}$ = 5.2, $^{4}J_{HH}$ = 3.2), 8.13 (m, 3H, H_b), 8.51 (s, 3H, H_e), 9.44 (s, 3H, H_d). $^{13}C\{^{1}H\}$ NMR: δ 115.44, 121.33, 122.58, 129.23, 132.39, 136.10, 146.95. TOF calcd for $C_{24}H_{15}N_9S_3$: 525.6312; found 526.0691. m.p. 296 – 298 °C. Yield: 0.24 g (91 %).

2.9 Synthesis of 2,5-Bis-(3,5-di-thiophen-2-yl-phenyl)-thiophene, 27

This compound was made by Negishi coupling according to Scheme 2.5. In a 500 mL three neck flask, 1,3,5-tri(2'-thienyl)benzene[12] (0.50 g, 1.5 mmol) was dissolved in 200 mL of THF and cooled to -78°C. A solution of n-BuLi in hexanes (1.6 M, 1 mL) was added dropwise *via* cannula to give a yellow solution. The mixture was stirred at -78 °C for 1.5 h. A solution of anhydrous $ZnCl_2$ (0.41g, 3.1 mmol) in THF (20 mL) was then added at -78°C and stirred for 1h and then allowed to warm to r.t. over 1 h. A solution of 1-bromo-3,5-(2'thienyl)benzene[12] and $Pd(PPh_3)_4$[12] (0.053 g, 0.03 mmol) in dry THF (40 mL) was added to the yellow solution. The mixture was stirred at 50 °C for

94 h. The reaction mixture was quenched with water (50 mL). The organic fraction was isolated and washed with brine, dried over $MgSO_4$ and concentrated. A white crystalline solid was obtained by flash column chromatography (1:9 DCM: hexanes, $R_f = 0.54$)

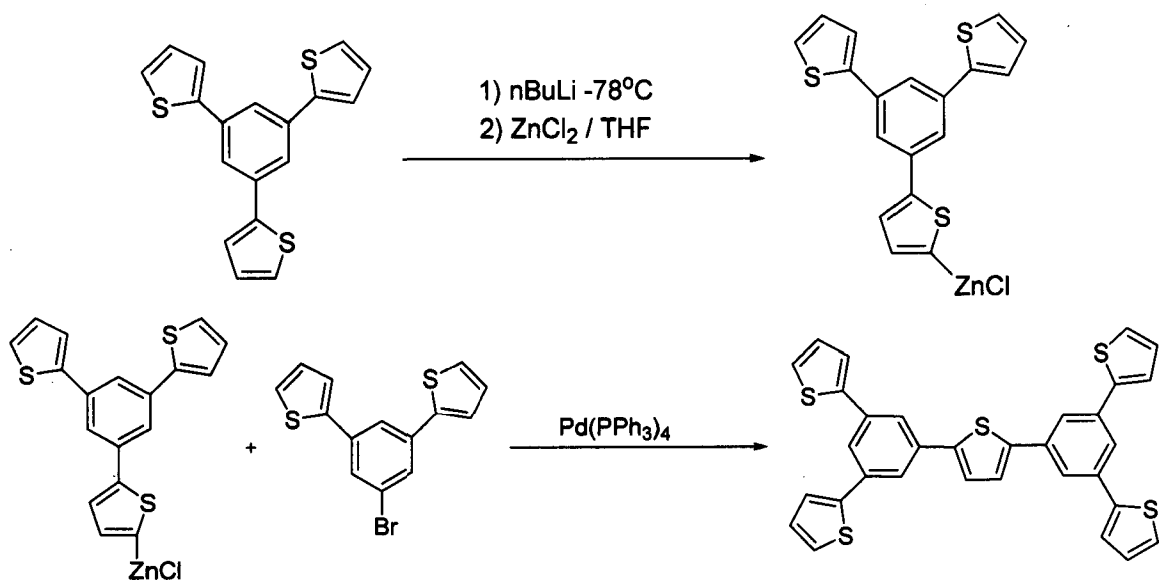

Scheme 2.5: Reaction scheme for the synthesis of 2,5-bis{3,5-di(2-thienyl)phenyl}thiophene

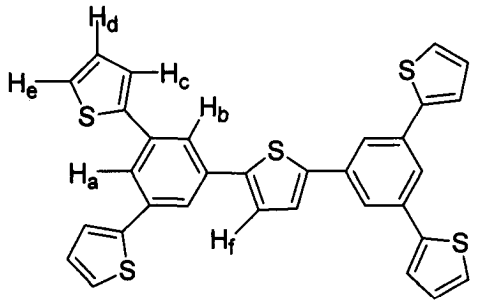

^{1}H NMR ($CDCl_3$): δ 7.14 (dd, 4H, H_e, $^3J_{HH}$ = 5.2, $^4J_{HH}$ = 3.6), 7.35 (dd, 4H, H_c/H_d, $^3J_{HH}$ = 5.2, $^4J_{HH}$ = 1.2), 7.43 (s, 2H, H_f), 7.44 (dd, 4H, H_c/H_d, $^3J_{HH}$ = 4, $^4J_{HH}$ = 1.2), 7.76 (t, 2H, H_a, $^4J_{HH}$ = 1.6), 7.78 (d, 4H, H_b, $^4J_{HH}$ = 1.2). $^{13}C\{^1H\}$ NMR ($CDCl_3$): δ 122.52, 123.05, 124.15, 124.96, 125.66, 128.36, 135.60, 135.96, 143.41, 143.69. HRMS calcd. For $C_{32}H_{20}S_5$: 564.0169; found 564.0152. m.p. 158 – 160°C. Yield: 0.27 g (31%)

2.10 References

(1) D.R. Lide, *CRC Handbook of Chemistry and Physics*, 84th ed., CRC Press LLC, Boca Raton, **2003**.
(2) K. M. Manness, R. M. Wightman, *J. Electroanal. Chem.* **1994**, *396*, 85
(3) Pollex, A.; Hierseman, M. *Org. Lett.* **2005**, *7*, 5707.
(4) Spinelli, D.; Zanirato, P. *Perkins. Trans.* 2. **1993** 1129.
(5) Carpita, A.; Rossi, R.; Veracini, C. *Tetrahedron Lett.* **1985**, *41*, 1919.
(6) Xie, Y.; Wu, B.; Xue, F.; Ng, S.; Mak, T.; Hor, T. S. A. *Orangometallics* **1998**, *17*, 3988.
(7) Gornowitz, S.; Zhang, Y.; Hornfelds, A. *Acta Chim. Scand.* **1992**, *46*, 654.
(8) Brandsma, L.; Verkruijsse, H. D. *Syn. Commun.* **1988**, *18*, 1763.
(9) Ladd, D.; Harrsch, P. B.; Kruse, L. *J. Org. Chem* **1988**, *53*, 417.
(10) Jayasuriya, N.; Kagan, J. *Heterocycles* **1986**, *24*, 2901.
(11) Koepp, E.; Wolfgang, O.; Czugler, M.; Csoregh, I. *Perkins. Trans. 2* **1988**, 1251.
(12) Cornacchio, A., *Master's Thesis*, University of Western Ontario, 2007.

3.0 Elaborated Thiophenes by Click reactions

3.1 General introduction

Thiophene-based materials, which are both semiconducting and fluorescent, are of great interest because of their diverse potential for use in optoelectronic devices.[1] Unfortunately, the syntheses of functionalized thiophene monomers and oligomers are labor-intensive and often plagued by low-yielding reactions. Generally, these compounds are prepared through various homo- and cross-coupling reactions. For example, quater and sexithiophene can be made by coupling of α-lithiated thiophenes in the presence of cupric chloride or organoboranes.[2] Grignard coupling of thiophenes in the presence of transition metal complexes has also been used extensively to functionalize various thiophene compounds. Although C-C couplings of this type are widely used, they are often not ideal: (i) slight changes in conditions may cause a reaction to fail; (ii) extensive functionalization of starting materials is typically required, which can greatly increase the number of steps to achieve the desired product; (iii) the starting materials (*e.g.*, boronic acids and Grignard reagents) are at times difficult to access, and are usually sensitive to moisture and oxygen; and (iv) lengthy work-up procedures are also usually required as undesirable by-products are commonly formed. A combination of all of these factors results in lengthy syntheses containing many steps and generally results in disappointing yields for many C-C coupling reactions.

We therefore used an alternative approach to synthesize elaborated thiophene compounds in this thesis. Here we took advantage of the copper-catalyzed Huisgen 1,3-dipolar cycloaddition reaction, or "Sharpless-type click reaction", between 3-azidothiophene and aromatic acetylenes.[3] Using this method, we were successful in

creating four different series of thiophene-containing compounds (Figure 3.1; only two are shown). Compounds in Series C and D are shown in Figures 3.11 and 3.12, respectively.

Series A

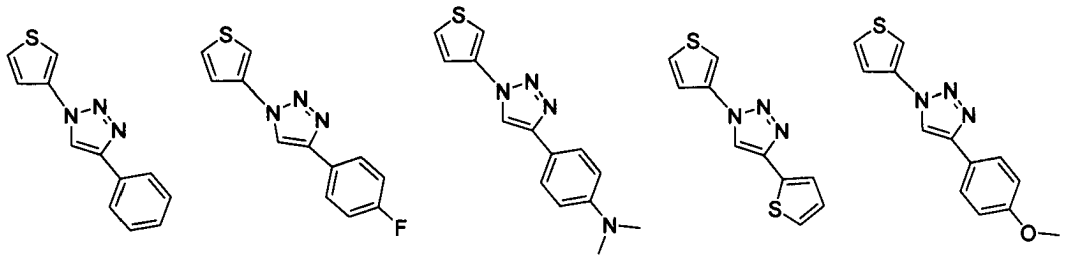

1 **2** **3** **4** **5**

Series B

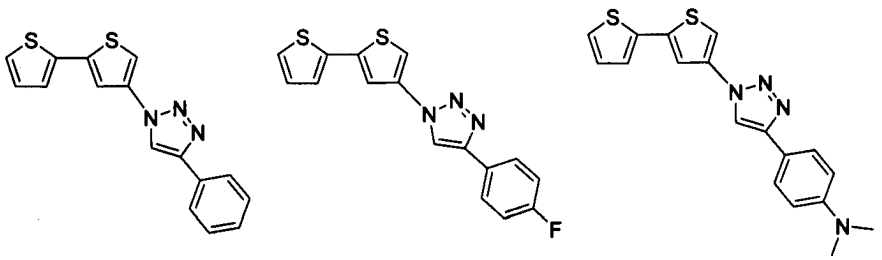

6 **7** **8**

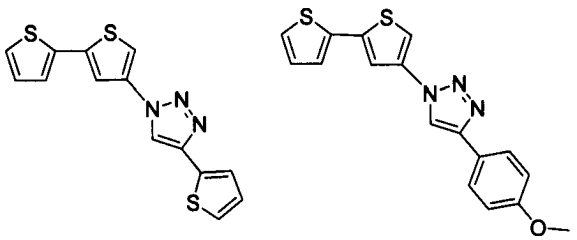

9 **10**

Figure 3.1: Mono- and bithienyl-substituted triazoles made in this work.

3.2 Synthesis of mono and bithienyl substituted triazoles

See Experimental Sections 2.4 and 2.5.

3.3 Results and Discussion

3.3.1 Synthesis of monothienyl triazole compounds (Series A)

These compounds were accessed through the precursor 3-azidothiophene which was synthesized from 3-bromothiophene according to published report (Scheme 3.1).[4]

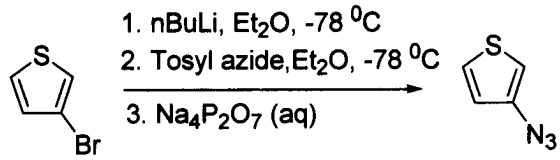

Scheme 3.1: Reaction scheme for the synthesis of 3-azidothiophene.[4]

We had first attempted to make 2-azidothiophene, but found it was very unstable, and only trace amounts could be isolated. A slight modification to the literature procedure[4] for the synthesis of 3-azidothiophene increased the yields from 36 % to 60 %: in the published report, the triazene salt that was formed after the addition of tosyl azide was isolated by filtration (Scheme 3.2).

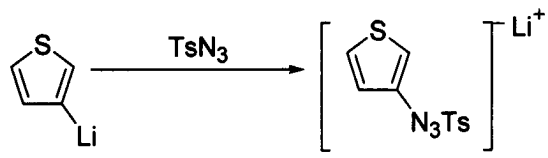

Scheme 3.2: Reaction scheme for the formation of the triazene salt.[5]

The isolated yellow salt was then added to an aqueous solution of $Na_4P_2O_7$. However, we found that the salt began to decompose on isolation and turned from a yellow powder to a sticky brown liquid. Pouring the reaction mixture directly into an aqueous solution of $Na_4P_2O_7$ without isolating the salt greatly increased yields of the 3-azidothiophene. The published procedure also called for the use of a fluorosil stationary phase for purification of the product by column chromatography; however, we found that this material was not very efficient at separating the different bands, and that silica gave much better separation.[4]

We then coupled 3-azidothiophene with various acetylenes containing both electron-donating and withdrawing-groups to make the compounds in Series A (Figure 3.2).

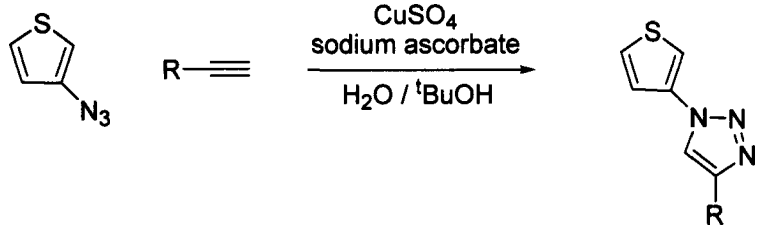

Figure 3.2: The synthesis of compounds in Series A.

All of the acetylene precursors were purchased from commercial sources and used without further purification. The "click" type reactions did not require inert conditions and were run under air. Originally, we followed a published report that described the use of copper metal and $CuSO_4$ to access the Cu(I) catalyst *in situ*; here the reaction mixture was heated to 125°C for 10 min.[6] However, the yields of our reactions under these conditions were low. We found that by using sodium ascorbate and $CuSO_4$ instead of copper metal and $CuSO_4$, and by decreasing the temperature to 80°C and increasing the

reaction time from 10 min to 120 min, the yields greatly increased (Table 3.1). One of the advantages of this reaction was that no chromatography was required for product isolation: all of the compounds **1** – **5** were isolated by filtration and purified by washing with dilute acid and Et_2O.

Table 3.1: Synthesis of Series A *via* Cu(I)-catalyzed cycloaddition.

Compound	$Cu_{(s)}/CuSO_4$ 125 °C, 10min Yield (%)	$CuSO_4$/sodium ascorbate 80 °C, 120 min Yield (%)
1	10	60
2	5	88
3	15	71
4	25	72
5	-	83

Crystals of **3** suitable for X-ray diffraction analysis were grown at 22 °C from CH_2Cl_2/Et_2O over a period of a week. The solid state structure was well defined (no disorder was seen in the thiophene ring) and the molecule was approximately planar (Figure 3.3)

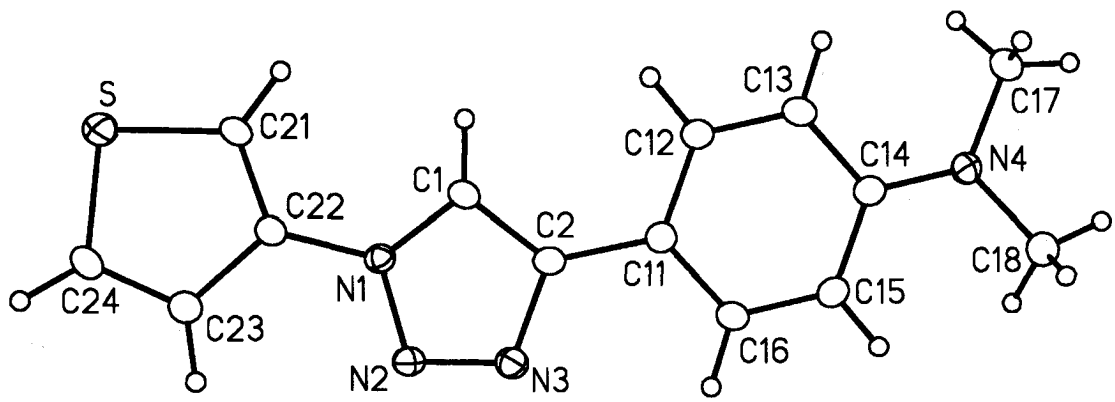

Figure 3.3: ORTEP representation of **3** with thermal ellipsoids drawn at 20%.

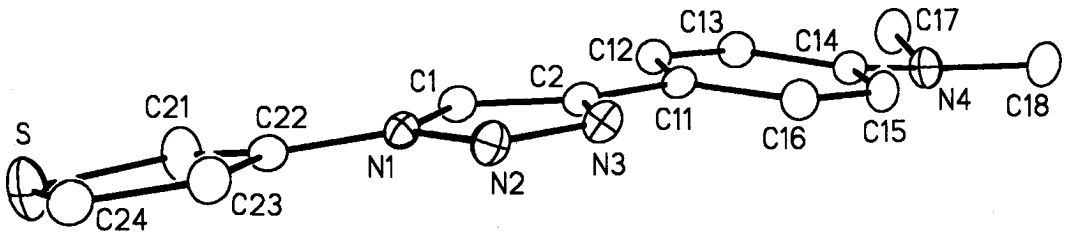

Figure 3.4: An alternative view of compound **3**.

Table 3.2: Selected bond distances (Å), interatomic angles (°) and torsion angles (°) for **3** with estimated standard deviations in parentheses.

S	C24	1.702(3)	C21	S	C24		92.70(14)
N1	N2	1.351(3)	N2	N1	C1		110.7(2)
N4	C14	1.387(3)	N1	N2	N3		107.2(2)
N4	C17	1.437(3)	C11	C12	C13		121.7(3)
C1	C2	1.372(3)	C17	N4	C18		115.7(4)
C2	C11	1.468(4)	N2	N1	C22	C23	5.1(3)
C12	C13	1.379(3)	N3	C2	C11	C16	6.9(4)
			N4	C14	C15	C16	-176.0(3)

Compound **3** was the only thienyl-substituted triazole made in the work that did not show any disorder of the thiophene ring. The very small intermolecular torsion angles show that it is also the most planar, relative to the other thiophene compounds obtained. We believe this is due to the fact that this compound contains an NMe_2 group and allows resonance structure B (Figure 3.5) to be the dominant form of this molecule. This is supported by the relatively short N4 – C14 bond length (1.387(3) Å relative to the standard value of (1.43 Å).[7]

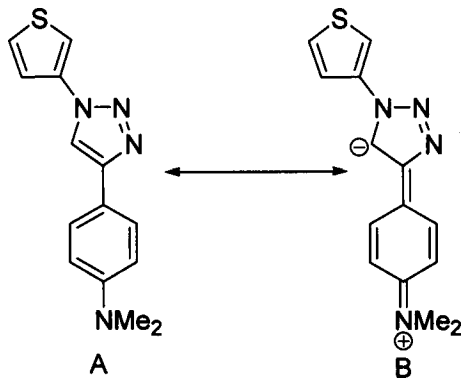

Figure 3.5: Resonance forms A and B of compound **3**.

3.3.2 Synthesis of bithienyl triazole compounds (Series B)

The first challenge in synthesizing these molecules was to make 4-azido-2,2'-bithiophene. The synthesis of the precursor 4-bromo-2,2'-bithiophene was easily accomplished by the Kumada coupling of the Grignard reagent derived from 2-bromothiophene and 2,4-dibromothiophene (Scheme 3.3).[8]

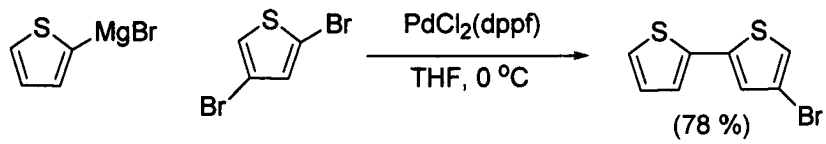

Scheme 3.3: Synthesis of 4-bromo-2,2'-bithiophene.[8]

4-azido-2,2'-bithiophene was made in a manner similar to that of 3-azidothiophene. Once again, not isolating the intermediate triazene salt dramatically improved the yield from 60 % to 80 %.[4] In a manner similar to the monothienyl azides, the bithienyl azides were coupled to various aromatic acetylenes having both electron-withdrawing and electron-donating groups. Again, we found that the yields dramatically increased when sodium ascorbate and $CuSO_4$ was used to make the Cu(I) catalyst *in situ*, and when the

reaction temperature was decreased to 80°C and the reaction time was increased to 120 min (Table 3.3.)

Table 3.3: Synthesis of Series B *via* Cu(I) catalyzed cycloaddition.

Compound	$Cu_{(s)}/CuSO_4$ 125 °C, 10min Yield (%)	$CuSO_4$/sodium ascorbate 80 °C, 120 min Yield (%)
6	13	73
7	27	84
8	15	71
9	24	72
10	-	98

Crystals of **6** suitable for X-ray diffraction analysis were grown at 25°C from CH_2Cl_2/Et_2O over a period of a week. The solid state structure of **6** had three crystallographically independent, but similar, molecules in its unit cell. The solid state structure was well defined, although the terminal thiophene ring was disordered over two positions corresponding to 180° rotation about the C25-C24 bond. The more highly occupied position of the disordered thiophene ring (60 %) is shown. The head-to-tail (HT) orientation of the bithiophene ring system is shown in Figure 3.6 and Figure 3.7.

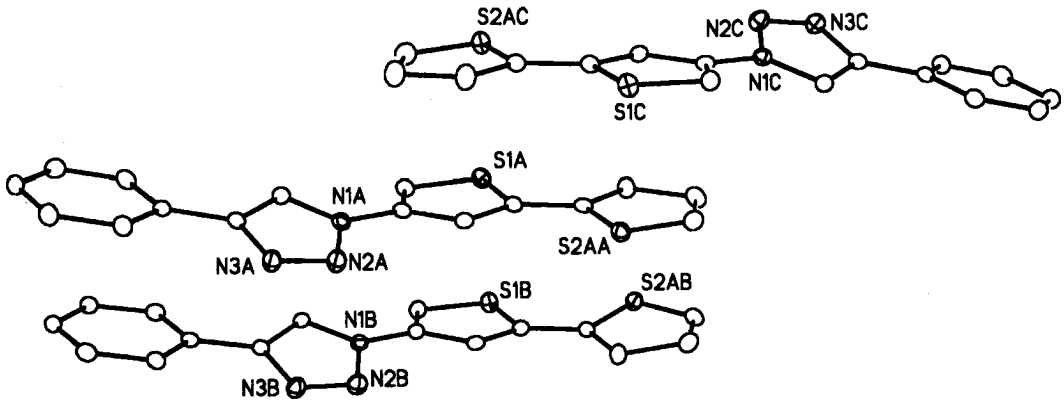

Figure 3.6: ORTEP representation of the three cystallographically independent molecules of **6** with thermal ellipsoids drawn at 20 %. Hydrogen atoms have been omitted for clarity. Only the more highly occupied of the two possible orientations of the thiophene ring is shown.

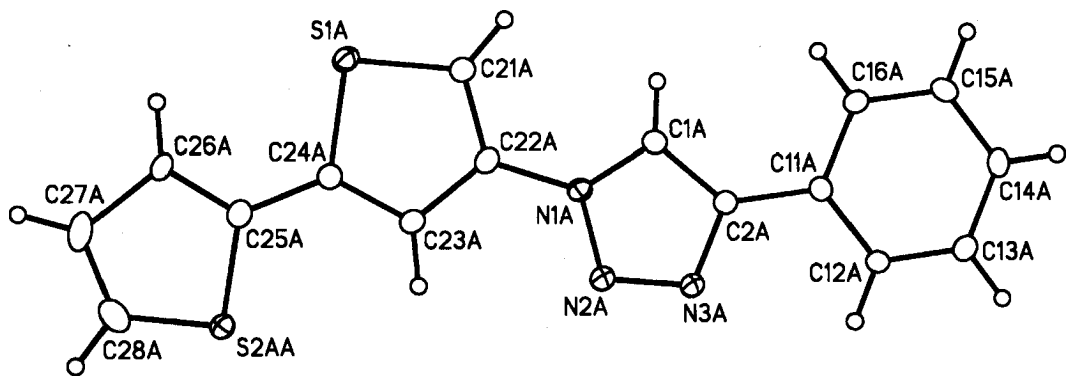

Figure 3.7: Alternative view of **6**

Compound **6** has a high degree of planarity in the bithiophene ring system. This can be seen from the small torsion angles between the two thiophene rings (Table 3.4). We believe this is possibly due to the fact that this bithiophene system is in the head-to-tail (HT) orientation.

Table 3.4: Selected bond distances (Å), interatomic angles (°) and torsion angles (°) for **6** molecule A with estimated standard deviations in parentheses

S1A	C21A	1.706(3)	C21A	S1A	C24A		92.87(14)
N1A	C1A	1.349(3)	C25A	S2AA	C28A		94.23(17)
N2A	N3A	1.316(3)	N1A	N2A	N3A		107.0(2)
C24A	C25A	1.456(4)	N1A	C1A	C2A		105.5(2)
S2AA	C25A	1.693(3)	C11A	C12A	C13A		120.8(3)
N1A	N2A	1.354(3)	S1A	C24A	C25A	C26A	-0.5(9)
N1A	C22A	1.416(3)	N2A	N1A	C22A	C23A	-19.2(4)
C2A	C11A	1.470(4)	N3A	C2A	C11A	C12A	13.5(4)
C12A	C13A	1.381(4)					

Crystals of **7** suitable for X-ray diffraction analysis were grown at 22 °C from CH_2Cl_2/Et_2O over a period of a week. The solid state structure was well defined, although not entirely planar. Once again, the terminal thiophene ring was disordered over two positions corresponding 180° rotation about the C25-C24 bond. The more highly occupied position of the thiophene ring (80 %) is shown in Figure 3.8. This gave the head-to-head (HH) orientation of the bithiophene system.

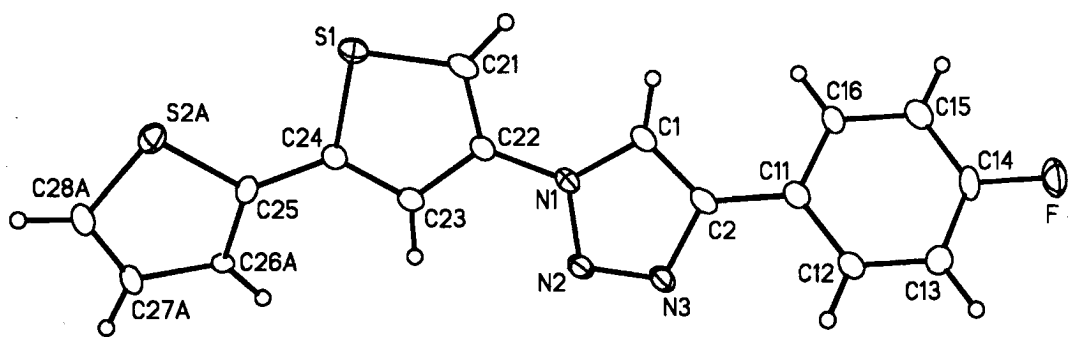

Figure 3.8: ORTEP representation of **6** with thermal ellipsoids drawn at 20 %. Only one of the two possible orientations of the thiophene ring is shown with an occupancy factor of 0.8.

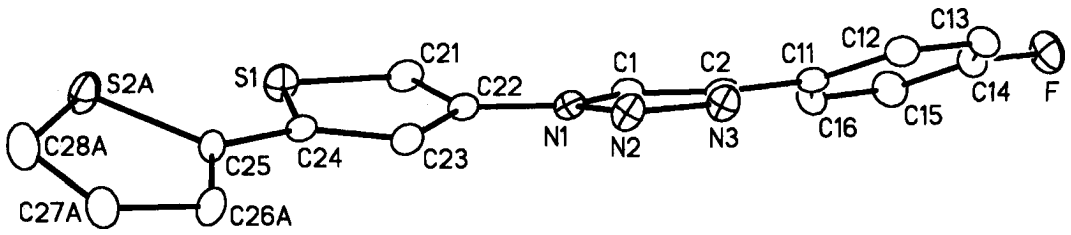

Figure 3.9: Alternative view of 7. Hydrogen atoms are omitted for clarity.

In compound **7** the bithiophene ring system is much less planar than in compound **6**. This can be seen from the increased torsion angle between the thiophene rings (Table 3.5). We believe this is because in this system the thiophene rings are HH and not HT.

Table 3.5: Selected bond distances (Å) interatomic distances (°) and torsion angles (°) for **7** with estimated standard deviations in parentheses.

S1	C21	1.693(5)	C21	S1	C24		92.4(2)
S2A	C28A	1.706(7)	C25	S2A	C28A		92.3(4)
S2B	C28B	1.705(7)	N1	N2	N3		107.5(3)
C24	C25	1.438(6)	N1	C1	C2		106.1(4)
C26A	C27A	1.389(11)	C11	C12	C13		121.9(4)
N1	C22	1.410(5)	S1	C24	C25	S2A	-16.4(5)
N2	N3	1.302(5)	N2	N1	C22	C23	-15.6(6)
C1	C2	1.345(6)	C23	C24	C25	C26B	166.0(14)
C2	C11	1.469(6)	N3	C2	C11	C16	159.6(4)
C11	C12	1.390(6)					
F	C14	1.363(5)					

3.4.1 Synthesis of 1-(3,5-di-thiophen-2-yl-phenyl)-substituted triazoles (Series C)

See Experimental Section 2.6

3.4.2 1-(3,5-di-thiophen-2-yl-phenyl)-substituted triazole compounds

A series of compounds similar to those reported in this section have previously been made by our group (Figure 3.10). These compounds had the general formula 1,3-

bis(thienyl)-5-R-benzene and were made to explore the effects that electron-withdrawing and -donating substituents had on the thienylbenzene ring system.[9]

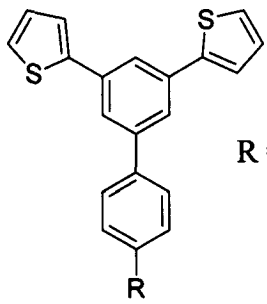

R = H **16**
= F **17**
= OMe **18**

Figure 3.10: 1,3-bis(thienyl)-5-R-benzene compounds made previously by our group.[9]

The compounds **16-18** were made using the Kumada cross-coupling reaction: 1-bromo-3,5-bis(2'-thienyl)benzene was coupled with the appropriate Grignard reagent in the presence of $PdCl_2$(dppf) as catalyst (dppf: 1,1'-bis(diphenylphosphino)ferrocene). These syntheses often required long reaction times to go to completion, were sensitive to air and moisture, and required column chromatography for purification of the products.[9]

By contrast, compounds **11 – 15** (Figure 3.11) were made in a manner similar to compounds **1 – 10**. The azide precursor was formed by lithiation of 1-bromo-3,5-bis(2'-thienyl)benzene followed by reaction with tosylazide.[4] To avoid lithiation of the carbon α to the sulfur on the thiophene ring in the first step, the lithiation reaction was conducted at -78 °C and not allowed to warm to r.t. (Scheme 3.4).

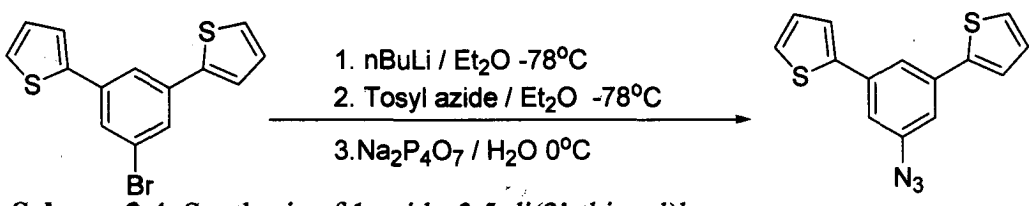

Scheme 3.4: Synthesis of 1-azido-3,5-di(2'-thienyl)benzene

Coupling of the azide and the various acetylenes was done in a similar manner to the procedure outlined in Section 3.3.2.

Series C

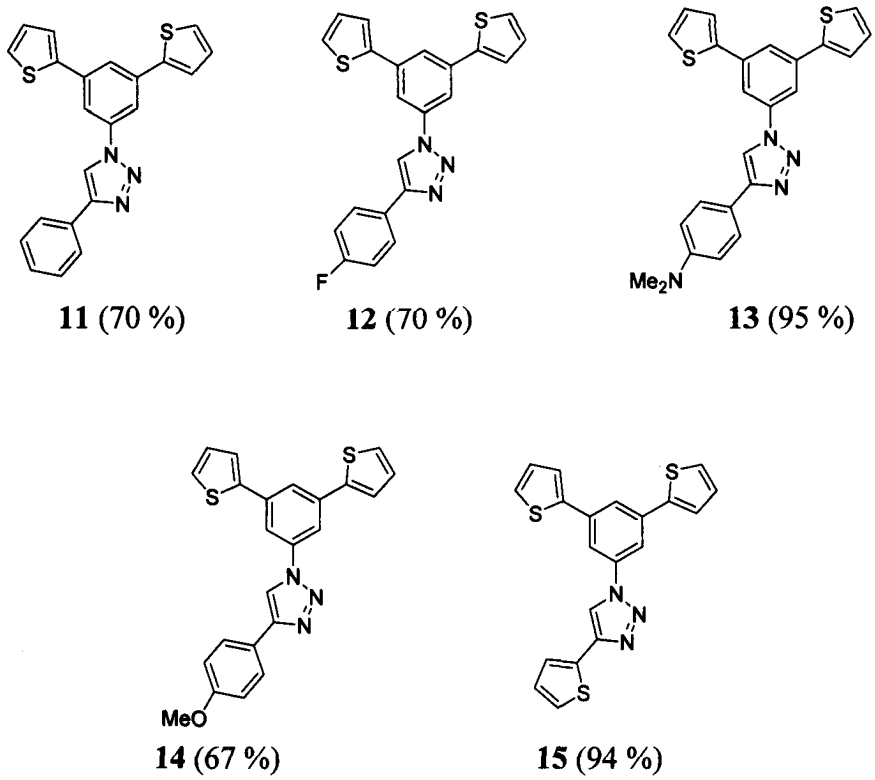

11 (70 %) **12** (70 %) **13** (95 %)

14 (67 %) **15** (94 %)

Figure 3.11: Target 1-(3,5-di-thiophen-2-yl-phenyl) substituted triazoles made in this work

Once again, these "click" reactions were conducted in air, and were not moisture sensitive. Workup consisted only of filtration followed by washing with water and Et_2O. Our new compounds had comparable yields (Table 3.6) and the required purification was much less tedious than the lengthy chromatography required for the analogous thienylbenzene compounds.

Table 3.6: Comparison of yields between "click" and Kumada coupling reactions for the synthesis of analogous compounds.

Compound	Coupling Reaction	Isolated Yield (%)
11	"click"	70
16	Kumada	68[9]
12	"click"	70
17	Kumada	84[9]
14	"click"	67
18	Kumada	52[9]

3.5 C_3 – Symmetric compounds

Dendrimers are well defined, monodisperse marcromolecules with a highly branched structure. Star-shaped dendrimers consist of a core connected to a number of branching units known as dendrons. Dendrimers can have aliphatic, non-conjugated dendrons, or the dendrimer can be conjugated in whole or in part. Dendrimers have advantages over conjugated polymers, including a defined molecular weight, reproducibility in synthesis and a higher degree of purity.[10] Conjugated dendrimers containing thiophene-based dendrons have attracted recent attention. These have the potential to be very useful because it is possible to tune both the optical and electrochemical properties of the dendrimer by varying the length of, or by introducing substituents into the dendrons.[10]

Despite the wide potential for applications of these star-shaped thiophene-based dendrimers, they have been rarely reported because they are very difficult to make. A typical approach is to use Pd-catalyzed cross-coupling reactions between 1,3,5-triiodobenzene and various substituted oliothiohpenes.[11] These syntheses often require

high catalyst loadings, harsh reactions conditions, and starting materials that are not easily accessed and are often sensitive to oxygen and moisture. The syntheses may involve many steps with lengthy purifications. Our goal was to develop a new synthetic route that would make these star-shaped thiophene dendrimers more accessible. The target compounds are shown in Figure 3.12.

Series D

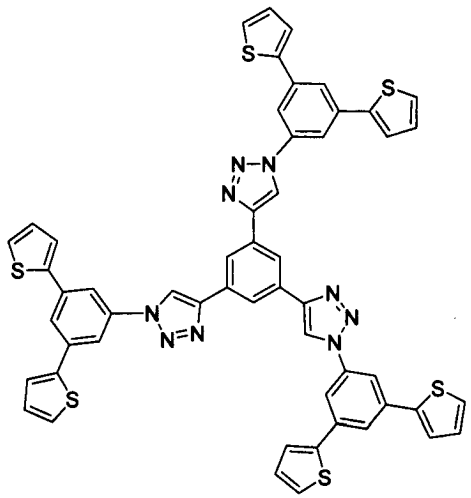

19

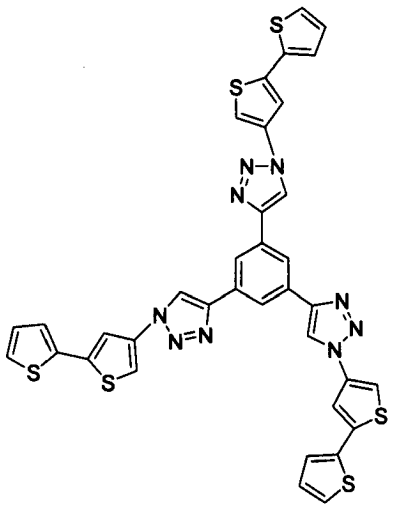

20

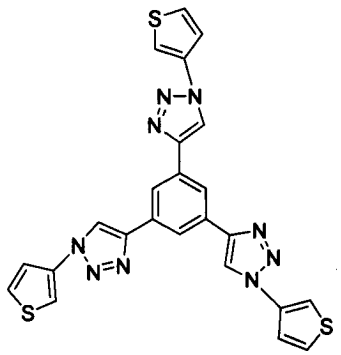

21

Figure 3.12: C_3 – symmetric thienyl benzene compounds made in this work.

Our group recently developed a new synthesis of 1,3,5-tris(2'-thienyl)benzene (**22**)[9] and 1,3,5 tris-{5'(2'2''-bithienyl)benzene (**23**).[9] The closely related 1,3,5-tris[4-2-thienyl)phenyl]benzene (**24**)[12] has been reported by Sunoj and coworkers (Figure 3.13).

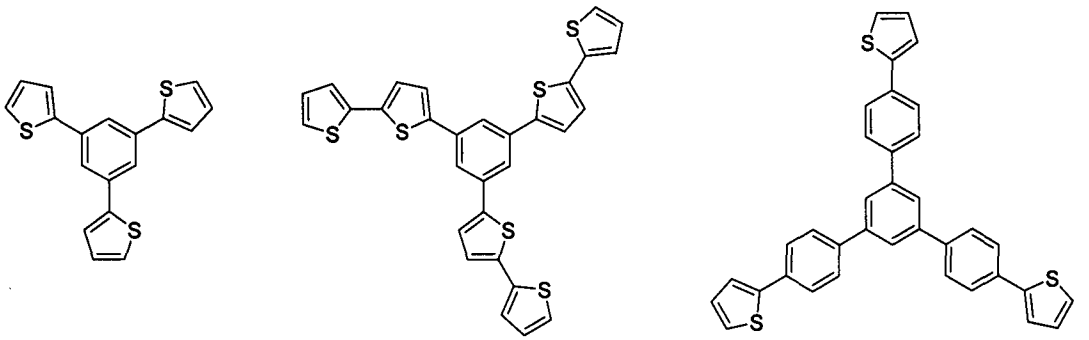

22[9] **23**[9] **24**[12]

Figure 3.13: Previously made C_3-symmetric thienyl compounds.

Compound **22** was synthesized using Pd-catalyzed Kumada coupling according to Scheme 3.5.

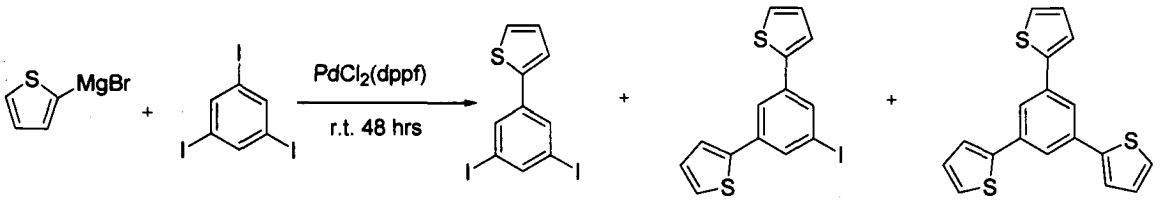

22

Scheme 3.5: Pd catalyzed coupling of 2-thienylmagnesium bromide and 1,3,5-triiodobenzene.[9]

Although the isolated yield of **22** was high (86%), the reaction was lengthy (48 h) and did not go to completion; undesired partially-substituted intermediates were identified after workup. To isolate the desired product, column chromatography was needed, and this was reported to be very tedious and time consuming due to the difficulty

of separating the various intermediates.[9] However, we were able to use a "click" type reaction to make a compound similar to **22** using a much more direct approach (Scheme 3.5).

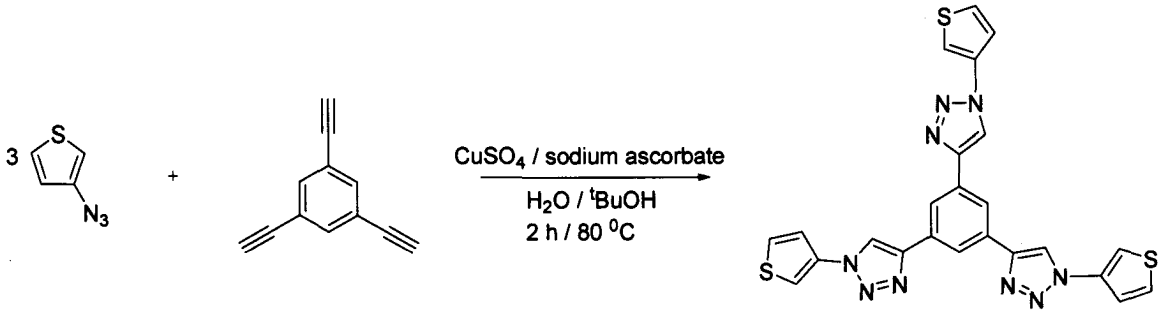

21 +

Scheme 3.6: Reaction scheme for the synthesis of **21.**

We used the same conditions as for the previous "click" coupling reactions (Section 2.7) and achieved an isolated yield of 91%. Our new method was far superior to the traditional coupling methods because it required no chromatography, only a short reaction time, and special precautions, such as keeping out oxygen and water were not needed. The reaction was done in air using a biphasic solution of H_2O / ^tBuOH from which the desired product was isolated by filtration.

The second target molecule was **20**. This compound was made in a manner similar to **21.** However, in this case, 4-azido-2,2'-bithiophene was used instead of 3-azidothiophene. Again, compounds similar to **20** have previously been made using traditional coupling reactions. For example, Stille cross-coupling between 1,3,5-triiodobenzene and tributylstannyl-2,2'-bithiophene using $PdCl_2$(dppf) as catalyst gave **23** in poor yields (Scheme 3.6).[9]

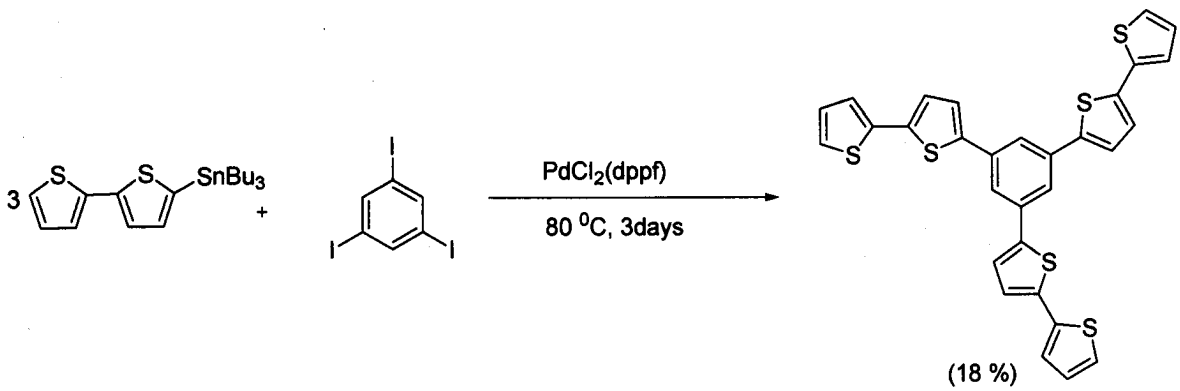

23

Scheme 3.7: Previously reported synthesis of **23**.[9]

The stannyl reagent for the synthesis of **23** was quite difficult to access as it required lengthy vacuum distillation at high temperature (~ 450 °C) for purification. As in the synthesis of **22**, the desired product was contaminated by partially substituted intermediates. In this case tetrathiophene, the most abundant impurity (32 %) was also formed. A more successful synthesis by previous members of our group used Suzuki coupling, which gave the desired product in 90 % yield. However, the synthesis of the required starting material, 2,2'-dithienyl-5-boronic acid was found to be very unreliable.[9] In this work, we were able to synthesize a compound similar to **23** in moderate yield using "click" reactions. Although the yield of this compound (**20**) was lower than that of most of our other "click" reactions, it far exceeded those of the more established coupling methods for generating similar compounds. Again, no chromatography was required, and the reaction was complete within 2 h while other reported reactions took up to 3 d.

C_3-symmetric compounds similar to **19** (*e.g.*, **24**) have been made previously by Sunoj and co-workers (Scheme 3.7) by Pd-mediated Suzuki-Miyaura cross-coupling of 2-thiophene-boronic acid with 1,3,5-tris(4-iodophenyl)benzene, which gave the coupled product in 60% yield; separation from the mono- and di-substituted intermediates was required. These researchers also attempted to make a compound, similar to our **19** (**25**, Scheme 3.8), but this was unsuccessful.[12]

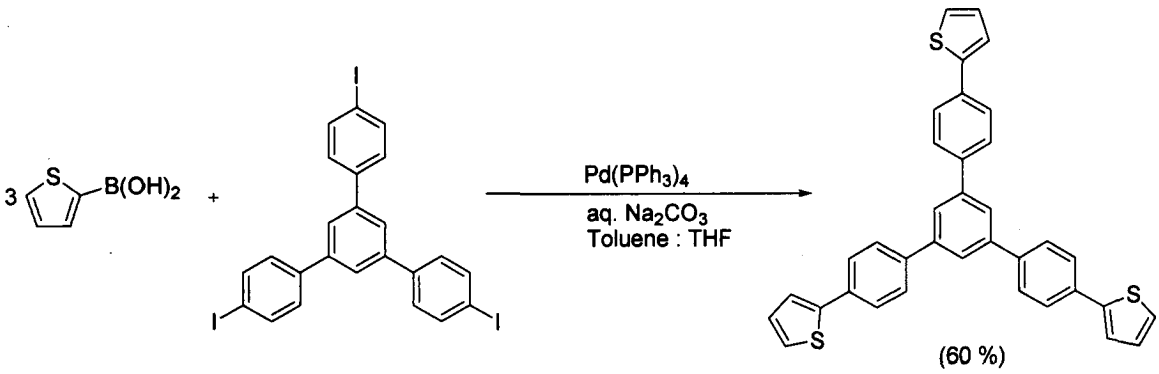

Scheme 3.8: Previously reported synthesis of **24**.[12] **24**

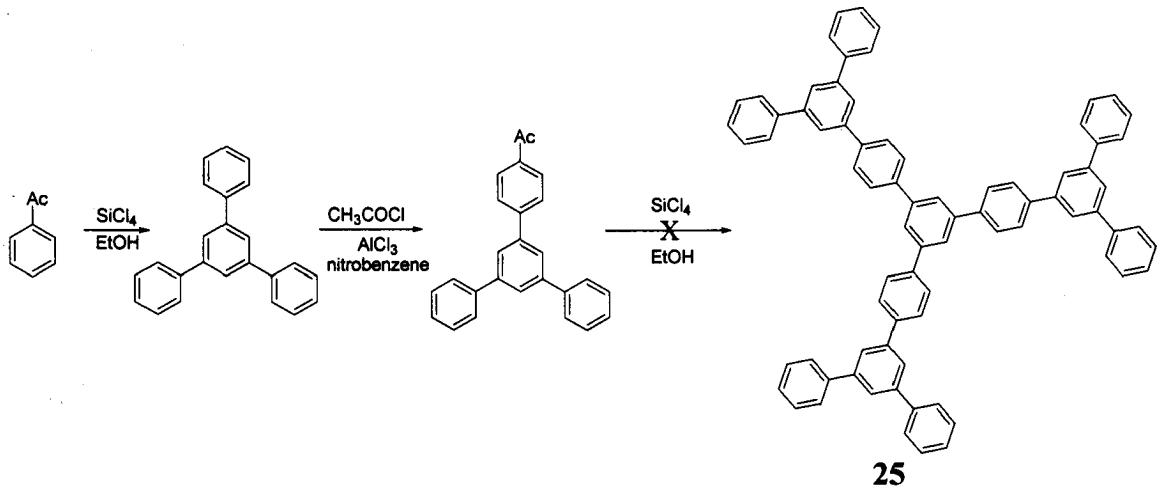

25

Scheme 3.9: Previously reported attempted synthesis of **25**.[12]

Sunoj and coworkers successfully trimerized acetophenone by treatment with $SiCl_4$. The 1,3,5-triphenyl benzene intermediate was then further acetylated but subsequent treatment with $SiCl_4$ failed to give the intended trimerized product **25**.[12] By contrast, we were successful in synthesizing **19**, which was similar to **25** in that it had C_3-symmetry and 13 contiguous aromatic rings, however, ours incorporated both triazole and thiophene heterocycles (Scheme 3.9).

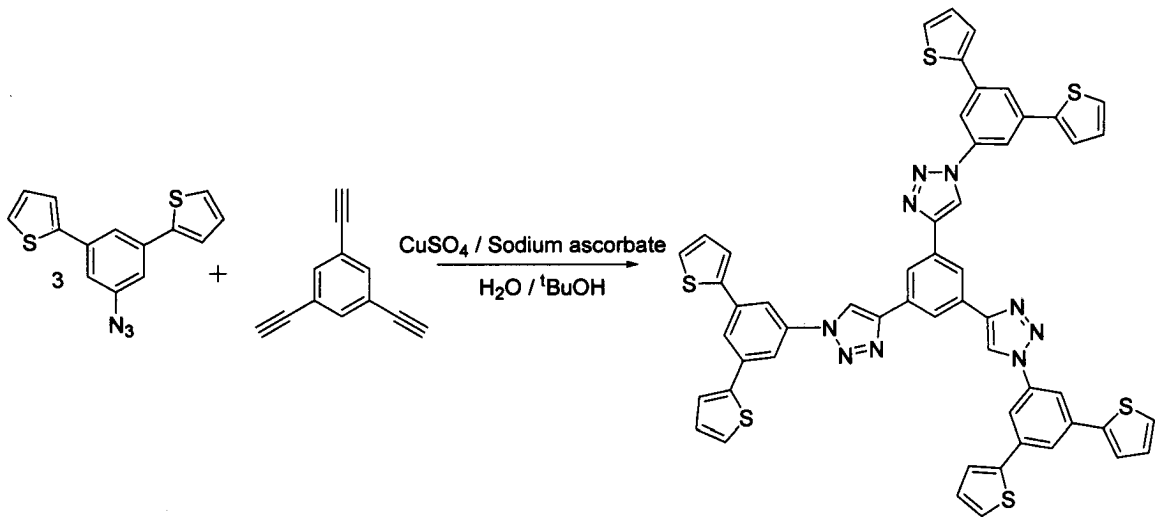

19 (95 %)

Scheme 3.10: Synthesis of **19**.

To make this compound, we first synthesized 1-azido-3,5-di(2'-thienyl)benzene from the precursor 1-bromo-3,5-di(2'-thienyl)benzene as described in Scheme 3.4. We then coupled 3 equiv. of the azide with 1 equiv. of 1,3,5-triethynylbenzene to yield the desired product **19** in an excellent 95% yield. Like the other C_3-symmetric compounds made in Series D, this product required no chromatography: filtration was all that was necessary.

3.6 Synthesis of 2,5-bis-(3,5-di-thiophen-2-yl-phenyl)-thiophene

The motivation behind the synthesis of the target compound **27** (Figure 3.13) was to enable a comparison of the electrochemiluminescence properties of analogous silole- and thiophene-based compounds. The silole **26** (Figure 3.14) had been made in the Pagenkopf laboratory by former M.Sc. student Xin Wang.

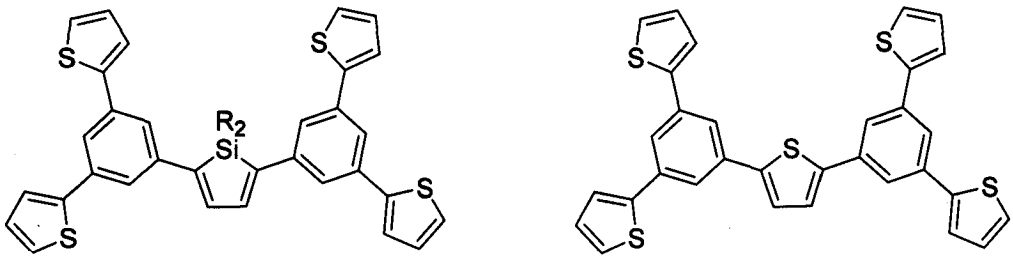

26 **27**

Figure 3.14: Silole **26** (R = Me, Bu) and our target thiophene derivative, **27**.

3.6.1 Synthesis of compound 2,5-bis-(3,5-di-thiophen-2-yl-phenyl)-thiophene

See Experimental Section 2.8

3.6.2 2,5-bis-(3,5-di-thiophen-2-yl-phenyl)-thiophene

The synthesis of **27** had previously been attempted by past members of our group; however, none of the early attempts were successful. In the past, Negishi conditions had been used in an attempt to couple 3,5-bis(2'-thienyl)benzene-1-zincchloride with 2,5-dibromothiophene according to Scheme 3.10.

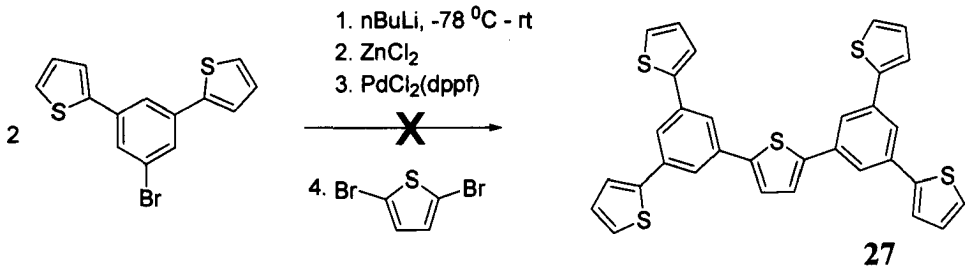

Scheme 3.11: Reaction scheme for the attempted synthesis of **27** by Nigishi coupling.

An alternative route was therefore needed. In this work, we were successfully able to synthesize the target compound **27**, also using Nigishi coupling: however, instead of using 5-bis(2'-thienyl)benzene-1-bromide and 2,5-dibromothiophene, we instead made the zinc chloride intermediate from **22** and coupled it to 1-bromo-3,5-(2'-thienyl)benzene using $Pd(PPh_3)_4$ as the catalyst. This gave the desired product in 31 % yield (Scheme 3.11).

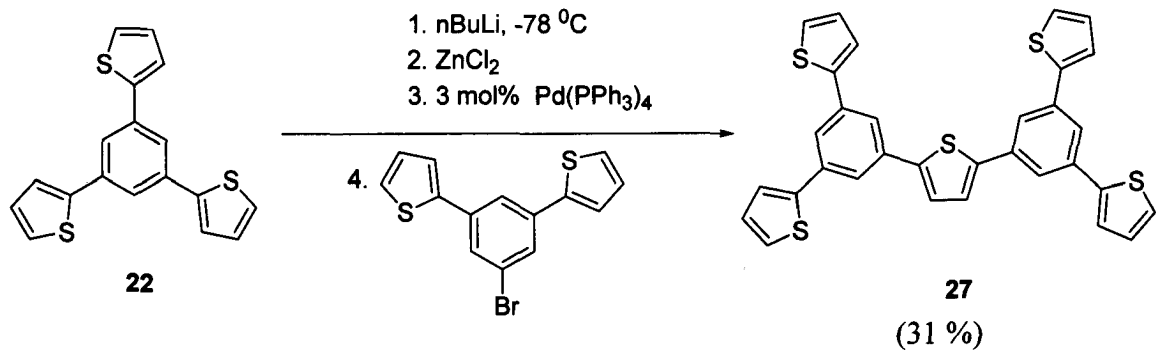

Scheme 3.12: Synthesis of compound **27**

An important aspect of the reaction was to keep the temperature low (-78 °C) for the lithiation of **22** and for addition of the zinc chloride. This gave more control and prevented over lithiation.

Crystals of **27** suitable for X-ray diffraction analysis were grown at 22 °C from CH_2Cl_2 over a period of a week. The solid state structure did not show any disorder in the thiophene rings (Figure 3.15 and Figure 3.16). Selected bond distances and angels are given in Table 3.7.

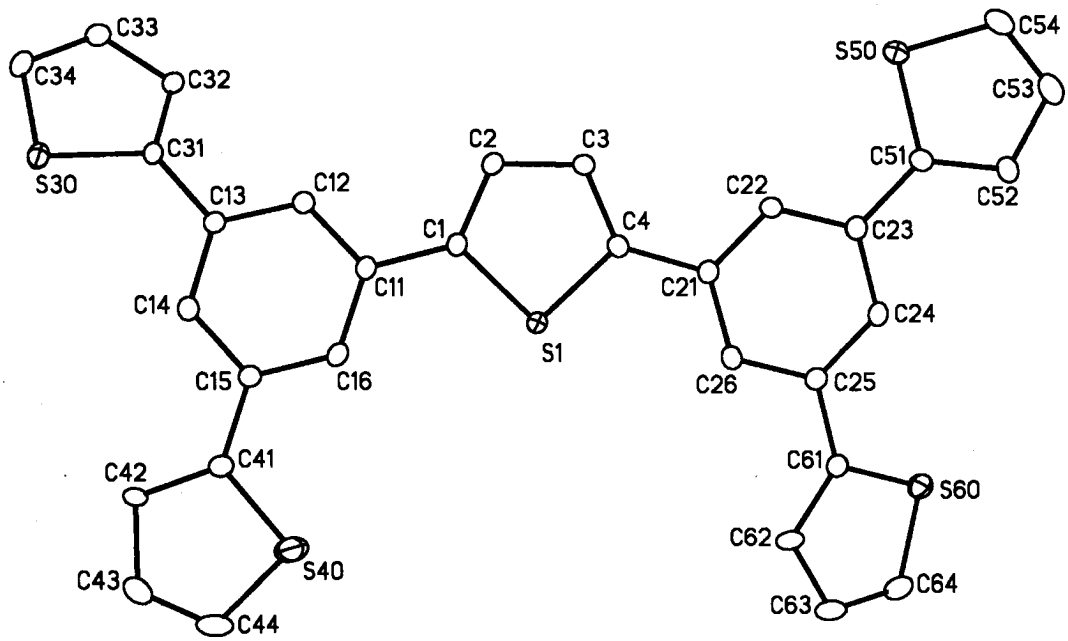

Figure 3.15: ORTEP representation of **27** drawn with ellipsoids at 20%. Hydrogen atoms have been omitted for clarity.

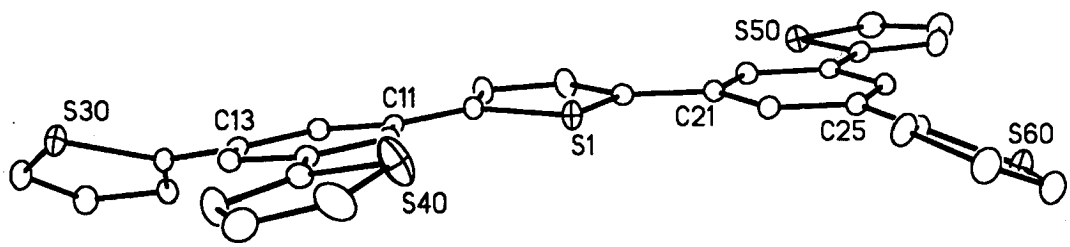

Figure 3.16: An alternative view of **27**.

Table 3.7: Selected bond distances (Å), interatomic distances (°) and torsion angles (°) for **27** with estimated standard deviations in parentheses.

S1	C1		1.732(3)	C41	S40	C44		92.9(2)
C1	C11		1.464(4)	C51	S50	C54		92.38(18)
C2	C3		1.415(5)	C61	S60	C64		92.71(18)
C11	C16		1.397(4)	C13	C14	C15		118.8(3)
C15	C41		1.471(4)	C23	C24	C25		120.8(3)
S40	C44		1.692(5)	C12	C13	C31	C32	30.8(5)
C42	C43		1.460(5)	C14	C15	C41	C42	4.8(5)
C1	S1	C4	92.86(15)	S1	C1	C11	C16	7.5(4)
C31	S30	C34	92.58(17)	C24	C25	C61	S60	-23.0(4)

The crystal structure of **27** had a planar core; however, the terminal thiophene rings were slightly twisted which can be seen by the larger intermolecular torsion angles between the thiophene and carbon atoms. Also, **27** crystallized with a molecule of chloroform, as did the analogous silole compound.

3.7 References

(1) Barabrella, G.; Melucci, M.; Sotgiu, G. *Adv. Mater.* **2005**, *17*, 1581.
(2) Roncali, J. *Chem. Rev.* **1992**, *17*, 711.
(3) Kolb, H. C.; Finn, M. G.; Sharpless, K. B. *Angew. Chem. Int. Ed.* **2001**, *40*, 2004.
(4) Spinelli, D.; Zanirato, P. *J. Chem. Soc. Perkin. Trans. 2* **1993**, 1129.
(5) Zanirato, P.; Cerini, S. *Org. Biomol. Chem.* **2005**, *3*, 1508.
(6) Appukkuttan, P.; Dehaen, W.; Fokin, V.; Van der Ecken, E. *Org. Lett.* **2004**, *6*, 4223.
(7) Sciau, P.; Moret, J.; Gros, N. *Acta Cryst. B* **1987**, 111.
(8) Jayasuriya, N.; Kagan, J. *Heterocycles* **1986**, *24*, 2901.
(9) Cornacchio, A., *Master's Thesis*, University of Western Ontario, 2007.
(10) Mitchell, W.; Kopidakis, G. R.; Ginley, D. S.; Shaheen, S. E. *J. Mater. Chem.* **2005**, *15*, 4518
(11) Pelter, A.; Jenkins, I. *Tetrahedron* **1997**, *53*, 10357.
(12) Kotha, S.; Kashinath, D.; Lahiri, K.; Sunoj, R. *Eur. J. Org. Chem.* **2004**, 4003.

4.0 Electrochemistry and Electrochemiluinescence

4.1 General Introduction

Electrochemiluminescence from conjugated organic molecules has recently become a highly investigated field.[1] Development in this area has been fueled by the exploration of new configurations of conjugated organic materials for luminescent devices.[1] Organic conjugated polymers are a very important group of photo-active materials.[2] These polymers exhibit both physical and optical properties that lend themselves to the development of display devices, transistors and sensors.[2] Also, the development of flexible and tunable organic polymers for light emitting diodes has received a great deal of attention[1]. Thiophene-based polymers and oligomers have been extensively studied for these applications. This is due to the large number of chemical modifications that can be made at the thiophene ring; these allow one to fine-tune the optical and physical properties of the materials.[3] Now that we have developed a simplified alternative route to C-C coupling for thiophene modification, a greater number of elaborated thiophene-containing compounds can be studied. We investigated the electrochemiluminescence and optical properties of our thiophene-containing compounds in Series A, B and D to determine whether these properties were rationally dependent on the incorporated electron-donating or withdrawing substituents and whether the compounds could potentially lead to future applications.

4.2 Cyclic voltammetry

The electrochemical properties of the elaborated thiophene compounds were studied using cyclic voltammetry (CV). Ferrocene was used as an internal standard ($E°$ (Fc/Fc^+) = 0.400 V *vs.* SHE) in DMF.[4]

4.2.1 The electrochemical properties of thiophene compounds in Series A

Quantum calculation of the electronic structure of the representative molecules in Series A allowed visualization of the HOMO and LUMO. The HOMO of **1** is spread over the entire molecule (Figure 4.1 (a)). It is from this orbital that electrons are lost during oxidation of the compound. Likewise, the LUMO into which the electrons are injected during reduction is fairly evenly distributed over all three rings. Therefore, it can be expected that both the oxidation and reduction potentials of compounds in Series A might have some dependency on the nature of the substituent attached to the triazole ring (Figure 4.1 (b)).

a)

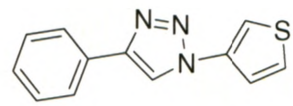

b)

Figure 4.1: Molecular orbital distributions for **1** calculated by Allison Brazeau (DFT/B3LYP/631G^{*++}) (a) HOMO and (b) LUMO

The redox potentials of compounds **1** – **5** are summarized in Table 4.1, and the cyclic voltammogram of **3** (Figure 4.2) and **1, 2, 4, 5** in DMF solution are shown in Figure 4.3.

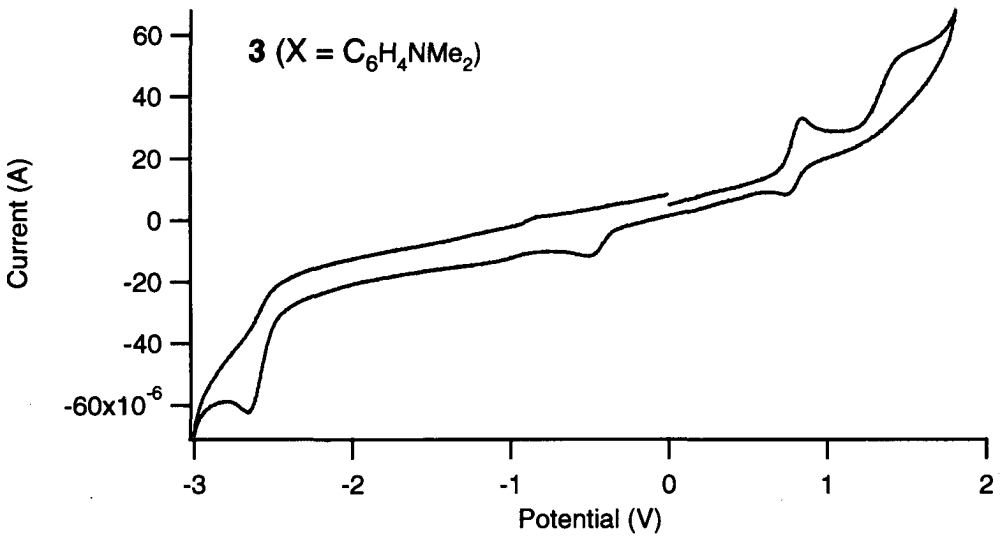

Figure 4.2: Cyclic voltamogramme of compound 3 [Scan rate = 0.1Vs-1 in DMF solution with 0.1 M TBAP]

Compound **3**, displays a quasi-reversible oxidation wave at 0.84 V; the radical cation produced by the oxidation of **3** is therefore relatively stable, possibly due to the introduction of a strong electron-donating (NMe_2) group.[5] Compound **3** also had a second irreversible oxidation peak at 1.52 V; the irreversibility of the second oxidation wave could be due to the fact that the produced dication is a highly reactive species and can easily undergo other chemical reactions. Also, it is evident that the oxidation potential of **3** is much smaller then the other Series A compounds possibly due to the introduction of an electron-donating group.[5]

Compounds **1**, **2**, **4** and **5** were all characterized by irreversible oxidation and reduction peaks due to the relatively unstable radical ions that were produced.

Comparing the relative reduction values of Series A, compound **2** has two irreversible reductions: the first a single reduction peak at -2.00 V and the second at -2.28 V consisting of multiple closely-spaced reduction waves. The first reduction potential of compound **2** was less negative than those of compounds **1**, **3**, **4** and **5**. This indicates that **2** is easier to reduce than the other compounds. This is probably due to the introduction of an electron-withdrawing group.[5]

Additionally, the small wave that is seen at - 0.5 V in the CV of compounds **2**, **3** and **5** probably corresponds to the possible formation of byproducts by electrochemical reaction (EC).[6]

Table 4.1: Oxidation and reduction potentials of Series A [Scan rate = 0.1 Vs^{-1} in DMF solution with 0.1 M TBAP].

Compound	Concentration x 10^{-3} mM	1st Oxidation (V) vs. Ag wire	2nd Oxidation (V) vs. Ag wire	1st Reduction (V) vs. Ag wire	2nd Reduction (V) vs. Ag wire
1	8.8	-	-	− 2.36	-
2	8.1	1.24	-	− 2.00	− 2.28
3	8.6	0.84/0.75*	1.52	− 2.67	-
4	7.4	1.28	-	− 2.31	-
5	7.8	1.56	-	− 2.59	-

* anode/cathode.

Series A

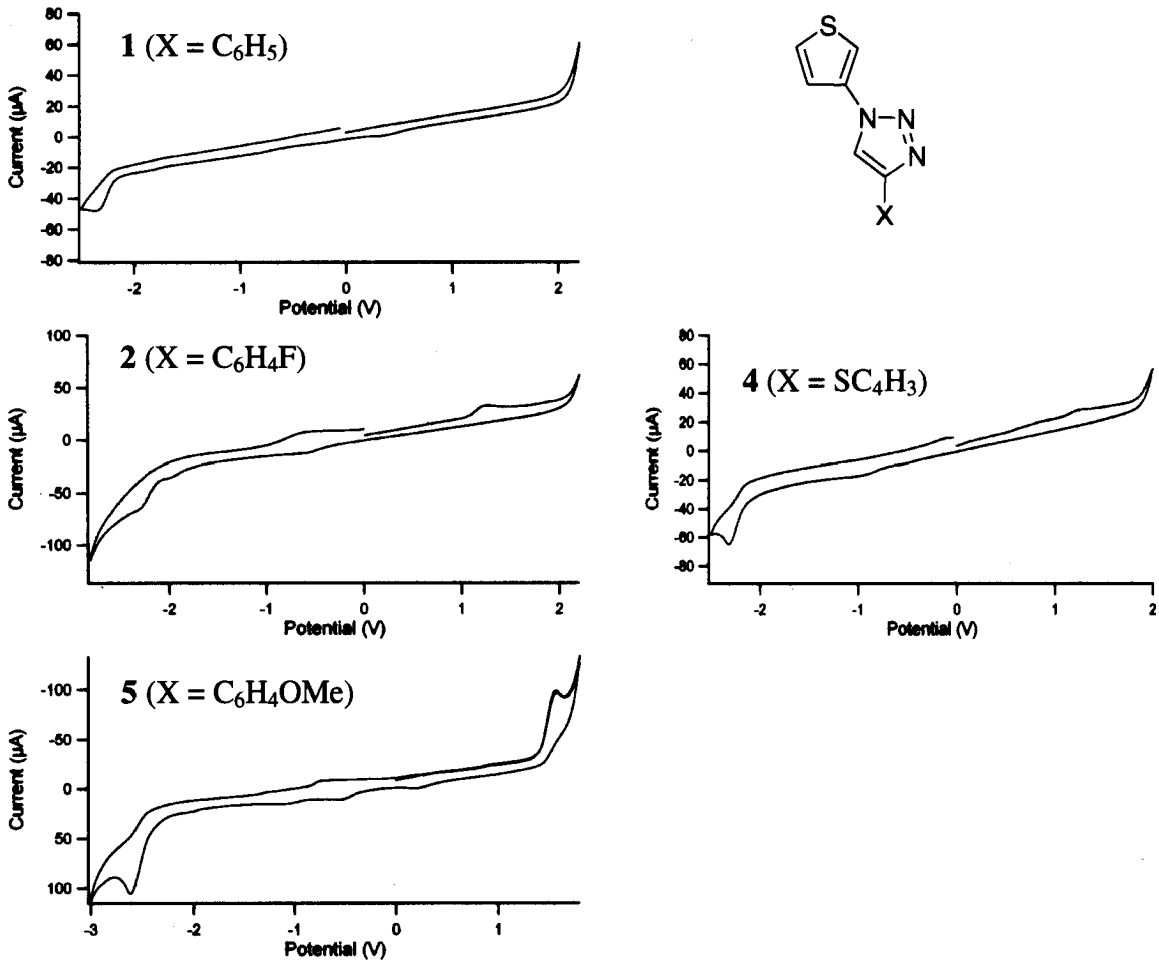

Figure 4.3: Cyclic voltammograms of compounds in Series A in DMF solution containing 0.1 TBAP M. Scan rate 0.1 Vs^{-1}.

The Hammett equation is used to predict the impact a substituent X has on the rate constant (k_x) of the reaction Z → Z`, where Z is a reactive group attached to the same aromatic ring as X, relative to the rate of the analogous reaction in the unsubstituted ring (k_0) (Figure 4.4).

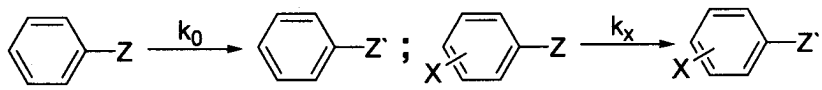

Figure 4.4: Relative rate of reaction in unsubstituted (k_0) and substituted (k_x) rings.

This relationship can be expressed quantitatively using the equation:

$$\log (k_x/k_0) = \rho\sigma_x$$

where k_x is the rate constant for the para- or meta-substituted aromatic compound

k_0 is the rate constant for unsubstituted aromatic compound

ρ is the reaction constant for a particular reaction under a given set of conditions

σ_x is a constant for a given substituent in a given position (*para* or *meta* to Z)[7]

Although the above equation relates different rates, analogous correlations can be made for thermodynamic data. In this work, we use the Hammett equation to evaluate the effect different substituents have on the oxidation and reduction potentials of the thiophene-containing compounds.

The oxidation and reduction potentials of compounds in Series A, were used to construct Hammett plots, in order to determine whether the various electron- donating and -withdrawing groups had predictable effects on the redox properties of the compounds (Figure 4.5 and 4.6).

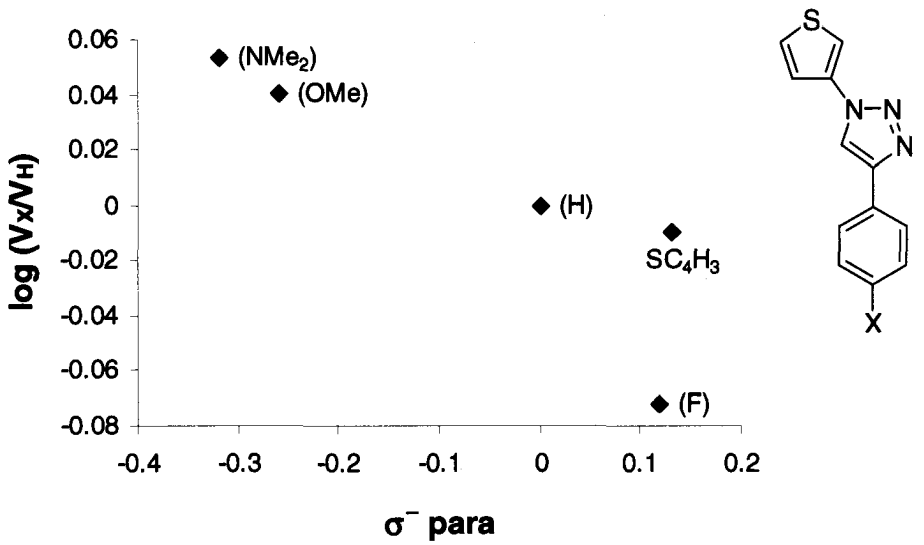

Figure 4.5: Hammett plot of the reduction potential *vs.* σ^-_p[8] for compounds in Series A.

From the Hammett plot in Figure 4.4 we see that there is an obvious trend for the reduction potential. As the para-substituent X becomes more electron-donating ($\sigma_p < 0$), the reduction potential becomes more negative, *i.e.* the compounds become harder to reduce, as expected.

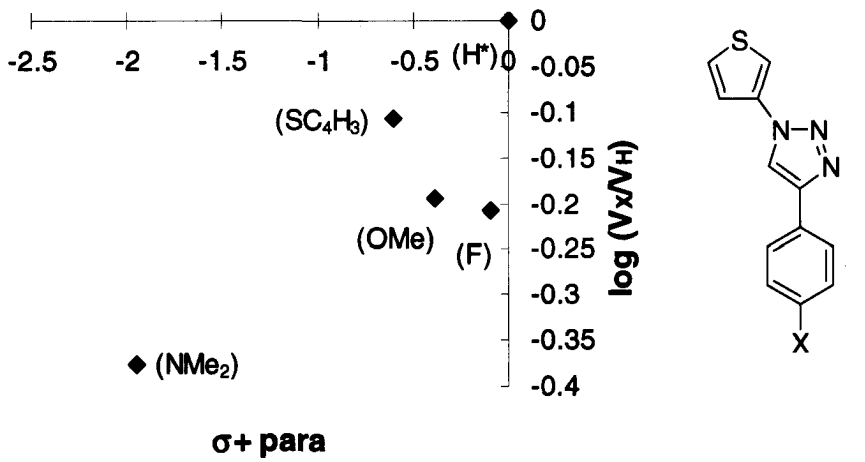

Figure 4.6: Hammett plot of the oxidation potential vs. σ^+_p[8] for compounds in Series A.
* The oxidation potential of **1** was estimated for the purposes of this graph.

Likewise, Figure 4.6 potential shows clearly that as the substituent becomes more electron-withdrawing, the compound becomes more difficult to oxidize; however this trend is not as obvious as it is in Figure 4.5.

4.2.2 Cyclic voltammetry of compounds in Series B

Quantum calculations of the electronic structure of representative molecules in Series B allowed visualization of the HOMO and LUMO. The HOMO of **6** is spread uniformly over the entire molecule (Figure 4.7 (a)). It is from this orbital that electrons are lost during the oxidation of the compound. By contrast, reduction of Series B compounds is thought to involve only the bithiophene and triazole ring systems because this is where the LUMO is concentrated (Figure 4.7(b)). This is in contrast to Series A compounds in which the LUMO is delocalized over all three rings.

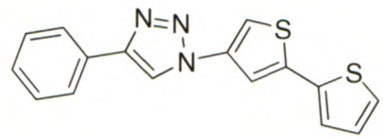

a)

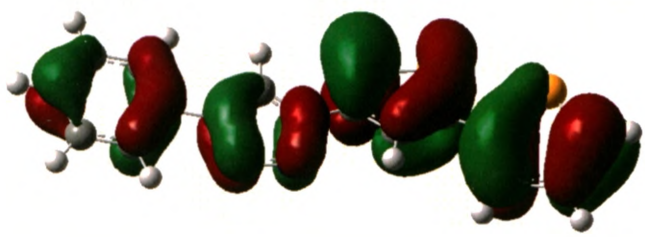

b)

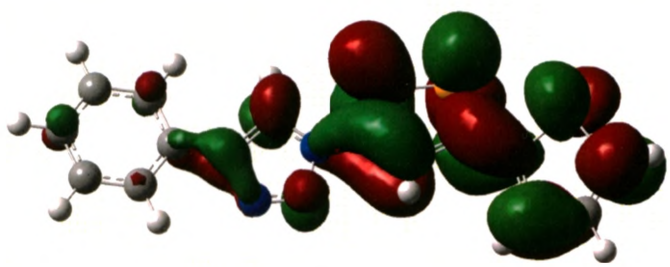

Figure 4.7: Molecular Orbital distributions for **6** calculated by Allison Brazeau (DFT/B3LYP/631G^{*++}) (a) HOMO and (b) LUMO.

The redox potentials of compounds **6** – **10** are summarized in Table 4.2, and the cyclic voltammograms of the Series B compounds in DMF solution are shown in Figure 4.8.

The compounds in Series B are characterized by irreversible oxidations and reductions due to the instability of the radical cations and anions, respectively. The first reduction potentials of compounds **6**, **8**, **9**, and **10** are more negative than that of compound **7**. This indicates that the reduction of **7** is much easier than that of the other compounds in this series. This is possibly due to the introduction of a strongly electron-withdrawing group. Comparison of the reduction potentials between Series A and Series B showed that the compounds containing two contiguous thiophene rings were more easily reduced, and, in the case of compounds **6**, **7** and **8**, could undergo multiple reductions. This could be due to the extended conjugation in Series B because of the extra thiophene ring present.

The oxidation potentials of the Series B compounds ranged from 0.76 V to 1.93 V. Compound **7** had an oxidation peak at the lowest potential followed by compounds **6**, **8**, **9** and **10** respectively. The facile oxidation of **7** was unexpected because this compound contains an electron-withdrawing group. Comparison of the oxidation potentials of the two series showed that compounds in Series B were more easily oxidized than the analogous Series A compounds. This is once again possibly due to the extended conjugation in the Series B compounds arising from the extra thiophene ring. Additionally, two small reduction waves are present in compounds **6**, **8**, **9** and **10**. These peaks could possibly correspond to the formation of byproducts by an EC (electrochemical) mechanism.

Series B

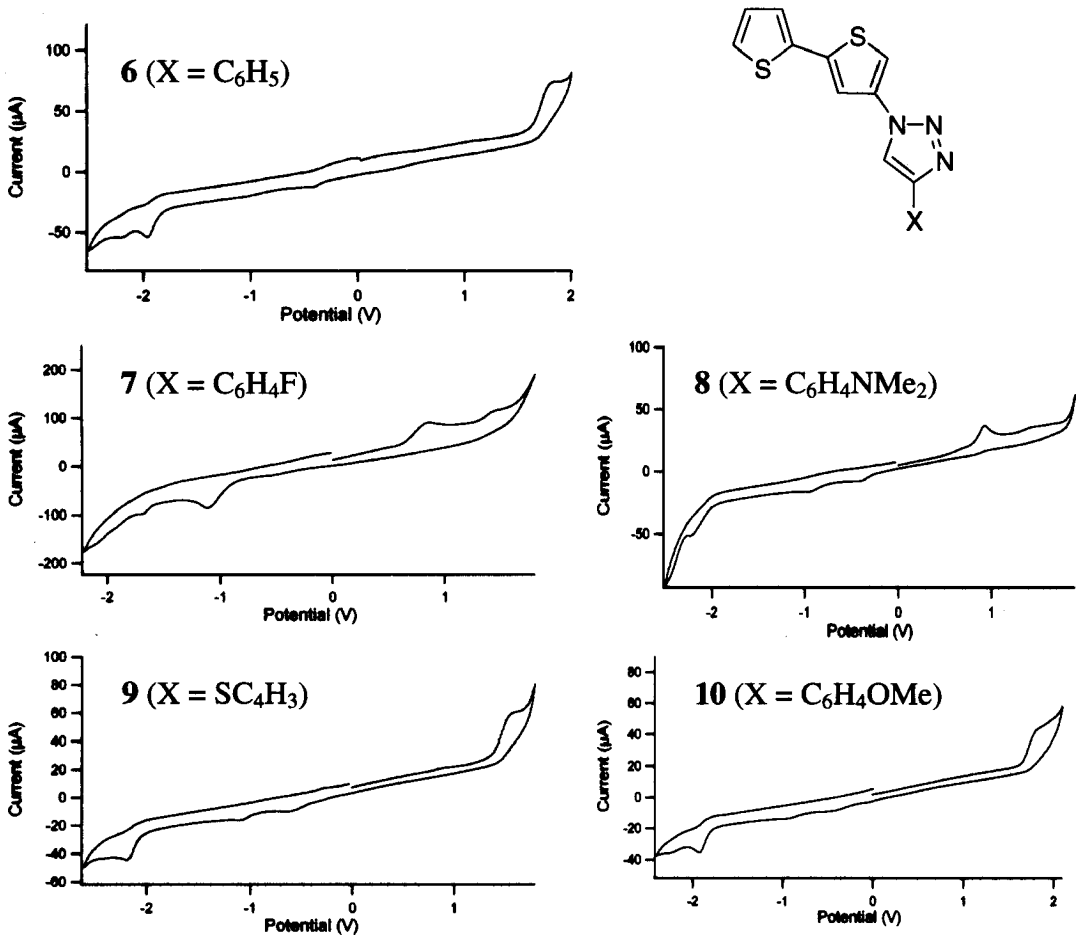

Figure 4.8: Cyclic voltammograms compounds in Series B in DMF solution containing 0.1 TBAP. Scan rate 0.1 Vs^{-1}.

Table 4.2: Oxidation and reduction potentials for Series B [Scan rate = 0.1 Vs^{-1} in DMF with 0.1 M TBAP].

Compound	Concentration (x 10^{-3} mM)	1st Oxidation Peak (V) vs. Ag wire	2nd Oxidation Peak (V) vs. Ag wire	1st Reduction Peak (V) vs. Ag wire	2nd Reduction Peak (V) vs. Ag wire
6	6.5	1.85	-	– 2.02	– 2.12
7	6.1	0.76	1.40	– 1.03	– 1.60
8	6.3	0.91	1.42	– 2.21	– 2.41
9	5.7	1.59	-	– 2.19	-
10	5.9	1.93	-	– 1.84	-

In order to visualize the effects that the various electron-donating or electron-withdrawing groups have on the Series B compounds, the reduction and oxidation potentials were plotted against the σ+ and σ– constant of the corresponding X group (Figure 4.9 and Figure 4.10 respectively).

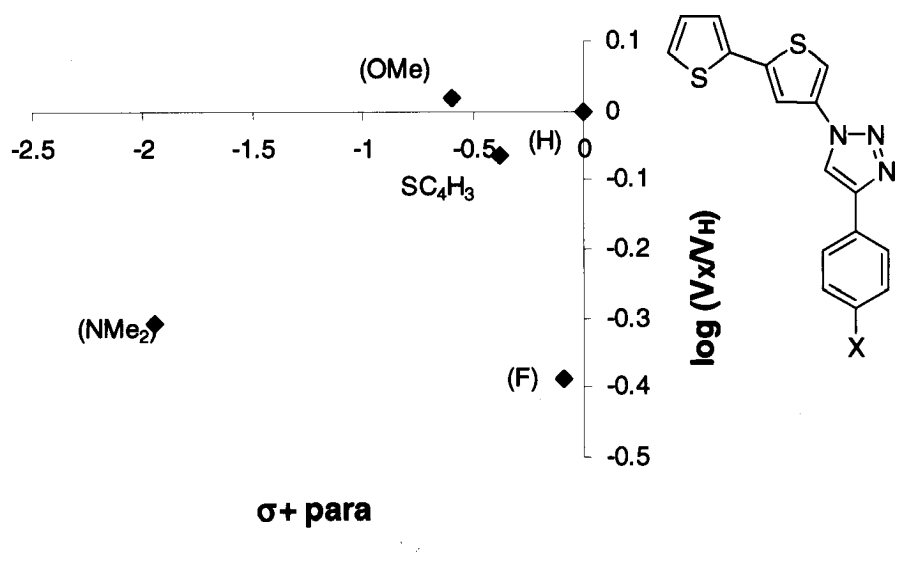

Figure 4.9: Hammett plot of the oxidation potential *vs.* $\sigma+_p$[8] of the X group in Series B compounds.

One would expect that compounds containing electron withdrawing groups ($\sigma_p > 0$) would be anodically shifted and would be more difficult to oxidize, and those containing electron-donating groups ($\sigma_p < 0$) would be cathodically shifted and be easier to oxidize. However, this is not the case for Series B. The bithienyl compounds containing electron donating-groups like OMe and NMe_2 were in fact harder to oxidize than that containing a fluoro-substituent.

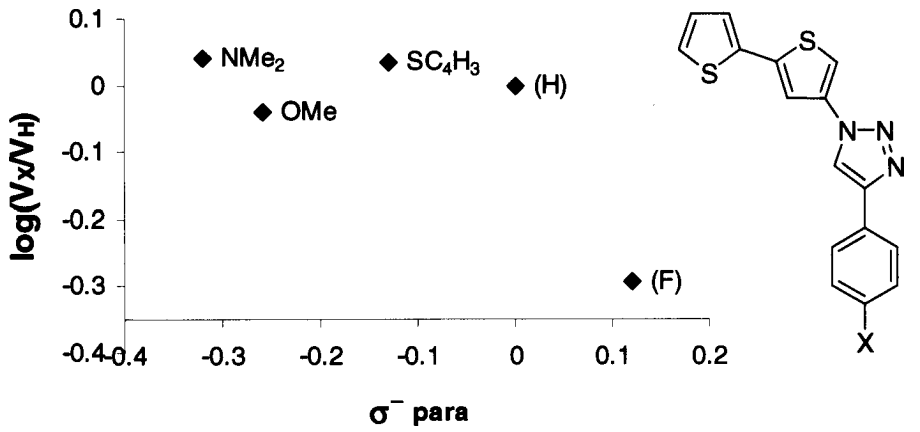

Figure 4.10: Hammett plot of the reduction potential of Series B compounds vs. σ_p^- [8]

As expected, the reduction of Series B compounds containing electron-donating groups ($\sigma_p < 0$) were shifted slightly cathodically and were slightly harder to reduce than the bithienyl compound containing an electron withdrawing fluoro- group, **7**; this compound was both the easiest to oxidize and reduce, whereas those containing electron-donating groups were both the hardest to oxidize and reduce, which is somewhat unexpected.

In Series B, the substituents have a greater affect on the reduction potential than the oxidation potential which can be seen from the Hammett plots. However, it seems that the electron-donating and -withdrawing substituents have a greater effect on the oxidation and reduction potentials in Series A compounds than in Series B compounds.

4.2.3 Cyclic Voltamogramms of Series D compounds

The redox potentials of the compounds in Series D were also studied and are summarized in Table 4.3; the cyclic voltammograms in DMF are shown in Figure 4.11

Table 4.3 : Oxidation and reduction potentials for series B [Scan rate = 0.1 Vs^{-1} in DMF with 0.1 M TBAP].

Compound	Concentration (x 10^{-3} mM)	1st Oxidaton (V) vs. Ag wire	2nd Oxidation (V) vs. Ag wire	1st Reduction (V) vs. Ag wire	2nd Reduction (V) vs. Ag wire
19	2.0	1.17	-	− 0.89	− 1.97
20	2.6	1.17	1.67	− 2.10	− 2.42
21	3.8	0.77	-	− 2.78	-

The compounds in Series D are characterized by irreversible oxidation and reduction waves. Compound **21** has the lowest oxidation potential, which is somewhat unexpected because it has the fewest aromatic rings of any of the compounds in this series. Compound **21** has a single oxidation peak, whereas compound **20** has two oxidation peaks and compound **19** displays a broad oxidation wave that probably consists of several closely spaced oxidation peaks.

In comparing the reduction potentials between the compounds in Series D, **19** and **20** display two distinct reduction waves, whereas compound **21** displays several closely spaced reduction waves. Compounds **19** and **20** displayed reduction waves at less

negative potentials than **21**. This could be due to the extended conjugation found in **19**, which aids in the reduction of the molecule compared to **20** and **21**.

Series D

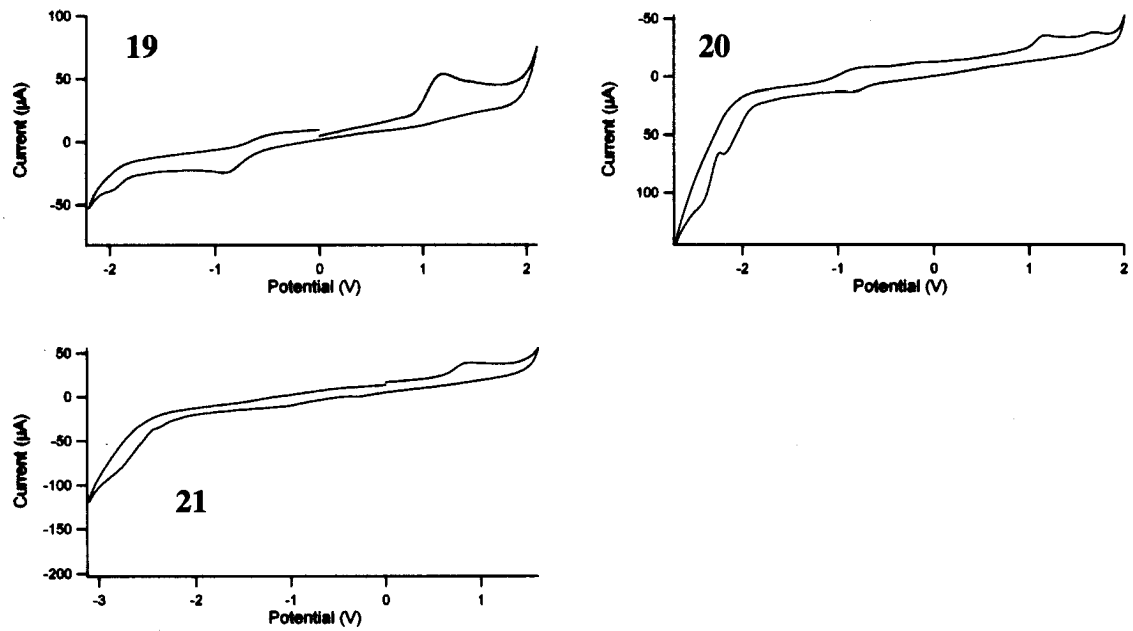

Figure 4.11: Cyclic voltammograms of compounds in Series D in DMF solution containing 0.1 M TBAP. Scan rate = $0.1 Vs^{-1}$

4.3 ECL experiments involving elaborated thienyl compounds

Electrochemiluminescence (also known as electrogenerated chemiluminescence, or ECL) involves the generation of species at an electrode surface that can undergo electron transfer reactions to form excited states that emit light. The first studies involved electron transfer reactions between an oxidized and a reduced species, both of which were generated at an electrode by sweeping the potential between positive and negative values. These experiments are called "annihilation" experiments (Figure 4.12).[9]

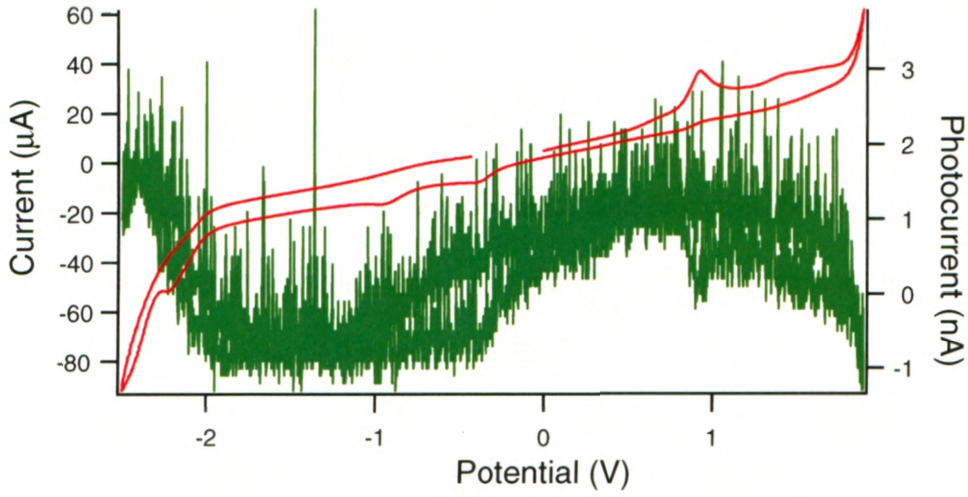

Figure 4.12: Cyclic voltammogram (red) and ECL-voltage curve (green) of **8** scanned at $0.1 Vs^{-1}$ in DMF solution containing 0.1 M TBAP.

The proposed mechanism for the annihilation of thiophene is shown in Scheme 4.1.

$$T + e^- \rightarrow T^{-\bullet}$$

$$T - e^- \rightarrow T^{+\bullet}$$

$$T^{-\bullet} + T^{+\bullet} \rightarrow T^* + T$$

$$T^* \rightarrow T + h\nu$$

Scheme 4.1: Proposed mechanism for the generation of light from thiophene, T.[9]

In the proposed mechanism, a radical cation is formed in the positive region of the potential range and a radical anion in the negative. These two radicals combine to form excited (T*) and ground state thiophenes. The excited thiophene then relaxes to the ground state with the emission of light (Scheme 4.1).[9]

4.3.1 Annihilation reactions of Series A

Compounds in Series A displayed minimal ECL in annihilation experiments. This is due to the fact that the produced radical ions were not stable in solution. This was also demonstrated by the irreversible oxidation and reduction peaks in the corresponding cyclic voltammograms (Figure 4.3). For ECL to occur, the cations and anions that are produced during the annihilation experiment must persist in solution long enough to interact with one another so that light can be produced; this was not the case for compounds in Series A. This is reflected in the poor ECL efficiencies displayed by compounds in Series A compared to the standard compound 9,10-diphenylanthracene (DPA) (Table 4.4).

Table 4.4: ECL efficiency of Series A compounds relative to DPA, measured at 0.1 Vs^{-1} in DMF solution containing 0.1 M TBAP.

Compound	Relative efficiency (%)
1	0.74
2	1.5
3	0.89
4	1.4
5	0.49

4.3.2 Annihilation reactions of Series B compounds

The ECL-voltage curve of compound **8** is shown in Figure 4.12. ECL is produced when the potential is swept through one full cycle, and in this case, light is detected in both the positive and negative potential regions. The same behaviour is also observed for compounds **6**, **9** and **10**. Since a photocurrent can be seen in both potential regions, these compounds must produce radical cations and anions that remain in solution long enough to interact during annihilation experiment. In Figure 4.12, a large amount of background noise is observed because the intensity of the photocurrent is very weak (measured in nA) compared to the current (μA). For compound **7** (Figure 4.13) the ECL is more intense in the negative region, so one could assume that the radical cation is relatively more stable than the radical anion being produced.

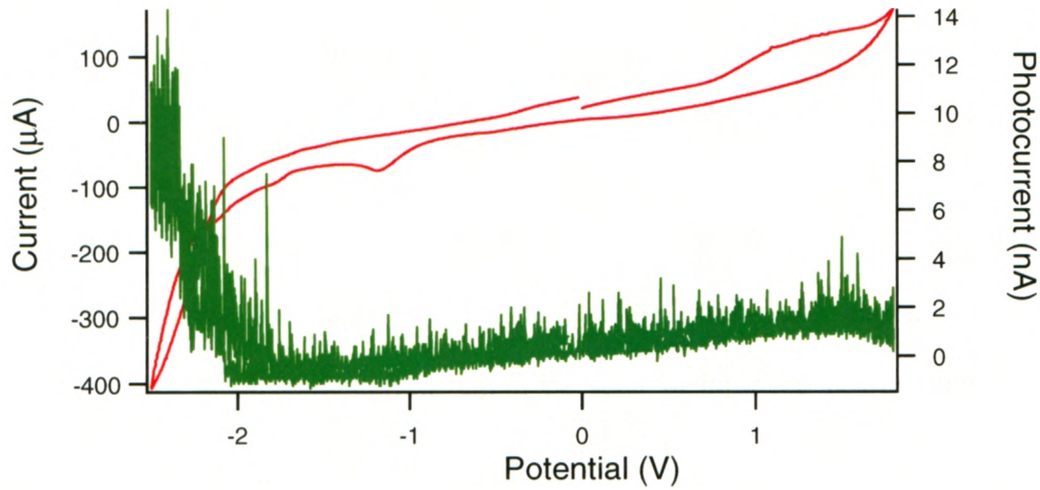

Figure 4.13: Cyclic voltammogram (red) and ECL-voltage curve (green) of **7** scanned at 0.1V/s in a DMF solution containing 0.1 M TBAP.

The efficiencies of the compounds in Series B are shown in Table 4.5. All of the compounds in Series B displayed low efficiencies compared to DPA. However,

cases (Table 4.5). This could be due to the longer π-conjugation system in the bithienyl compounds which supports easier oxidation and reduction of the compounds. Compounds **6** and **8** displayed the lowest efficiencies at 0.37 % and 0.40 % of DPA, respectively, while the efficiencies for **7, 9, 10** were a bit higher ranging from 1.20 to 1.69 % of DPA. The increase in efficiency for **7**, **9** and **10** could possibly be due to enhanced stability of the radical cation and anion produced during the annihilation experiments.

Table 4.5: ECL efficiency of Series B compounds relative to DPA, measured at 0.1 Vs^{-1} in DMF solution containing 0.1 M TBAP.

Compound	Relative efficiency (%)
6	0.37
7	1.20
8	0.40
9	1.30
10	1.69

4.3.3 Annihilation reactions of compounds in Series D

Series D also displayed minimal ECL in the annihilation experiments. As in Series B, a very weak photocurrent could be seen in both the positive and negative potential regions. The relative efficiencies ranged from 0.92 – 1.5 % (Table 4.6). One would expect **19** to have the highest efficiency due to the fact that it has a more highly conjugated structure than compounds **20** and **21**; however, this was not the case.

Table 4.6: ECL efficiency of Series D compounds relative to DPA, measured at 0.1 Vs^{-1} in DMF solution containing 0.1 M TBAP.

Compound	Relative efficiency (%)
19	1.09
20	1.5
21	0.92

4.4 Coreactant experiments

ECL can be generated by annihilation reactions between an oxidized and a reduced species produced at a single electrode by using an alternating potential; however, the potential window allowed by a particular solvent may be too narrow to generate the radical ions and this can result in weak ECL.[10] By the addition of a coreactant, ECL can instead be produced with a single potential step, or by scanning over one potential range (Scheme 4.2). Depending on the applied potential, both the coreactant and the luminophore are first oxidized or reduced at the electrode to form radical ions. The ions resulting from the coreactant then decompose to produce either strong oxidizing or reducing species that go on to react with the oxidized or reduced luminophore to produce the exited states that produce light. Using a coreactant has many advantages compared to ECL produced by annihilation experiments because it does not require the generation of both the oxidized and reduced forms of the luminophore. Thus, even in solvents that have a narrow potential window, allowing *only* the oxidized *or* reduced form of the luminophore to be produced, but not both, a coreactant makes it still possible to generate ECL. When the annihilation experiments are not efficient due to the instability of one or

the other of the radical, the use of coreactant can greatly increase the intensity of light produced.[10]

In our experiments benzoyl peroxide (BPO) was used as the coreactant. This required us to scan only the negative potential region because peroxides produce reactive oxidizing agents when they are reduced (in this case, $PhCO_2^{\bullet}$).[11] The first of two possible mechanisms for the generation of light is shown in Scheme 4.2 and Figure 4.14.

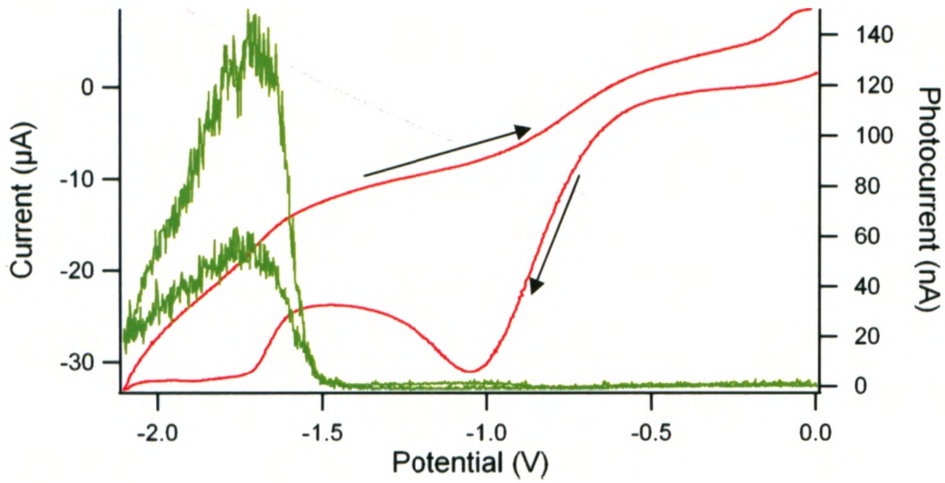

Figure 4.14: Cyclic voltammogram (red) with superimposed ECL-voltage curve (green) for **3** in DMF solution with added BPO (0.5 mM) and TBAP (0.1 M) scanned at 0.1 Vs^{-1} over 0/-2.1V

$$BPO + e^- \rightarrow BPO^{-\bullet}$$

$$BPO^{-\bullet} \rightarrow C_6H_5COO^- + C_6H_5COO^{\bullet}$$

$$C_6H_5COO^{\bullet} + T \rightarrow T^{+\bullet} + C_6H_5COO^-$$

$$T + e^- \rightarrow T^{-\bullet}$$

$$T^{+\bullet} + T^{-\bullet} \rightarrow T^* + T$$

$$T^* \rightarrow T + h\nu$$

Scheme 4.2: Possible negative potential (reducing) "coreactant mechanism" for the generation of ECL, where T = thiophene.[11]

In the proposed mechanism BPO gains one electron to form a radical anion. This leads to decomposition of $BPO^{\bullet -}$ *via* cleavage of the O-O bond to yield $C_6H_5COO^-$ and $C_6H_5COO^{\bullet}$.[10] The benzoyl radical is a very strong oxidizing agent and is able to oxidize the thiophene compound in solution to a radical cation. In Scheme 4.2, the electrogenerated thiophene radical anion combines with the thiophene radical cation to give thiophene in its excited state which produces light.

In many of our compounds we observed two photocurrent peaks (Figure 4.15), and we believe that the first peak occurs due to the second proposed mechanism (Scheme 4.3).

$$BPO + e^- \rightarrow BPO^{-\bullet}$$

$$BPO^{-\bullet} \rightarrow C_6H_5COO^- + C_6H_5COO^{\bullet}$$

$$C_6H_5COO^{\bullet} + T \rightarrow T^{+\bullet} + C_6H_5COO^-$$

$$BPO^{-\bullet} + T^{+\bullet} \rightarrow T^* + BPO$$

$$T^* \rightarrow T + h\nu$$

Scheme 4.3: 2nd Possible "coreactant mechanism" for the generation of ECL, where T = thiophene.

a)

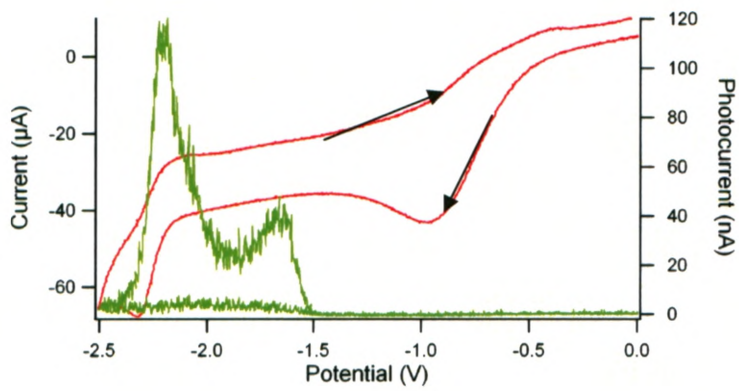

b)

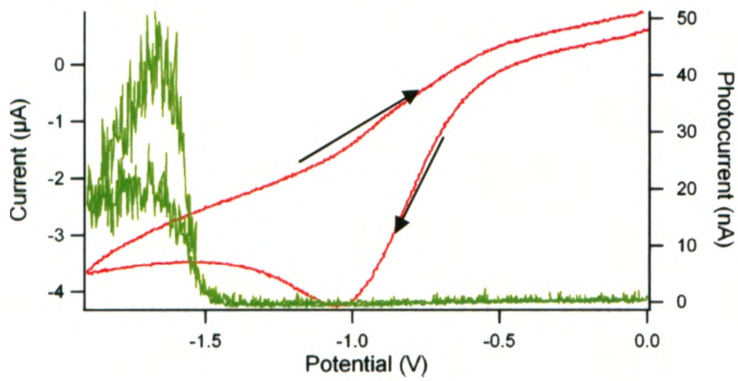

Figure 4.15: Cyclic voltammogram (red) with superimposed ECL-voltage curve (green) for **6** in DMF solution with added BPO (0.5 mM) and TBAP (0.1 M) scanned at 0.1 Vs−1 over (a) 0/-2.5 and (b) 0/-1.9 V. Arrows show the sweep direction.

One can see that there are two peaks in the photocurrent: the first appears "before" reduction of **6** (-2.3 V), however after the reduction of BPO (-1.0 V). In addition, this light is still generated even when the potential is restricted in the range of 0 to -1.9 V, which is insufficient to reduce **6**. The first peak in the photocurrent is therefore not dependent on the generation of the radical anion of **6** and the first proposed mechanism for ECL generation (Scheme 4.2) does not apply. It is possible that the path

taken to generate this photocurrent is by Mechanism 2 (Scheme 4.3), which does not rely on reduction of the luminophore at the electrode. A second possible mechanism is shown in Scheme 4.3. This second mechanism proposes that $C_6H_5COO^{-\bullet}$ combines with the chemically generated thiophene radical cation ($T^{\bullet+}$) to give thiophene in its excited state, which produces the emission of light when it relaxes down to its ground state.

The second photocurrent peak appears "after" the reduction of **6**, and presumably arises from the more established route (Scheme 4.2). The ECL efficiencies for the thiophene containing compounds with BPO coreactant relative to DPA + BPO are listed in Table 4.7.

Table 4.7: ECL efficiencies relative to DPA + "coreactant" for ECL experiments containing 5mM BPO and 0.1M TBAP in a DMF solution. Scan rate = 0.1 V^{-1}

Series A Compound	1st photocurrent peak (V)	2nd photocurrent peak (V)	Relative efficiencies*
1	-1.58	-2.23	0.74
2	-1.54	-2.24	0.90
3	-	-1.68	4.9
4	- 1.62	-2.29	0.70
5	-1.59	-2.24	1.4
6	-1.62	-2.18	10.0
7	-	-2.27	0.26
8	-	-2.36	1.06
9	-1.58	-2.08	1.00
10	-1.55	-2.14	0.78
19	-1.62	-2.27	0.95
20	-1.54	-	17.0
21	-1.56	-2.28	8.0

*The potential window used to determine the efficiencies was from 0 to -2.5 V.

By not scanning to positive potential, the time delay between the production of the radical anion and cation is much smaller and therefore decay of the radical ions is

lessened and a greater intensity of light is produced. Only compounds **6**, **19** and **20** had large increases in relative ECL efficiency when BPO was added.

4.5 Pulsing experiments of the elaborated thiophene compounds

In these experiments, the working electrode was pulsed in DMF between 2 and -2.5 V at a rate of 10 Hz. Under these conditions, an increase in photocurrent should be observed because the decreased delay between the production of radical anions and cations should allow more productive collisions between them relative to other non radiative decomposition pathways. However, in these annihilation experiments, the photocurrent was very weak and the predicted increase in efficiency was not seen.

The pulsing experiments were also done with added coreactant over the range of 0 to -2.5 V. The photocurrent in these experiments was affected by the potential range (Figure 4.14). When the potential was pulsed to the 1st reduction potential where a photocurrent peak was seen in the coreactant experiments (e.g., -2.0 V for **19**), the photocurrent was weaker than when a larger potential window was used (Figure 4.16). The larger potential window allows an increase in redox reactions and a greater photocurrent to be produced through mechanism 1 and 2 (Scheme 4.2 and 4.3, respectively).

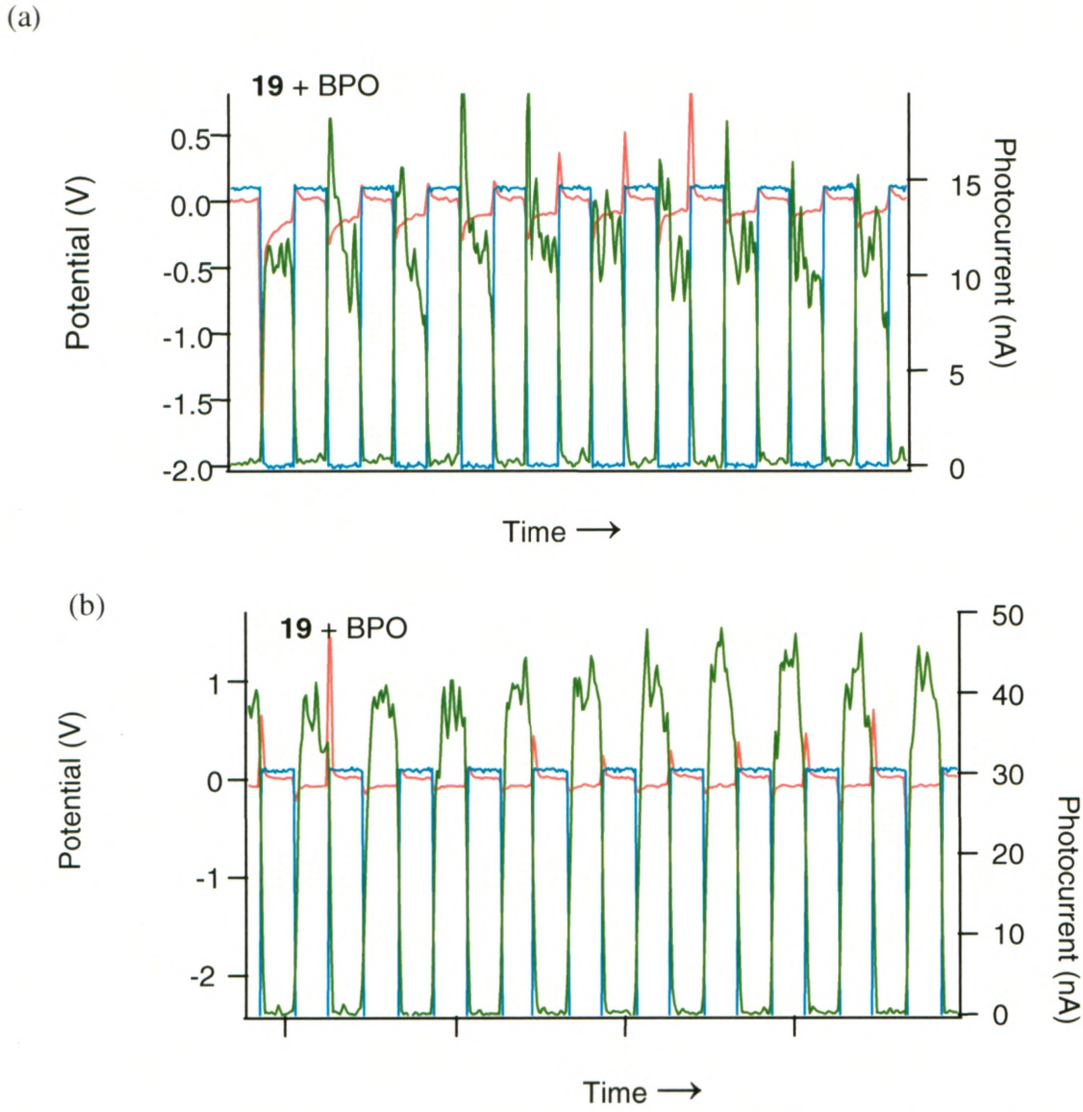

Figure 4.16: Photocurrent (green), electrochemical current (red) and applied potential (blue) over time in pulsing experiment. (a) 0/-2.0 V (b) 0/-2.5 V at a rate 10 Hz for **19** in DMF solution containing 5 mM BPO and 0.1 M TBAP.

Also with many of the compounds, we observed weak efficiencies because of a decay in the photocurrent over repeated cycles (Figure 4.17).

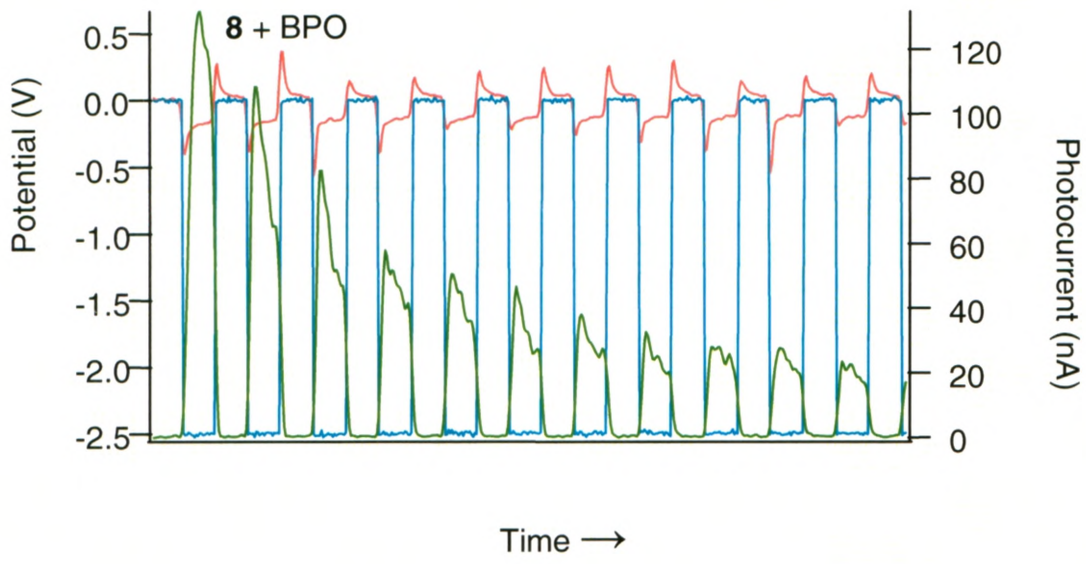

Figure 4.17: Photocurrent (green), electrochemical current (red) and applied potential (blue) over time in pulsing experiment at a rate 10 Hz for **8** in DMF solution containing 5 mM BPO and 0.1 M TBAP.

This decay in the photocurrent is possibly due to the generation of polymer on the electrode or other byproducts.[12] It was seen for compounds **1**, **2**, **7**, **8**, **9**, **10**, and **19**.

4.6 Spectroscopy of elaborated thienyl compounds.

UV-vis absorption spectra were obtained for compounds in Series A, B and D. The compounds in Series A absorbed light at a shorter wavelength and higher energy than the analogous compounds in Series B. Also compounds **3** and **8** had the widest Stokes' shift between the UV-vis absorption and the photoluminescence. This could possibly be due to changes in the molecular structure of the compound upon excitation.[6]

Table 4.8: Quantum yields, Absorbance and Photoluminescence maxima for the elaborated thiophene compounds.

Compound	Absorbance λ_{max} (nm)	Photoluminescence λ_{max} (nm)	Φ_{PL} (%)*	ECL λ_{max} (nm)	$ECL_{max} - PL_{max}$ (nm)
1	250	331	0.16	432 / 641	101 / 310
2	252	321	0.017	610	289
3	266	423	0.76	449 / 637 / 743	26 / 226 / 320
4	255	328	0.301	719	391
5	258	330	0.052	646	316
6	255	368	0.34	509 / 642	141 / 274
7	249	367	0.25	477 / 553 / 738	110 /186 / 371
8	295	482	1.23	568 / 745	86 / 263
9	287	366	0.41	454 / 608	88 / 242
10	274	371	4.79	430 / 557	59 / 186
19	290	371	0.51	570 / 675	199 / 304
20	282	368	0.43	462 / 597	94 / 229
21	274	345		439 / 597	94 / 252

*determined with reference to DPA.

It is clear from the photoluminescence (PL) data that the Series B compounds are red shifted by 31-60 nm from Series A and this is possibly due to the extended conjugation found in Series B. In addition, the compounds containing an NMe_2 group (**4** and **8**) are much more red shifted (~100 nm) than the other compounds in these series. This could possibly be due to changes in the molecular structure of the compound center upon the excitation.[6] Also from Table 4.8, we can see that there is a large difference between the ECL spectrum and the photoluminescence. It is possible that this is due to self-absorption since; compared to the concentrations needed for photoluminescence high concentrations of thiophene were needed to obtain measurable ECL spectra. The formation of excimers was also a possible contributing factor (See section 4.7).[6]

The photoluminescence quantum efficiency for the elaborated thiophene compounds was low, compound **19** having the highest relative efficiency of only 4.79 %. It is possible that the extended conjugation and rigid structure in **19** allowed for a higher quantum yield.

4.7 Spectra of electrogenerated chemiluminescence (ECL)

The ECL spectra of the elaborated thiophene compounds were acquired in DMF solution by pulsing between the oxidation and reduction potentials of the compounds under study. We found that using a larger potential window increased the intensity of the ECL peak while a narrow window decreased the intensity. We also noticed that many of the compounds displayed peaks at longer wavelengths than the normal emission (Figure 4.18). These peaks have been attributed to emission from excimers (*excited dimers*). The ECL process for the formation of excimers is represented below (Scheme 4.4); here excimers are represented as T_2*.[12]

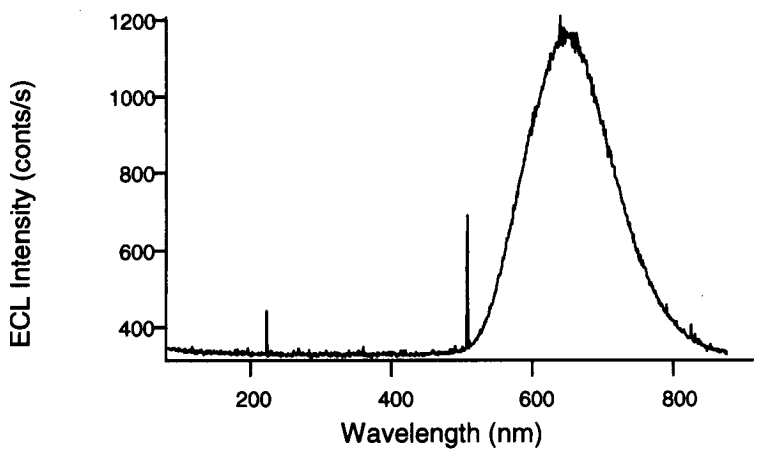

Figure 4.18: ECL spectra of compound **3** in DMF solution containing 5 mM BPO, 0.1 M TBAP pulsed for 60 seconds at 10 Hz.

$$T + e \rightarrow T^{\bullet -}$$

$$T - e \rightarrow T^{\bullet +}$$

$$T^{\bullet -} + T^{\bullet +} \rightarrow T^* + T \text{ or } T_2^*$$

$$T^* \rightarrow T + h\nu_1$$

$$T_2^* \rightarrow 2T + h\nu_2$$

Scheme 4.4: Proposed mechanism for the emission from excimers; T = thiophene-containing compounds.

The formation of excimers decreases the fluorescence quantum yield because of the slower radiative rate and the greater number of available nonradiative decay pathways. It also increases the contribution of lower energy photoluminescence compared to the monomer photoluminescence.[13]

For all compounds in Series A except **1**, the ECL emission was red shifted compared to the fluorescence emission and consisted of only a single emission peak between 600 and 700 nm (*e.g.*, as shown in Figure 4.15), compound **1** instead displayed two peaks, one at 450 nm and one at 641 nm. According to Bard and coworkers, the broad, featureless low energy band between 600 and 700 nm is characteristic of the excited-state dimer species, which is favored under the high concentrations of the ECL experimental conditions.[13] Bard and coworkers found similar results when studying the ECL of poly(fluorene).[13] They found that the ECL spectrum was strongly dependent on concentration. As the concentration of the sample in solution increased so did the relative

excimer emission (Figure 4.19).[13] This is because dimmers are favoured at higher concentrations.

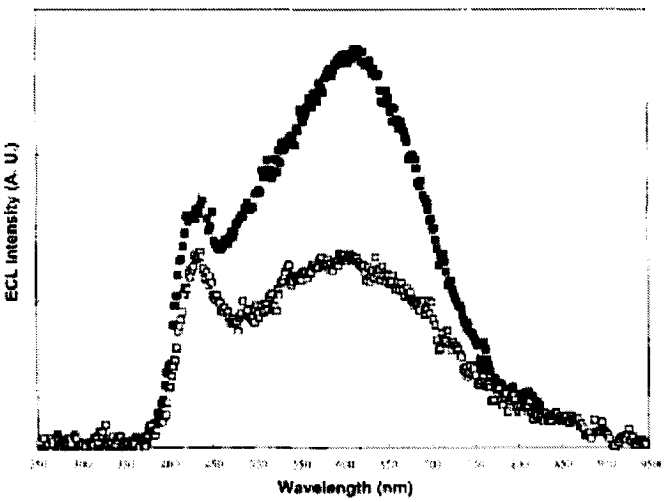

Figure 4.19: ECL emission spectra of 3.3 x 10-5 M (open squares) and 6 x 10-5 M (filled squares) of poly(9,9-dioctylfluorene) (taken from ref. 13)

We also found that with some compounds, excimer formation was dependent on the applied potential that was applied (Figure 4.20). In these experiments, when the potential was pulsed between 0 and -2.5 V there were two peaks at 450 nm and 780 nm, however, when the potential was pulsed between 0 and -1.8 V there was only one peak present at 680 nm. We are uncertain as to why the there is a peak shift between the two potentials and this requires further investigation.

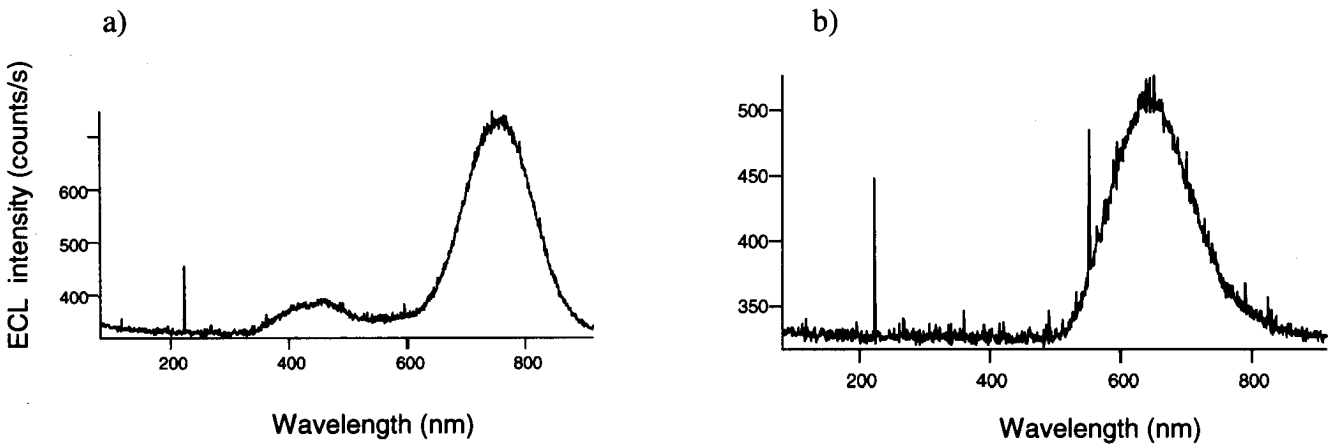

Figure 4.20: ECL spectra of **1** in DMF solution containing 0.1 M TBAP and 5 mM BPO pulsed at 10 Hz, (a) 0/-2.5 V and (b) 0/-1.8 V.

With the exception of **7**, the ECL spectra in Series B could only be obtained in the presence of coreactant. In the coreactant system, when a smaller potential window was used, the emission from the excimer dominated the ECL spectra (Figure 4.18). It is possible that Mechanism 2 for ECL generation (Scheme 4.3) favors the excimer (T_2*) formation rather than the excited monomer (T*). For compounds in Series D, dominant peaks were observed around 600 nm (possibly due to excimer emission) and as well as small peaks near the baseline (monomer emission).

4.8 References

(1) Dini, D. *Chem. Mater.* **2005**, *17*, 1933.
(2) Barbarella, G.; Melucci, M.; Sotgiu, G. *Adv. Mater.* **2005**, 1581.
(3) Perepichka, I.; Perepichka, D.; Meng, H.; Wudl, F. *Adv. Mater.* **2005**, *17*, 2281.
(4) Lide, D. R. *CRC Handbook of Chemistry and Physics*; 84 ed. Boca Raton, **2003**.
(5) Yang, X.; Jiang, X.; Zhao, C.; Chen, R.; Qin, P.; Sun, L. *Tetrahedron Lett.* **2006**, 4961.
(6) Lai, R.; Kong, X.; Jenekhe, S.; Bard, A. *J. Am. Chem, Soc.* **2003**, *125*, 12631.
(7) McDaniel, D. H.; Brown, H. C. *J. Org. Chem* **1957**, *23*, 420.
(8) Hansh, C.; Leo, A.; Hoekman, D. *Exploring QSAR - Hydrophobic, Electronic and Steric Constants* Washington, DC, **1995**.
(9) Richter, M. *Chem. Rev.* **2004**, *104*, 3003.
(10) Miao, W.; Choi, J. P. In *Electrgenerated Chemiluminescence*; Bard, A., Ed. **2004**, p 213.
(11) Choi, J. P.; Wong, K. T.; Chem, Y. M.; Yu, J. K.; Chou, P. T.; Bard, A. *J. Phys. Chem.* **2003**, *107*, 14407.
(12) Omer, K.; Kanibolotsky, A.; Skabara, P.; Perpichka, I.; Bard, A. J. *J. Phys. Chem.* **2007**, *111*, 6612.
(13) Prieto, I.; Teetsov, J.; Fox, M. A.; Bout, D. A.; Bard, A. *J. Phys. Chem.* **2001**, *105*, 520.

5.0 Conclusions and Future work

In our search to develop new ways to increase the functionality of thiophene, the Huisgen 1,3-dipolar addition or "click" reaction using Cu(I) as the catalyst has emerged as an extremely reliable and useful reaction. Using this method we were able to make 18 new thiophene compounds with various functional groups in moderate to high yields and we were no longer restricted to complicated and unreliable C-C bond forming reactions to functionalize thiophene.

The synthesis of the elaborated thiophene compounds was straightforward, requiring only the synthesis of the azidothiophene precursor; the aryl acetylenes were all commercially available except for 1,3,5-triethynylbenzene. We found that changing our pre catalyst combination of Cu/Cu(II)SO_4 to a combination of Cu(II)SO_4 and sodium ascorbate, lowering the temperature and increasing the reaction time enabled us to achieve much higher yields. We also took advantage of using a biphasic system of water and ^{t}BuOH, which allowed us to isolate the desired products by filtration without column chromatography.

We were able to study the redox and optical properties of compounds in Series A, B and D. We found by calculation done the HOMO was spread over the entire molecule, and that the LUMO was located on the thiophene and triazole ring systems for Series B.

The UV-vis absorption spectrum of the elaborated thiophene compounds provided evidence that the more conjugated systems in Series D had the smallest energy gap between the HOMO and LUMO, followed by compounds in Series B, then A. The photoluminescence of the compounds were also studied and compounds containing the functional group NMe_2 (compounds **3** and **8**) had a large Stokes shift compared to other

compounds in the respective series and emitted light at a much lower energy then the other elaborated thiophene compounds. We believe that this could possibly be due to a change in the molecular structure of the compound center upon the excitation. Also the fluorescence quantum yield was calculated for all compounds; **19** was the most efficient at 4.79% of DPA.

From CV experiments, we found that the elaborated thiophene compounds lack stability when they are oxidized or reduced. We also found from the Hammett plots that the electron-donating and -withdrawing substituents had a greater effect on the oxidation and reduction potentials of compounds in Series A. In Series B these substituents had very little effect on the oxidation potential of the bithiophene ring system.

ECL experiments were also done: in the annihilation reaction, all of the compounds had a low efficiency. However, with the addition of coreactant the efficiency was increased. The most efficient compounds were **6** (10 %) and **20** (17 %) relative to DPA. We also observed excimer formation for all of the elaborated thiophene compounds. This was inferred from the low energy emission between 650 – 800 nm in the ECL spectra. However, further experimentation is required. These experiments would include varying the concentration of the thiophene-containing compounds in solution during the ECL experiments. If we were to see an increase in intensity of the low energy peak at higher concentration of thiophene in solution, this would provide further evidence that excimer formation is in fact responsible for the low energy emission during the ECL experiments.

Future experiments to complement this work would include polymerization of the thiophene compounds and studying the physical and optical properties of the polymer

through ECL and cyclic voltammetry. Also, the physical and optical properties of Series C compounds need to be examined.

Appendix

Appendix 1: Crystal Structure Data for 3

Table 1. Crystallographic Experimental Details

A. Crystal Data	
formula	$C_{14}H_{14}N_4S$
formula weight	270.35
crystal dimensions (mm)	0.53 × 0.05 × 0.05
crystal system	orthorhombic
space group	$P2_12_12_1$ (No. 19)
unit cell parameters[a]	
a (Å)	6.0478 (9)
b (Å)	12.876 (2)
c (Å)	16.732 (3)
V (Å^3)	1302.9 (3)
Z	4
ρ_{calcd} (g cm^{-3})	1.378
μ (mm^{-1})	0.240
B. Data Collection and Refinement Conditions	
diffractometer	Bruker PLATFORM/SMART 1000 CCD[b]
radiation (λ [Å])	graphite-monochromated Mo Kα (0.71073)
temperature (°C)	–80
scan type	ω scans (0.3°) (45 s exposures)
data collection 2θ limit (deg)	51.60
total data collected	9682 ($-7 \le h \le 7$, $-15 \le k \le 15$, $-20 \le l \le 20$)
independent reflections	2507 (R_{int} = 0.0625)
number of observed reflections (*NO*)	1919 [$F_o^2 \ge 2\sigma(F_o^2)$]
structure solution method	direct methods (*SHELXS–97*[c])
refinement method	full-matrix least-squares on F^2 (*SHELXL–97*[c])
absorption correction method	multi-scan (*SADABS*)
range of transmission factors	0.9881–0.8836
data/restraints/parameters	2507 [$F_o^2 \ge -3\sigma(F_o^2)$] / 0 / 174
Flack absolute structure parameter[d]	0.02 (11)
goodness-of-fit (S)[e]	1.034 [$F_o^2 \ge -3\sigma(F_o^2)$]
final R indices[f]	
R_1 [$F_o^2 \ge 2\sigma(F_o^2)$]	0.0439
wR_2 [$F_o^2 \ge -3\sigma(F_o^2)$]	0.0889
largest difference peak and hole	0.182 and –0.215 e Å^{-3}

[a]Obtained from least-squares refinement of 2357 reflections with $5.80° < 2\theta < 40.32°$.

[b]Programs for diffractometer operation, data collection, data reduction and absorption correction were those supplied by Bruker.

[c]Sheldrick, G. M. *Acta Crystallogr.* **2008**, *A64*, 112–122.

[d]Flack, H. D. *Acta Crystallogr.* **1983**, *A39*, 876–881; Flack, H. D.; Bernardinelli, G. *Acta Crystallogr.* **1999**, *A55*, 908–915; Flack, H. D.; Bernardinelli, G. *J. Appl. Cryst.* **2000**, *33*, 1143–1148. The Flack parameter will refine to a value near zero if the structure is in the correct configuration and will refine to a value near one for the inverted configuration. In this case the relatively large standard uncertainty indicates that the structural data alone should not be used to confirm absolute structure, but no stereochemical implications are being made here (since the compound is achiral).

[e]$S = [\Sigma w(F_o^2 - F_c^2)^2/(n-p)]^{1/2}$ (n = number of data; p = number of parameters varied; $w = [\sigma^2(F_o^2) + (0.0349P)^2 + 0.1820P]^{-1}$ where $P = [\mathrm{Max}(F_o^2, 0) + 2F_c^2]/3$).

[f]$R_1 = \Sigma||F_o| - |F_c||/\Sigma|F_o|$; $wR_2 = [\Sigma w(F_o^2 - F_c^2)^2/\Sigma w(F_o^4)]^{1/2}$.

Appendix 2: Crystal Structure Data for 6

Table 1. Crystallographic Experimental Details

A. Crystal Data	
formula	$C_{16}H_{11}N_3S_2$
formula weight	309.40
crystal dimensions (mm)	0.67 × 0.35 × 0.16
crystal system	orthorhombic
space group	$Pna2_1$ (No. 33)
unit cell parameters[a]	
a (Å)	31.455 (5)
b (Å)	5.6198 (8)
c (Å)	23.722 (3)
V (Å^3)	4193.4 (10)
Z	12
ρ_{calcd} (g cm^{-3})	1.470
μ (mm^{-1})	0.376
B. Data Collection and Refinement Conditions	
diffractometer	Bruker PLATFORM/SMART 1000 CCD[b]
radiation (λ [Å])	graphite-monochromated Mo Kα (0.71073)
temperature (°C)	–80
scan type	ω scans (0.5°) (10 s exposures)
data collection 2θ limit (deg)	52.00
total data collected	29164 ($-38 \le h \le 38$, $-6 \le k \le 6$, $-29 \le l \le 29$)
independent reflections	8192 (R_{int} = 0.0429)
number of observed reflections (*NO*)	7095 [$F_o^2 \ge 2\sigma(F_o^2)$]
structure solution method	direct methods (*SHELXS–97*[c])
refinement method	full-matrix least-squares on F^2 (*SHELXL–97*[d])
absorption correction method	multi-scan (*SADABS*)
range of transmission factors	0.9423–0.7868
data/restraints/parameters	8192 [$F_o^2 \ge -3\sigma(F_o^2)$] / 6[e] / 586
Flack absolute structure parameter[f]	0.00 (5)
goodness-of-fit (*S*)[g]	1.028 [$F_o^2 \ge -3\sigma(F_o^2)$]
final R indices[h]	
R_1 [$F_o^2 \ge 2\sigma(F_o^2)$]	0.0403
wR_2 [$F_o^2 \ge -3\sigma(F_o^2)$]	0.0929
largest difference peak and hole	0.357 and –0.175 e Å^{-3}

[a]Obtained from least-squares refinement of 4727 reflections with $5.18° < 2\theta < 50.34°$.

[b]Programs for diffractometer operation, data collection, data reduction and absorption

correction were those supplied by Bruker.

[c]Sheldrick, G. M. *Acta Crystallogr.* **1990**, *A46*, 467–473.

[d]Sheldrick, G. M. *SHELXL-97*. Program for crystal structure determination. University of Göttingen, Germany, 1997.

[e]Distances involving the carbon atoms disordered with sulfurs were given fixed values during refinement: d(C25A–C29A) = d(C25B–C29B) = d(C25C–C29C) = 1.35(1) Å; d(C28A–C29A) = d(C28B–C29B) = d(C28C–C29C) = 1.54(1) Å.

[f]Flack, H. D. *Acta Crystallogr.* **1983**, *A39*, 876–881; Flack, H. D.; Bernardinelli, G. *Acta Crystallogr.* **1999**, *A55*, 908–915; Flack, H. D.; Bernardinelli, G. *J. Appl. Cryst.* **2000**, *33*, 1143–1148. The Flack parameter will refine to a value near zero if the structure is in the correct configuration and will refine to a value near one for the inverted configuration.

[g]$S = [\Sigma w(F_o^2 - F_c^2)^2/(n-p)]^{1/2}$ (n = number of data; p = number of parameters varied; $w = [\sigma^2(F_o^2) + (0.0441P)^2 + 1.3083P]^{-1}$ where $P = [\mathrm{Max}(F_o^2, 0) + 2F_c^2]/3$).

[h]$R_1 = \Sigma||F_o| - |F_c||/\Sigma|F_o|$; $wR_2 = [\Sigma w(F_o^2 - F_c^2)^2/\Sigma w(F_o^4)]^{1/2}$.

Appendix 3: Crystal Structure Data for 7

Table 1. Crystallographic Experimental Details

A. Crystal Data	
formula	$C_{16}H_{10}FN_3S_2$
formula weight	327.39
crystal dimensions (mm)	0.84 × 0.19 × 0.02
crystal system	triclinic
space group	$P\bar{1}$ (No. 2)
unit cell parameters[a]	
a (Å)	6.060 (2)
b (Å)	7.962 (3)
c (Å)	15.135 (5)
α (deg)	97.682 (6)
β (deg)	93.700 (5)
γ (deg)	96.533 (6)
V (Å^3)	716.7 (4)
Z	2
ρ_{calcd} (g cm^{-3})	1.517
μ (mm^{-1})	0.381
B. Data Collection and Refinement Conditions	
diffractometer	Bruker PLATFORM/SMART 1000 CCD[b]
radiation (λ [Å])	graphite-monochromated Mo Kα (0.71073)
temperature (°C)	–80
scan type	ω scans (0.4°) (10 s exposures)
data collection 2θ limit (deg)	50.50
total data collected	5883 ($-7 \le h \le 7$, $-9 \le k \le 9$, $-17 \le l \le 18$)
independent reflections	2586 (R_{int} = 0.1589)
number of observed reflections (*NO*)	1316 [$F_o^2 \ge 2\sigma(F_o^2)$]
structure solution method	direct methods (*SHELXS–97*[c])
refinement method	full-matrix least-squares on F^2 (*SHELXL–97*[d])
absorption correction method	Gaussian integration (face-indexed)
range of transmission factors	0.9908–0.9172
data/restraints/parameters	2586 [$F_o^2 \ge -3\sigma(F_o^2)$] / 7[e] / 213
goodness-of-fit (S)[f]	0.928 [$F_o^2 \ge -3\sigma(F_o^2)$]
final R indices[g]	
R_1 [$F_o^2 \ge 2\sigma(F_o^2)$]	0.0638
wR_2 [$F_o^2 \ge -3\sigma(F_o^2)$]	0.1443
largest difference peak and hole	0.302 and –0.336 e Å^{-3}

[a]Obtained from least-squares refinement of 874 reflections with $5.20° < 2\theta < 44.44°$.

[b]Programs for diffractometer operation, data collection, data reduction and absorption correction were those supplied by Bruker.

[c]Sheldrick, G. M. *Acta Crystallogr.* **1990**, *A46*, 467–473.

[d]Sheldrick, G. M. *SHELXL-97*. Program for crystal structure determination. University of Göttingen, Germany, 1997.

[e]Pairs of corresponding distances within the disordered thienyl group were constrained to be equal (within 0.01 Å) during refinement: d(S2A–C25) = d(S2B–C25); d(S2A–C28A) = d(S2B–C28B); d(C25–C26A) = d(C25–C26B); d(C26A–C27A) = d(C26B–C27B); d(C27A–C28A) = d(C27B–C28B). A planar geometry was imposed upon the minor (20%) conformer of the disordered thienyl group by constraining the five-atom unit (S2B, C25, C26B, C27B, C28B) to define a polyhedron with a volume of no more than 0.01 Å (through use of the *SHELXL-97* FLAT instruction; see reference *d*).

[f]$S = [\Sigma w(F_o^2 - F_c^2)^2/(n-p)]^{1/2}$ (n = number of data; p = number of parameters varied; $w = [\sigma^2(F_o^2) + (0.0242P)^2]^{-1}$ where $P = [\text{Max}(F_o^2, 0) + 2F_c^2]/3$).

[g]$R_1 = \Sigma||F_o| - |F_c||/\Sigma|F_o|$; $wR_2 = [\Sigma w(F_o^2 - F_c^2)^2/\Sigma w(F_o^4)]^{1/2}$.

Appendix 4: Crystal Structure Data for 27

Table 1. Crystallographic Experimental Details

A. Crystal Data	
formula	$C_{33}H_{21}Cl_3S_5$
formula weight	684.15
crystal dimensions (mm)	0.61 × 0.20 × 0.17
crystal system	monoclinic
space group	$P2_1$ (No. 4)
unit cell parameters[a]	
a (Å)	8.8067 (6)
b (Å)	14.1463 (9)
c (Å)	12.3041 (8)
β (deg)	93.0458 (9)
V (Å^3)	1530.71 (17)
Z	2
ρ_{calcd} (g cm^{-3})	1.484
μ (mm^{-1})	0.665
B. Data Collection and Refinement Conditions	
diffractometer	Bruker PLATFORM/SMART 1000 CCD[b]
radiation (λ [Å])	graphite-monochromated Mo Kα (0.71073)
temperature (°C)	–80
scan type	ω scans (0.3°) (15 s exposures)
data collection 2θ limit (deg)	54.98
total data collected	13239 (-11 ≤ h ≤ 11, -18 ≤ k ≤ 18, -15 ≤ l ≤ 15)
independent reflections	6946 (R_{int} = 0.0216)
number of observed reflections (*NO*)	6339 [$F_o^2 \geq 2\sigma(F_o^2)$]
structure solution method (*DIRDIF–99*[c])	Patterson search/structure expansion
refinement method	full-matrix least-squares on F^2 (*SHELXL–97*[d])
absorption correction method	multi-scan (*SADABS*)
range of transmission factors	0.8954–0.6873
data/restraints/parameters	6946 [$F_o^2 \geq -3\sigma(F_o^2)$] / 0 / 370
Flack absolute structure parameter[e]	-0.01 (7)
goodness-of-fit (*S*)[f]	1.061 [$F_o^2 \geq -3\sigma(F_o^2)$]
final R indices[g]	
R_1 [$F_o^2 \geq 2\sigma(F_o^2)$]	0.0484
wR_2 [$F_o^2 \geq -3\sigma(F_o^2)$]	0.1322
largest difference peak and hole	0.976 and –0.643 e Å^{-3}

[a]Obtained from least-squares refinement of 7816 reflections with $4.64° < 2\theta < 54.88°$.

[b]Programs for diffractometer operation, data collection, data reduction and absorption correction were those supplied by Bruker.

[c]Beurskens, P. T.; Beurskens, G.; de Gelder, R.; Garcia-Granda, S.; Israel, R.; Gould, R. O.; Smits, J. M. M. (1999). The *DIRDIF-99* program system. Crystallography Laboratory, University of Nijmegen, The Netherlands.

[d]Sheldrick, G. M. *SHELXL-97*. Program for crystal structure determination. University of Göttingen, Germany, 1997.

[e]Flack, H. D. *Acta Crystallogr.* **1983**, *A39*, 876–881; Flack, H. D.; Bernardinelli, G. *Acta Crystallogr.* **1999**, *A55*, 908–915; Flack, H. D.; Bernardinelli, G. *J. Appl. Cryst.* **2000**, *33*, 1143–1148. The Flack parameter will refine to a value near zero if the structure is in the correct configuration and will refine to a value near one for the inverted configuration. In this case the relatively large standard uncertainty indicates that the structural data alone should not be used to confirm absolute stereochemistry. The 2,5-bis{3,5-di(2-thienyl)phenyl}thiophene molecule contains no stereogenic centers, so the Flack parameter would only be used to assess the stereochemistry of the crystal packing (if this were of interest).

[f]$S = [\Sigma w(F_o^2 - F_c^2)^2/(n-p)]^{1/2}$ (n = number of data; p = number of parameters varied; $w = [\sigma^2(F_o^2) + (0.0745P)^2 + 0.9185P]^{-1}$ where $P = [\mathrm{Max}(F_o^2, 0) + 2F_c^2]/3$).

[g]$R_1 = \Sigma||F_o| - |F_c||/\Sigma|F_o|$; $wR_2 = [\Sigma w(F_o^2 - F_c^2)^2/\Sigma w(F_o^4)]^{1/2}$.

Appendix 5: Background Cyclic voltammogram

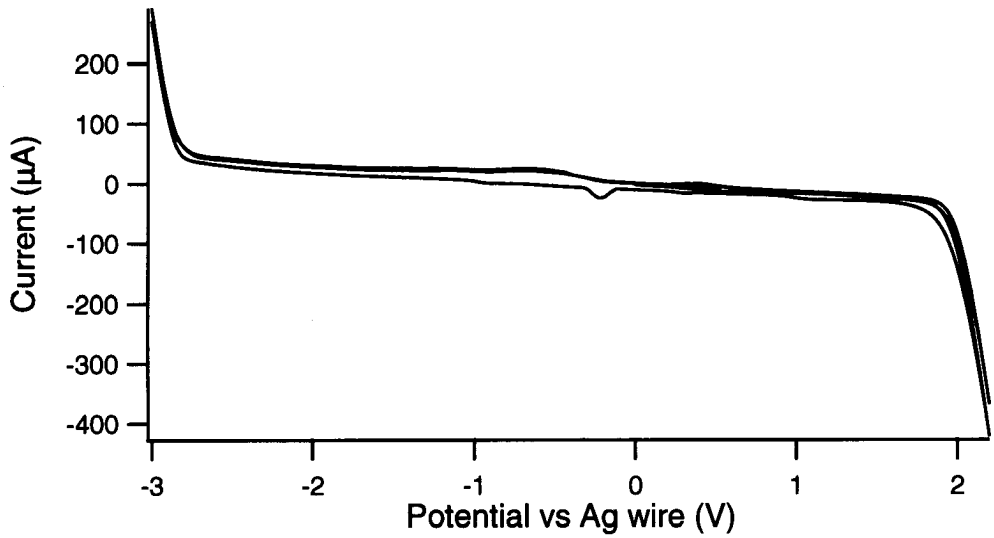

Cyclic voltammogram of DMF (3 ml) and 0.1 M of TBAP scanned at a rate of 0.1 Vs^{-1}